3-21-2016

West Florida Shelf Connectivity: An Exploratory Study

Amanda Sue Reinert

West Florida Shelf Connectivity: An Exploratory Study

by

Amanda Sue Reinert

A thesis submitted in partial fulfillment
of the requirements for the degree of
Masters of Science
with a concentration in physical oceanography
College of Marine Science
University of South Florida

Major Professor: Robert H. Weisberg, Ph.D.
Andrea Mask, Ph.D.
Lianyuan Zheng, Ph.D.
Yonggang Liu, Ph.D.

Date of Approval:
March 15, 2016

Keywords: synoptic forcing, deep-ocean forcing, backward, Isopycnic Trajectories

DEDICATION

Without my amazing family and all of its variegation, I never would have completed this step. For my children, my darlin's Donovan and Gabriel- whom my every waking moment and breath taken is an effort to make your lives better and filled with more joy than puddles, happy birthday sprinkles and excavators can provide. For my Mom and my other-mother Dolly- your prodding, poking, kicking-in-the-butt, smacks through the phone and unending support in every facet of my life is something I strive to emulate and provide to my boys as they grow into wonderful men. I don't have the words to properly express how truly necessary your support and love (in all its forms) has been through this process and the Life that happened along the way. Thank you for believing in me when I didn't believe in myself and for giving me the support and room I needed to allow me to find myself again. For my brother- Your tat, indignation on my behalf, and righteous fury when I needed it were amazing displays of love and support. Thank you for always having my back. For my Daddy- your rumbling love gave me something constant to touch back to when everything felt like it was swirling (and sometimes hitting me) in a tornado. For my sisters-by-choice Josy, Allie, and Amanda- Your phone and FaceTime hugs were so important. Your joy, life adventures, puppies, wine, care packages, Vera, families, and crazy dancing made my soul smile when the rest of me wanted to cry. You three are the models of the woman I strive to be. For E&R- thank you for your support, friendship, and accepting me for me from day one. For Sarah- the hugs, food, and line dancing made all the difference in the world. For Joan- always.

ACKNOWLEDGMENTS

This work could not have been accomplished without the strong support and mentorship of my committee. My advisor, Dr. Robert Weisberg, helped me to stretch as a scientist and to define what I am truly interested in while adding a creative flair to my science. Dr. Andrea Mask of the Naval Oceanographic Office provided excellent mentorship from outside the realm of academia as well as personally endorsing my selection as a Department of Defense Science, Math and Research Technology Fellowship recipient to assist in the funding of this research, summer internships, and follow-on funding and employment in the field of mission-oriented oceanography. Dr. Lianyuan Zheng showed more patience and endurance while working with a student with no programing or modeling experience on a modeling project than I thought any person had. His suggestions of new ways to look at problems were instrumental to this research. Dr. Yonggang Liu's advice and teachings for script writing, data analysis, and altimetry data were a huge help, highly practical, and incredibly instructive.

I would like to thank the Ocean Circulation Group's thorough answering of random (sometimes panicky) questions I would come up with (Clifford, Dennis, and Jeff). The continued support and mentoring in achievement of my academic and professional goals by David Smith, Patrick Dixon, and Sam Wilson were also invaluable.

I have been supported financially by the College of Marine Science Anne and Werner von Rosenstiel Endowed Fellowship, a Research Assistantship, the Post 9-11 G.I. Bill, and the Department of Defense Science, Math and Research Technology Fellowship.

TABLE OF CONTENTS

LIST OF TABLES

LIST OF FIGURES

LIST OF ACRONYMS AND ABBREVIATIONS

°T: Degrees True, referencing True North as 0° and True East as 90° in the clockwise direction
EOF: Empirical Orthogonal Function
FD: Finite Difference
FE: Finite Element
FVCOM: Finite Volume Coastal Ocean Model
GOMEX: Gulf of Mexico
GOMHYCOM: Gulf of Mexico Hybrid Coastal Ocean Model
HYCOM: Hybrid Coupled Ocean Model
km: kilometer
KSRQ: Sarasota-Bradenton International Airport
kt: knot
LC: Loop Current
m: meter
NAVGEM: Navy Global Environmental Model
RK: Runge-Kutta
Sv: Sverdrup
TS: Tropical Storm
UN: United Nations
WFCOM: West Florida Coastal Ocean Model
WFS: West Florida Continental Shelf

ABSTRACT

This Thesis explores the connectiveness of the West Florida Shelf's various areas of economic and ecological importance by considering five case studies of varying dynamic forcing influences and time. The advection of water about the shelf moves nutrients and has a direct impact on the shelf's ecology and the determination of whether or not the shelf will be oligotrophic at any given time or location. The case studies are analyzed both quantitatively and qualitatively after quasi-isopycnal particle trajectory calculations are completed for each. The findings support a combination of local and deep-ocean forcing being ideal for the maximum advection and opportunity for potential connectivity between areas of the shelf, and provide a solid guide for moving forward with a considerable ensemble of studies in the future to approach the question from a statistical perspective. The numerical scheme used to calculate the particle trajectories is a 4^{th} order Runge-Kutta method. The scheme is investigated for it appropriateness and pitfalls as a backward trajectory calculation tool by direct comparison between forward trajectory calculations and attempting to replicate the result in the backward direction. The findings support that the more linear the trajectory and the more restrictive the dynamics acting upon a particle at any given location, the better the backward and forward replication will be, although it is still an approximation, much like any other iterative tool used for approximating a solution to an ordinary differential equation.

CHAPTER 1

INTRODUCTION

1.1 Objectives

The coastal ocean may be described as follows: Seaward from the shoreline, the continental shelves around the world are the areas where the landmass of the continent submerges underwater, with a relatively gentle slope as it extends into the ocean. At the end of this extension, at times reaching hundreds of kilometers horizontally, the continental shelf experiences an abrupt bottom slope change at what is referred to as the continental shelf break. Seaward of the shelf break, the continental slope continues to proceed towards the ocean floor as it transitions into the continental rise. This marks the transition from the continental landmass to the oceanic crust made primarily of basalt (ocean floor). The shelf break and slope are the hurdles that deeper, cooler and inorganic nutrient-rich oceanic waters need to cross in order to upwell onto a shelf and provide new deep ocean-derived nutrients to the organisms living in coastal ocean waters.

Upwelling as a physical process has been clearly described in multiple articles such as *Smith* [1995] with specific regard for coastal upwelling systems, *Weisberg et al.* [2014a] with a focus on the West Florida Shelf (WFS) in 2010 when the Loop Current and recently shed eddy in the Gulf of Mexico interacted with the shelf slope, *Weisberg et al.* [2000] focusing on the WFS inner shelf and the Ekman-geostrophic upwelling response to wind forcing observed there, and in *Pitcher et al.* [2010] specifically regarding the eastern boundaries of oceans and their

proclivity to develop harmful algal blooms as a result of their upwelling. Because this study focuses on the West Florida Shelf comparing deep-ocean forcing and local forcing for water parcel advection including upwelling and downwelling, the description provided in *Weisberg et al.* [2014a] serves as an informative introduction for deep-ocean forced upwelling in the local study area. The interaction of either the Loop Current or an eddy with the shelf slope sets into motion a series of responses. The relatively high height (and resulting high pressure) of the Loop Current to the surrounding Gulf of Mexico and WFS waters causes a pressure variation, resulting in a northward flow along isobaths. This flow then results in a pressure gradient force directed toward the right (towards the shallower waters), which is balanced by a Coriolis force induced by a southward flowing geostrophic current. This geostrophic flow tends to be along isobath, and it continues in such a manner until the prompting pressure gradient force is gone or the friction dissipates it [*Taylor*, 1921]. This geostrophic flow interacts with the bottom forming an Ekman layer in which the flow turns toward the left, allowing for an onshore directed flow component and the upwelling of waters from the shelf slope across the shelf break and onto the shelf itself.

Along with such deep ocean influences, there is also a correlation between the local winds and sea level by virtue of surface Ekman layer divergence and the set of an across shelf pressure gradient force, and as a corollary there is a correlation between the winds and the along-shelf currents allowing for similarities in properties of the shelf circulation, and differences based on each shelf's unique geometry, river input distribution, and boundary currents [*Weisberg et al.*, 2005]. The world's continental shelves have been investigated by a number of groups in many different fashions. Some such examples include *Strub et al.* [1987] which considers the Northeast Pacific Continental Shelf and its seasonality, while *Lucas et al.* [2005] diagnose the water origins, seasonal periods, persistent fronts and distinct sections of the Northern Argentine

Continental Shelf. *Holligan et al.* [1983] studied the North-West European continental shelf specifically to work towards improving remote sensing techniques for the estimation of chlorophyll in oceanic waters by using observations from cruises, unprocessed Coastal Zone Color Scanner graphics and other weather and imagery for the area. *Milliman et al.* [1985] looked at the Changjiang Estuary and its adjacent continental shelf in terms of sediment transport and sink pathways, dependent upon tidal fluctuations, river run-off, and other influences. A wonderfully thorough review (through that time) of the history of the circulation on the east coast of the US works is provided by *Bumpus* [1973], in which he covers experiments from drift bottles and other methods and provides a detailed recommended pathway for further studies and ensuring the struggles and limitations from previous studies are taken into consideration for making future experiments more successful.

The present works provides further clarification on the driving forces of water parcel advection to include upwelling and downwelling responses throughout the West Florida Shelf region. Further understanding of West Florida Shelf responses to both local and deep-ocean forcing is a necessary step to understanding ecological phenomena such as red tides, juvenile marine life cycles, nursery and adult habitat locations, estuary connectivities, and inorganic nutrient transports across the shelf.

<u>The present study strives to answer the following two questions:</u>

1. Under primarily deep-ocean or local forcing influences, what are the ranges of upwelling and advection of water parcels both vertically and horizontally across the various regions of the West Florida Shelf (WFS)?

- Given a period of time when we know the deep-ocean influence was strong on the WFS, what were the pathways of water parcel delivery from the region of the shelf slope to the near shore?
- Given a period of time when we know the local forcing influence was strong on the WFS, what were the pathways of water parcel advection across the WFS?

2. Is it reasonable to expect forward and backward particle trajectory calculations to have the same results? If so under what conditions?

For the purposes of continuity and comparison with previous works, "local forcing" and "deep-ocean forcing" will be defined as in *Weisberg and He* [2003] and specified below:

- Local forcing: shelf-wide inputs of momentum by winds and buoyancy by surface heat and freshwater flux and river inflows.
- Deep-Ocean forcing: inputs of momentum and buoyancy by currents at the shelf break.

1.2 Significance of the Study

1.2.1 The Florida Economy

Florida's Gross Domestic Product (GDP) total for 2012 was $777.2 billion [*Program*, 2014]. According to the Florida Department of Agriculture and Consumer Services report statistical overview encompassing 2012 [*Florida Department of Agriculture and Consumer Services*, 2013] Florida had 47,500 commercial farms, utilizing 9.25 million acres of land, employing 2 million people and contributing more than $104 billion to the state's economy in 2012. Comparatively, Florida is even more dependent upon the financial input it gets from the economic activity physically located in coastal counties (coastal economy: $599.8 billion in 2012)

and economic activity using the Atlantic ocean as an input (ocean economy: $24.5 billion in 2012) [*Program*, 2014]. These contribution amounts are ~5.8 (coastal) and ~6 (coastal + ocean) times the agriculture contribution amount (~$104 billion). Some specific aspects of the agricultural, coastal and oceanic economies include commercial fishing, aquaculture, and the recreational fishing and tourism.

In 2012 there were over 93 million pounds of fish, crab, clams (wild harvest only), lobster, shrimp and other invertebrates caught coming in at $205 million dockside value [*Florida Fish and Wildlife Conservation Commission*, 2015]. Of the coastal regions, the Gulf Coast has, on average, landed 70-75% of Florida's domestic seafood catch by weight and 70-80% by value. The Commercial fishing industry in Florida is the 2nd largest in the United States with $12 million in-state sales supporting 64,744 jobs (2009). The Saltwater Products Licenses sold brought in $925,000 (fiscal year 2012/2013) (not including wholesale dealers). In addition to traditional commercial fisheries, the aquaculture industry contributed $66.1 million (2005) in commercial income to the state [*Kildow*, 2008].

While the fishing industry brought in millions of dollars to the state as described above, the difference between those millions of contributed dollars and the billions brought in as a whole by the ocean and coastal economy is filled largely by the recreation and tourism sectors of the coastal economy. In 2005, the recreational marine-related industry statewide generated $18.5 billion in annual economic impact and 220,000 jobs (~100,000 of which were in manufacturing) [*Kildow*, 2008]. Florida is the leading state in terms of marine recreational fishing participation, and accounted for 33% of all marine angler trips taken in the United States in 2006 [*Kildow*, 2008].

Florida is ranked as the most popular recreational fishing state [*Allen and Southwick*, 2007] in the United States, with the saltwater anglers in Florida making up over 23.5% of the US total, and generating almost $3 billion in expenditures and retail sales (27% of the US total). Nearly half of the recreational fishing trips in Florida are made by visitors to the state. This clearly demonstrates the ocean tourism industry's direct impact on Florida's economy strictly by considering the recreational fishing aspect of the industry and not the 2nd and 3rd order industries supporting such an increase like those of the lodging, food, and transportation industries in the area.

The total economic impact of the Florida oceanic and coastal industries is approximately six times larger than that of the land-based agriculture industry in the state. This large difference in the economic impact for the state of Florida is one of the many reasons why the study of fisheries and recreational-impacting events such as red tides, the spawning of various sport fishes and the overall transport and advection of the inorganic nutrients across the shelf are so important. The better the scientific community becomes at adding another level of understanding to the system, the more impactful and widely applicable the research will be to the fisheries and economic health of the state.

1.2.2 Red Tides

With the coastal area being of such great import to Florida's economy, harmful algal blooms, or red tides, are a strong concern (e.g. *Heil et al.* [2014]). They can be incredibly detrimental to the fisheries and recreational events in a large area, as documented by *Walsh et al.* [2006], resulting in an economic loss some years of more than $25 million. Over a 6 year period, the red tides originating on the West Florida Continental Shelf (WFS) accounted for roughly half of the annual average economic loss to the United States, estimated then to be a total of ~$49

million [*Anderson et al.*, 2000]. As potentially damaging as red tides and other harmful algal blooms can be, these do not occur independent from the environment in which they exist. It is therefore imperative to gain a thorough understanding of the ocean circulation, resultant water properties, and interactions between the continental shelf and the deep-ocean and estuaries, all of which have a strong impact on the formation and advection of the bloom [*Weisberg et al.*, 2009a; *Weisberg et al.*, 2014a].

Typically, the wind driven upwelling scenario (the most frequent) on the WFS is a key factor for *Karenia brevis* (*K. brevis*) red tide blooms to manifest along the coastline [*Weisberg et al.*, 2009a] while the less frequent, prolonged deep-ocean induced upwelling scenario acts to suppress *K. brevis* red tides (as occurred in 1998, 2010 and to some degree in other years). This suppression occurs due to the resetting of the WFS water properties to a roughly Redfield ratio nutrient structure favoring other phytoplankton, and becoming non-conducive to the blooming of *K. brevis* [*Walsh et al.*, 2003; *Weisberg and He*, 2003; *Weisberg et al.*, 2014a]. This permits the diatoms to flourish in the environment rather than the microflagellates or toxic dinoflagellates.

In addition to the wind driven upwelling scenario, iron concentrations play a large role in controlling the periodic blooms of the diazotroph cyanobacterium *Trichodesmium erythraeum* (*T.E*), whose biomass levels have in turn been shown to significantly impact the blooms of *K. brevis* [*Lenes et al.*, 2008; *Walsh et al.*, 2009]. Upwelling plays a key role in the circulation and water properties on and around the shelf, and has a highly interdisciplinary impact from fisheries, geology, chemistry, and biology.

1.2.3 Upwelling Systems and Their Inter-Disciplinary Importance

The importance of the various upwelling systems in the oceans were discussed from a perspective beyond physical oceanography in 1995 at the 18th Dahlem Workshop in

Environmental Sciences in Berlin, Germany, upon which the primary editors of the workshop results (C.P. Summerhayes, K.-C Emeis, M.V. Angel, R.L. Smith, and B, Zeitzschel) stated unequivocally that "upwelling systems are important socially as well as scientifically, not only because they sequester nutrients that control ocean chemistry, biology, and fisheries, but also because they are intensely productive, and so by increasing the 'drawdown' of CO_2 in glacials they may influence climate. They are the sites of accumulation of oil-prone petroleum source rocks and of mineral resources such as diatomites and phosphorites" [*Summerhayes et al.*, 1995]. To be even more specific, as "open ocean and coastal upwelling dominate primary productivity in the world's oceans, accounting for 80-90% of world new production [*Brink et al.*, 1995]. The relevance to humans is undisputed and considerable, as some 50% of the world fish catch comes from the coastal waters [specifically known for their strong upwelling]. Changes in upwelling are known to have a considerable effect on fish stocks" [*Summerhayes et al.*, 1995]. In addition to the commercial fisheries aspect of the importance of upwelling systems, they "are important agents in the carbon cycle because of their exceptionally high productivity and the high rate of sequestration of organic matter in the bottom sediments beneath them" [*Summerhayes et al.*, 1995].

Upwelling systems play a large role in the distribution of other ocean water properties that are directly involved in biological processes which modulate seawater chemical composition and increase particulate matter and sedimentation of particles. Upwelling zones are particularly important because their high biological productivity leads to sequestration of nutrients in the water column and their associated high rates of sediment accumulation lead to concentrations of biogenic components like carbon, phosphate, and opaline silica on the seabed [*Summerhayes et al.*, 1995]. Continuing with the importance of sedimentation, "much oil is derived today from

organic-rich rocks that were deposited beneath upwelling systems, […] from which oil is obtained by drilling beneath the modern upwelling system […] Phosphate mineral deposits are abundant on the seabed in upwelling areas and fossil phosphorite deposits that formed in such environments provide most of the world's sources of phosphate fertilizer" [*Summerhayes et al.*, 1995].

1.3 Organization of this Manuscript

This manuscript is organized as follows:

Chapter 2 provides an overview of the Gulf of Mexico, the West Florida Continental Shelf (WFS), and the physical processes that occur on the WFS and have a direct impact on this study. The information provided in this chapter is intended to give the reader a thorough understanding of the current state of knowledge of the area of interest as well as the physical principles involved (i.e. Ekman layer transport, upwelling, tidal fluctuations, etc.).

Chapters 3 and 4 each start with an abstract, discuss the specific tools used in the study, describe the experiment design, the limitations and assumptions made, the data analysis methods used and concludes with a discussion of the results obtained. Chapter 3 specifically addresses Question #1 and associated sub-questions while Chapter 4 specifically addresses Question #2 as defined in section 1.1.

Chapter 5 provides a summary of the study and manuscript as a whole, followed by the reference list, and appendices.

CHAPTER 2

SETTING THE SCENE

2.1 The Gulf of Mexico

The Gulf of Mexico's (GOMEX) coastal ocean consists of three interconnected domains: a) the deep-ocean or the region seaward from the shelf break, b) the coastal ocean or the continental shelf region between the shelf break and the shoreline, and b) the estuaries, where the rivers transition to the sea [*Weisberg*, 2011].

As with any body of water, it is important to understand the deep circulation. *Sturges* [2005] used a three-layer analog to describe the deep GOMEX circulation. Below the upper layer of the water column being transported into the GOMEX (and eventually becoming the LC-Florida Current system), there are three deep layers. The uppermost deep layer is from approximately 800 m- 1100 m depth, and is driven primarily as an extension of the upper layer flow, also flowing into the GOMEX. The middle of the deep layers functions as a return mean flow into the Caribbean between approximately 1100 m and 1900 m. The bottom-most deep layer reaches from approximately 1900 m -2000 m (the average sill depth at the Yucatan Channel into the GOMEX). This deepest layer has sporadic flow into the GOMEX from the Caribbean. The majority of the flux both in and out of the GOMEX is accomplished in the upper layer. It has, however, been observed by *Oey* [1996] that during times of increased bottom inflow to the GOMEX, there is an inhibition of the eddy shedding process from the Loop Current (LC), lending further support to the importance of understanding the deep circulation.

The origination of the water masses is also described by *Sturges* [2005]. The net inflow into the Caribbean Passages and then into the GOMEX is approximately 40% of South Atlantic origin. This water of South Atlantic origin is in the Florida Current concentrated in two comparatively fresh water masses. High current regimes with temperatures greater than ~ 24ºC are found on the left hand and central segments of the Florida straits in the upper ~100 m. There is an additional significant contribution of deeper, mostly upper Antarctic Intermediate Water. The rest of the upper ocean water entering the Caribbean Sea and the LC and Florida Current is of North Atlantic origin.

2.2 The West Florida Continental Shelf

A comprehensive review of the physical oceanographic works that have been completed on the WFS is provided by *Weisberg et al.* [2009a] which builds upon previous similar compilations of *Weisberg et al.* [2005] and *Boicourt et al.* [1998]. Looking a little bit broader, *Oey et al.* [2005] summarizes previous works on the various continental shelves in the GOMEX and describes the differences and interconnectivities of the circulation questions that many of the research groups studying the area have been able to answer.

2.2.1 A Physical Description

The WFS for its majority is equal in breadth to the portion of the Florida peninsula which currently resides above water, approximately 200 km wide (Figure 2.1). It is one of the world's broadest continental shelves with a gentle slope, and a sharp gradient that drops to over 3000 m in the span of 50-100 km in the GOMEX [*Meyers et al.*, 2001]. Its isobaths generally parallel the coastline which at mid-shelf is oriented approximately 333ºT, and the 100 m isobath is located some 150-200 km offshore [*Weisberg et al.*, 1996]. It stretches south to north from the steep area

by the Dry Tortugas up to the Big Bend area of Florida, and then bends sharply 90º to the west, encompassing De Soto Canyon as it reaches towards the Mississippi River delta in Louisiana. The De Soto Canyon can be characterized as the almost perpendicular intersection of two different slopes: the rough Mississippi-Alabama slope and the broader WFS, which becomes very steep below 1000 m (this area is called the Florida Escarpment) [*Hamilton and Lee*, 2005].

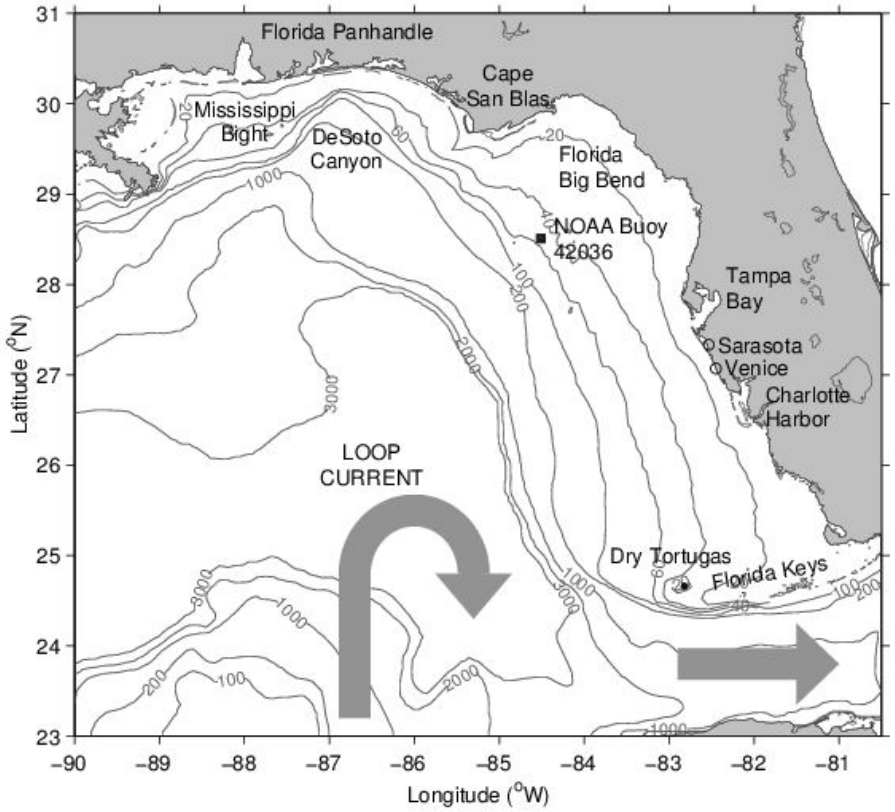

Figure 2.1: The WFS with annotated isobaths and points of interest [*Weisberg et al.*, 2005].

The Dry Tortugas and De Soto Canyon each have a significant relevance to the dynamics on the WFS. The Dry Tortugas are an area in which the shelf break is located at approximately the 25 m isobath. This bears considerable importance because if the LC or an eddy impinges upon the shelf slope in that particular region, the shallow water isobaths that extend into the inner shelf along the rest of the WFS are able to be impacted directly at the Dry Tortugas location because pressure gradient disturbances propagate along isobath with shallow water to

the right (in the northern hemisphere). This would permit isobaths encompassing all three regions of the shelf (inner, middle and outer) to be dynamically set into motion at once, potentially affecting the entirety of the shelf. Similarly, the De Soto Canyon is an area in which an eddy might get trapped in the Canyon and impact many of the isobaths at one time. The inner shelf in that region extends out past the shelf break due to its narrow width, allowing any dynamic impacts originating in the Canyon itself to affect the inner shelf and potentially propagate to along the shelf to the west. Moreover, while propagation of disturbances may be with shallow water to the right, once on the shelf water properties may be carried in any direction by either the local or the deep-ocean driven currents.

As a result of its broad nature and relatively small amount of river discharge directly to the shelf, the waters of the WFS are often characterized as oligotrophic [*Lenes et al.*, 2008]. Oligotrophic waters are generally described as having a low accumulation of dissolved nutrients, high oxygen content, and low growth of algae and other organisms [*Zhang*, 2000]. *Weisberg et al.* [2009a] noted that nutrients tend to concentrate near the bottom of the water column on the WFS, so the circulation on the shelf bottom (including bottom Ekman transport) is responsible for uniting nutrients with the euphotic zone. Contrary to this description of the shelf being oligotrophic, however, there is a large biomass present on the WFS, spanning from primary producers through sea turtles and large sport fish [*Arnold et al.*, 2002]. One of the ways the shelf may be able to support such biomass is by the replenishment of nutrients from the deeper, comparably nutrient rich waters via upwelling.

2.2.2 A Dynamic Description

The WFS circulation is driven by local wind, atmospheric heat fluxes and resulting buoyancy forcing at the surface, the offshore LC system in the GOMEX, the fresh water influx

from contributing rivers, and density-driven buoyancy forcings at depth [*He et al.*, 2003; *Liu et al.*, 2006; *Weisberg et al.*, 1996]. It is dynamically linked to varying water properties, particularly to temperature, which exerts a primary control on density [*He et al.*, 2003], driving the transport of nutrients relative to the euphotic zone, affecting both primary and secondary production, controlling the shelf ecology [*Weisberg et al.*, 2005].

The tidal influences on the WFS must be taken into consideration when discussing the flow on and off the shelf and surrounding areas. The determination of 8 tidal constituents: M2, S2, N2, K2, O1, K1, P1, and Q1, accounting for more than 95% of the WFS tidal variance when quantitatively gauged against available coastal sea level and offshore velocity profiler data [*He and Weisberg*, 2002; *Weisberg et al.*, 1996] is further supported by *Weisberg and Zheng* [2006a] and *Zheng and Weisberg* [2010].

Beyond the tidal flux, *He et al.* [2003] found that while deep-ocean forcing should be relatively ineffective at generating shelf currents extending onto the WFS by more than a Rossby radius of deformation, there are instances where deep-ocean effects are quite apparent due to the narrow shelf width within the area of the De Soto Canyon, and the region of shallow, convergent isobaths near the Dry Tortugas.

A definitive work on the local and deep-ocean forcing effects on the WFS was *Weisberg and He* [2003]. In this study the authors separate local forcing effects from deep-ocean forcing by running separate model simulations over the 1998-1999 timeframe with and without deep-ocean forcing. Quantitative comparisons between the model simulations and in situ observations enabled discussions on what aspects of the water column observations were attributable to local and deep-ocean forcings. It was found for 1998, when both the deep-ocean and local forcings were anomalously upwelling favorable, that "while deep-ocean processes set the depths of

material isopleths along the shelf slope, local forcing is generally necessary to upwell materials across the shelf break. Once on the shelf local forcing is also the motive agent for distribution from the shelf break and the inner shelf with the bottom Ekman layer playing a major role. Deep-ocean effects under special circumstances may augment the distribution by local forcing, as occurred during the spring-fall seasons of 1998 (and also inferred in 1997)." That year, there was strong upwelling onto the shelf. This strong ventilation of deep-water origin played a huge role in supporting the shelf ecology, and we need to further understand how, when, and why such occurrences happened as well as the advection of water properties across the shelf and the resulting connectivity.

Due to its broad width, the WFS is able to be dynamically separated into multiple regions where the influences and driving forces are different [*Lentz*, 1995; *Li and Weisberg*, 1999; *Mitchum and Clarke*, 1986; *Weisberg et al.*, 2005]. Various approaches to this idea have emerged over the last few decades. *Mitchum and Clarke* [1986] assumed a linear, rigid lid, barotropic, simple constant eddy viscosity model to try and find a solution valid over the entire shelf, including shallow water. They found that if a fictitious coastal wall is placed in water of depth about 3 times the Ekman scale thickness, neglecting the inner shelf does not degrade the solution in deeper water. While this is a great development for flow studies on the outer shelf area of the WFS, it left room for growth and further investigation specifically in the area of the inner shelf region since it was cut off from the rest of the shelf flow by virtue of the "wall" being inserted.

Lentz [1995] focused his study on whether the inner-shelf circulation was sensitive to the form of the turbulent mixing profile, specifically on the subinertial motions and the cross-shelf divergence in the Ekman transport over the inner shelf. His results suggest the inner shelf is

strictly defined by the area in which there is enough interior stress able to be transmitted from the surface directly to the bottom of the water column, promoting the cross-shelf divergence in the Ekman transport. Similarly to the definition used by *Mitchum and Clarke* [1986], this requires the direct overlap of the surface and bottom Ekman layers, and does not take into account the stratified case.

Later, *Li and Weisberg* [1999] approached the question from a different perspective. They isolated each of the individual dynamic influences on the shelf flow and showed how the dynamic balances at various locations across the shelf, once evolved to a quasi-steady state, varied between locations. This difference between the locations allowed for an inner, outer, and midshelf to be defined by the dynamic balances inherent to each. Expanding on the *Li and Weisberg* [1999] study, *Weisberg et al.* [2001] took the same model setup and general approach of isolating the dynamic influences on shelf flow on the WFS, and looked at the stratified and unstratified cases off the Sarasota, Florida coast in April 1998 to further define the dynamic and kinematic differences in the balances between inner and outer shelf regions during upwelling and downwelling events.

According to *Li and Weisberg* [1999] the inner shelf is defined as the transition region between the coastline and the point where offshore-directed surface Ekman transport balances the alongshore wind-stress. This divergence leads to the development of a coastal jet which induces the bottom Ekman layer as a response [*Li and Weisberg*, 1999], and a change in sea surface slope [*Weisberg et al.*, 2001]. While the approaches were different, there are similarities to the *Mitchum and Clarke* [1986] and *Lentz* [1995] definitions of the inner shelf. They define it as the area where the surface and bottom Ekman layers overlap. *Li and Weisberg* [1999] share the general description, but stress that it is the interaction between surface and bottom Ekman

layers via divergence, (without a requirement for any direct overlap between the surface and bottom Ekman layers) that distinguishes the inner shelf. A further and complemental definition of the inner shelf is given by *Weisberg et al.* [2001] where the inner shelf, defined with respect to vertically integrated vorticity, is the region where the primary vorticity balance is between the bottom stress and bottom pressure torques, regardless of stratification.

Li and Weisberg [1999] define the outer shelf as the area of the shelf break where the across-isobath flow is constrained by the stretching of planetary vorticity filaments and where density and pressure effects of the adjacent ocean are established. *Weisberg et al.* [2009a] further defines the outer shelf as the transition area where the deep-ocean processes are expected to penetrate onto the shelf over a distance equal to the Rossby radius of deformation consistent with previous studies by *Kelly and Chapman* [1988]. Also consistent with these arguments and the inner shelf definition *Weisberg et al.* [2001] further defined the outer shelf by the primary balance between the bottom pressure torque and the material rate of change of relative vorticity, which is indicated by eddy-like motions.

The midshelf region is the remaining area between the inner and outer shelf. For the WFS, the partial closure of the Florida Keys may result in a return flow and reversal in the across shelf pressure gradient across the mid-shelf [*Weisberg et al.*, 2005].

Based on the *Li and Weisberg* [1999] inner shelf definition, the De Soto Canyon is an interesting case as it is an area in which the inner shelf extends beyond the shelf break [*Weisberg et al.*, 2009a]. Another example of a location with a wide inner shelf is the relatively broad, shallow shelf off of northwest Africa, in which case *Barton et al.* [1977] found that the defining conditions for the inner shelf extend to the shelf edge and result in upwelling into the surface layer occurring close to the shelf edge.

Further support for the dynamic separation of the inner and outer shelves is seen in the variability of the current structure on the WFS. The along-shelf pressure gradient sets up in opposition to the along shelf wind stress (local forcing), and it serves to decelerate the along-shelf currents relative to those that would other-wise exist under the wind stress alone [*Weisberg et al.*, 2005]. The inner shelf current behavior has been shown to be visually coherent with the winds, suggesting that they are the main driving force for the currents over the inner shelf, a finding which is also consistent with the observed turning in the implied surface and bottom Ekman layers [*Liu and Weisberg*, 2005b, 2007]. However, neither the strong northward or southward currents at the shelf break coincide with the wind events seen locally (local forcing), but rather they appear to be driven by oceanic forcing (deep-ocean forcing): for instance see *Meyers et al.* [2001]. This is in contrast to the inner-shelf region where the currents are wind driven. The partitioning of the WFS dynamic regimes from the outer shelf to the nearshore region is also summarized in *Liu and Weisberg* [2012].

2.3 Fresh Water Influx to the WFS

For the WFS, the largest riverine fresh water inflows are in the spring season and over the northern portions of the WFS [*Weisberg et al.*, 2005]. Direct discharge of fresh water onto the WFS is accomplished by the multiple rivers in Florida (Figure 2.2). These rivers include but are not limited to the Escambia River, Chipola River, Apalachicola River, Suwannee River, Withlacoochee River, Peace River, and Caloosahatchee River, along with others that flow into bays and estuaries prior to making their way to the actual WFS. The northern rivers provide a drainage mechanism for the southeastern United States, peaking in the spring. The southern Florida rivers get their waters from local fresh water inputs, which peak in the summer. The

Mississippi River, while not directly discharging onto the WFS, still impacts the water properties of the WFS and GOMEX. *Hu et al.* [2005] was able to confirm the Mississippi River plume had the ability to remain a coherent feature over large distances (1000-2000 km) when entrained in the LC-Florida Current-Gulf Stream system as far a distance as off the coast of Georgia in the

Figure 2.2: Map of the major rivers in Florida [*Mapsofworld.com*, 2013]

Atlantic via in situ observations and satellite imagery. Draining 41% of the continental United States, the Mississippi River is the largest river in North America and ranks as the 8th largest worldwide in terms of discharge mean $1.35 \pm 0.2 \times 10^4$ m^3s^{-1} based on 64 years of USGS data [*Hu et al.*, 2005]. *Weisberg et al.* [2005] discussed three mechanisms by which the Mississippi River water can be advected south in the GOMEX. It can take the WFS route via wind and buoyancy driven spring transition currents, use the direct LC entrainment option when the LC is positioned far to the north, or indirectly use LC entrainment beginning with a circulation either along the shelf or around eddies shed by the LC. By using the first option, the Mississippi River

waters can make it onto the WFS and at times can be advected (while remaining on the shelf) as far south as the Dry Tortugas [*Oey et al.*, 2005; *Weisberg et al.*, 2003].

2.4 Physical Processes on the WFS

2.4.1 Eddy Shedding and Impact on the WFS

In addition to the LC's direct impact on the WFS affecting upwelling and water dynamics, eddies are a mechanism which can help drive water exchange between the shelf and the deep-ocean waters, both as single eddies or as eddy pairs. Eddies are shed from the LC, and at times are trapped by the topography along the shelf. This has been observed to happen at times for relatively prolonged periods of more than a month [*Hamilton and Lee*, 2005]. The eddies can be trapped near the De Soto Canyon or near the Dry Tortugas, making contact with the shelf slope. When near the De Soto Canyon, the eastward surface jet that is found in the area can take discharge from the Mississippi River and bring it to the outer WFS. The predominance of the eastward jet and anticyclonic currents promotes upwelling at the head of the canyon and along the shelf break of the WFS, where water is approximately 2ºC colder on average than further west [*Hamilton and Lee*, 2005].

The vorticity flux over the shelf slope and rise is typically greater than the contribution from wind stress curl [*Schmitz et al.*, 2005]. When eddies are impinged near the Dry Tortugas for a prolonged period of time, the resulting flows are significant. As the dynamic height of the LC and associated eddy are relatively high, a pressure perturbation on the ambient fluid is exerted and propagated along the isobaths due to continental shelf wave dynamics in the form of continental shelf waves. With the WFS located in the northern hemisphere, the waves travel north, propagating with the shallower water to the right. The resulting relatively high pressure on the shelf slope in turn imposes a pressure gradient force stretching across the shelf slope to the

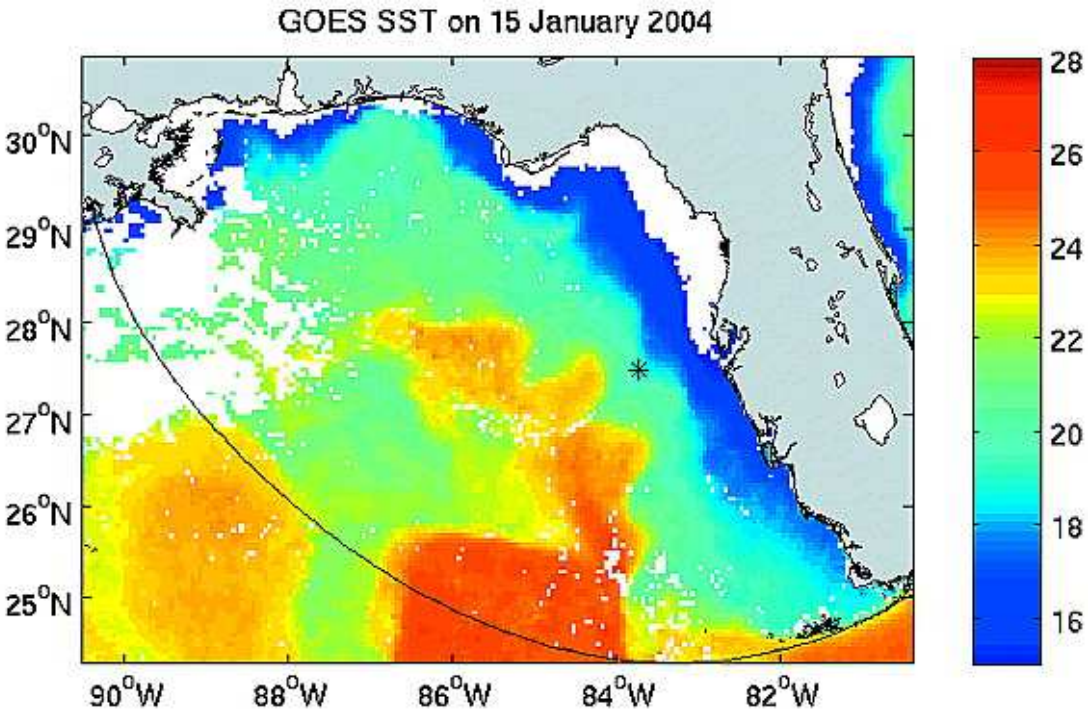

Figure 2.3: Filament visible in the GOES SST on 15January 2004, denoted by the tongue of warmer SST temperatures on the shelf [*Barth et al.*, 2008].

shelf, supporting a geostrophic current flowing toward the south [*Weisberg et al.*, 2014a]. It has been found that the propagation of eddies in the GOMEX from the LC is caused mainly by the vorticity component due to the gradient of ambient potential vorticity rather than advection [*Barth et al.*, 2008]. When considering the impact eddies from the LC play upon the WFS flow and upwelling, it is important to note that they are less frequent than filaments (Figure 2.3) reaching the shelf from the LC, but manage to play an equally important role in transporting LC water onto the shelf due to their ability to transport more LC water than the filaments do, as found via observations and model studies [*Barth et al.*, 2008].

2.4.2 Loop Current and Impact on the WFS

Many studies of the LC have been conducted, to include *Hurlburt and Thompson* [1980] who used a 1.5 and 2-layer barotropic model with bottom topography in the GOMEX to

investigate the LC and its eddies. This particular model is what all the models since have been compared to. *Hetland et al.* [1999] used satellite-tracked surface drifters to find the LC has "mature" and "young" phases throughout its cycle, and the shelf-edge jet along the WFS was able to be observed and verified to be pressure-induced, directly relative to the LC's position. *Weisberg et al.* [2005] studied the multiple time scales applicable to the various circulation patterns on the WFS. It was found that on an inter-annual timescale (by using the results of *Hetland et al.* [1999] as a prompt to control part of the open boundary in their model with a sea level perturbation consistent with the edge of the LC making contact with the WFS slope), the LC's proximity to the WFS and its level of penetration into the GOMEX as a deep-ocean forcing event was helpful in supporting the upwelling process over the shelf break. However, in addition to the LC the local forcing effects and bottom Ekman layer transport were necessary to get the cooler, inorganic nutrient rich waters to the shore and into the areas important to for fisheries recruitment. By impinging on the WFS slope, the LC is able to increase the slopes of the isotherms at the shelf break, and make it possible for the deeper waters to breach the shelf break and make it up onto the shelf with the help of local forcing [*Weisberg and He*, 2003]. *Meyers et al.* [2001] reported on a year-long study during which the LC impacted the central WFS three times, amounting to a total of about 13% of the year, showing current reversals (up to 100 cm s^{-1}) occurring within a window of a few days. Similar LC intrusion cases were observed in 2000 and 2010 respectively [*He and Weisberg*, 2003; *Liu et al.*, 2011a] A LC vortex was observed in altimetry and reproduced in a model and subsequently studied in addition to using a tracer experiment [*Barth et al.*, 2008], looking at the movement of the LC eddy and the LC's impingement upon the WFS shelf slope and the resulting pressure changes.

2.4.3 Near-Shore Upwelling

Sverdrup [1938] described an experiment off the coast of Port San Luis, California in which a case of locally forced near-shore upwelling is identified, explored, and analyzed. The work showed the development of a cellular region unlike any that had previously been described as a product of the upwelling process. Building on this initial model of the cellular system for a coastal upwelling system, *Johnson and Killworth* [1975] and later *Werner* [1987] used a model to study shelf-break upwelling, and found that it is a consequence of the interaction between the onshore Ekman transport in an upwelling system and the topographic change at the shelf break.

There are many types of upwelling, and they can be caused by a variety of triggers in multiple environments. Generally, upwelling is wind-driven and as such, wherever winds act on the surface of the ocean to make surface waters diverge horizontally this horizontal divergence is compensated for by the upwelling of relatively colder water from depth [*Summerhayes et al.*, 1995]. The definition of coastal upwelling provided in *Smith* [1995] agrees with Summerhayes' previous description, as he says it is the response of the coastal ocean to wind-induced divergence in the surface boundary layer. The magnitude of wind-stress curl driven upwelling is proportional to the wind-stress curl and inversely proportional to the Coriolis parameter at the location.

Upwelling provides not only a new mass of water into an area, but in most instances it also provides a temperature change (normally a decrease) and makes available inorganic nutrients that had previously been sequestered at depth. As the original water mass vacates the area of interest through divergence, a new (potentially inorganic nutrient-rich) water mass is brought up on the principle of continuity of mass, helping to support the local ecosystem and in the case of the WFS, allowing for specific regions of the shelf to not be oligotrophic for a time.

Specifically for the WFS, the upwelling is primarily and most often coastal and wind driven (e.g. [*Liu and Weisberg*, 2005a; 2007]. Due to the width of the WFS and the distance the deep-ocean water needs to be transported to be impactful to the coastal areas, such upwelling tends to raise only relatively shallow, inner shelf water [*Weisberg et al.*, 2014a], which is often depleted of nutrients compared to the more seaward, outer shelf waters which would have the stronger possibility of having a beneficial impact to the shelf ecology.

The Taylor-Proudman theorem, through a combination of vorticity and mass conservation, constrains water to flow along isobaths. The movement of water across (rather than along) isobaths requires that the Taylor-Proudman constraint be broken either by frictional boundary layers, time dependence, or a large Rossby number [*Weisberg et al.*, 2005]. In areas where the shelf is narrow (like the De Soto Canyon), eddies may result in flows across the isobaths, elsewhere it is primarily the bottom Ekman layer in which across isobaths flow may be observed.

The deep-ocean origin upwelling onto the outer shelf of the WFS can reach all the way up to the inner shelf at times, as documented by *Weisberg and He* [2003] and *Weisberg et al.* [2005] when cold water originating from the shelf break some 300-400 km away was observed upwelling between Tampa Bay and Charlotte Harbor. An unexpected finding was that a strong asymmetry exists in the responses to upwelling and downwelling favorable winds on the WFS. The upwelling responses to favorable winds are larger and extend farther offshore than downwelling. This is due in part to the along shelf component of vorticity and thermal wind effects in relation to the bottom Ekman layer, which tends to be more developed under upwelling conditions [*Weisberg et al.*, 2005].

2.4.4 Seasonal Variability

On the WFS, there is a strong seasonal circulation variability overlaid on long-term mean upwelling currents, especially on the inner shelf region [*Liu and Weisberg*, 2012; *Weisberg et al.*, 2009b]. Generally, the winter tends towards an upwelling circulation and summer sees a downwelling circulation as described in [*Weisberg et al.*, 2005]. The largest monthly mean velocities are found in the spring and late-summer to early-fall, which were accompanied by large vertical sheer. In an experiment that attempted to bring clarity to the spring transition on WFS, the strong currents seen at midshelf were explained based on the interactions between the barotropic and baroclinic responses to wind and surface heat-fluxing forcing. The evolution of the currents shows that an initially strong near-shore wind-driven current in March progressively moves further offshore, becoming a shelf break current in May that is continuous from the Mississippi River to the Dry Tortugas. This shelf break jet is maintained due to the baroclinic current tendency, which is cyclonic around the spring cold tongue. This cold tongue allows for the advection of Mississippi River water onto the WFS.

The fall sees a different circulation. The local forcing on the WFS is found to largely control the inner shelf circulation, while the deep-ocean forcing of the LC provides reinforcement for the midshelf currents, allowing the across shelf transports of the bottom Ekman layer to increase. This increase helps to move the colder, inorganic nutrient-rich waters of deep-ocean origin shoreward. By November, the shoreward-directed density gradient is positioned farther offshore so the near-shore currents are primarily wind-driven, while the shelf break currents are largely buoyancy-driven.

The seasonality of the WFS is supported by long term measurements of the currents showing the varying background circulation and velocity fluctuations [*Liu and Weisberg*, 2012;

Weisberg et al., 1996; 2009b], as well as the use of Self Organizing Maps (SOM) to pick up some fluctuations that were unable to be noted using the traditional linear empirical orthogonal function method, specifically that the spatial patterns extracted are asymmetric [*Liu and Weisberg*, 2005b; 2007]. SOM allowed for the fall-winter circulation to be noted as southeastward in the along-shelf direction with a coastal jet located around the 30 m isobath, and near bottom currents have an obvious onshore component in the nearshore region. The summer circulation shows weaker currents, in the northwestward direction on the inner shelf with a weak current core around the 20-25 m isobaths. SOM was also able to detect inter-annual variations in the dominant flow patterns [*Liu and Weisberg*, 2005b].

There is a robust seasonal cycle in velocity found in long-term moored observations on the inner WFS. Seaward from about the 50 m isobath, the seasonal variations are less pronounced. Over the outer shelf and near the southwestern end of the WFS, the seasonal variations are obscured by the deep ocean influences [*Liu and Weisberg*, 2012]. The seasonal variations in sea level are also robust, but unlike the velocity, these extend across the entire WFS and into the deep GOMEX [*Liu and Weisberg*, 2012].

Additional seasonal changes that occur on the WFS are those of SST [*He and Weisberg*, 2003; *Liu et al.*, 2006] and iron concentrations. The SST adjusts seasonally in part due to hurricane/tropical storm activity. The latent heat released from the passage of a tropical system (hurricane season in the Atlantic is 01JUN-30NOV) out of the surface waters of the Atlantic, Caribbean and GOMEX is transported into the atmosphere and advected into the upper levels, condensing into rain and then falling again on the waters, helping to decrease the SSTs again in the cycle [*Virmani and Weisberg*, 2006]. The iron concentrations in the summer months on the WFS are controlled primarily by the riverine inputs and the Saharan dust traveling from Africa in

the trade winds [*Lenes et al.*, 2008]. Observations taken in Miami, Florida have shown that the maximum concentrations of Saharan dust in the air occur between June and August. The large increase in atmospheric iron (many times between 3 and 30 times the normal background levels), help to support an increase in *Trichodesmium erythraeum* (*T.E*) on the WFS up to 100-fold as it is deposited into the water column from the atmosphere. *T.E* has been shown to support the growth and blooms of the toxic red-tide dinoflagellate (*K.brevis*) by assisting with the elevated nitrogen levels and nitrogen fixing that *K. brevis* needs to have a sustainable, substantial bloom on the WFS. The *T.E.* is iron and phosphorous limited, so the substantial increase in iron concentrations led to a substantial increase in the amount of *T.E.* in the area [*Lenes et al.*, 2008].

2.4.5 Inter-Annual Variability

The WFS sees a strong inter-annual variation as well as the seasonal shifts previously discussed. Each year is not the same dynamically or otherwise. Occasionally, there are vast anomalies, such as in 1998. *Weisberg et al.* [2005] and *Walsh et al.* [2003] showed that in 1998, the entire WFS was involved in the upwelling of the deep-ocean water onto the shelf break. Normally, this upwelling occurs due to the impetus of the LC on the shelf break at one location or another on the WFS. In 1998, the entire WFS was able to be involved in the deep water upwelling across the shelf break due to anomalies in the local forcing (wind) combined with the anomalies in the deep-ocean forcing (LC and coastal jets). The anomalies with the deep-ocean forcing occurred due to the LC impinging on the WFS in the vicinity of the Dry Tortugas, and this not only set the WFS currents into motion throughout the shelf, but also helped to precondition the isotherms along the shelf slope so that the local forcing (wind) was capable of driving these past the shelf break. The impact of the LC at the Dry Tortugas was verified with altimetry SSH analysis, and it was determined the impact occurred from spring into fall of 1998.

Looking back through the altimetry record (to 1993), there are very few such impacts of the LC at the Dry Tortugas. When such an impact occurs, the WFS as a whole responds due to the pressure perturbation that is able to propagate along the isobaths up the shelf as a continental shelf wave [*Barth et al.*, 2008; *Hetland et al.*, 1999; *Weisberg and He*, 2003].

CHAPTER 3

QUESTION #1

3.1 Abstract

Deep-ocean and local forcing effects and the resulting connectivities between regions of the WFS are investigated using five case studies in 2007 and 2012. A case of primarily deep-ocean forcing is considered via a 45-day timeframe of upwelling, while a comparative 45-day local forcing study is conducted during a downwelling event. The primarily local forcing investigation is supported with three additional case studies, specifically two cold front passages (2007, 2012) and Tropical Storm Debby (AL042012). Particle trajectory calculations are completed for all case studies both at the surface and at the bottom of the water column along seven transects spanning the breadth of the WFS. Basic statistics that include mean particle displacement, mean transport direction, and standard deviation of particles that originated outside of the Florida Panhandle (specifically east of 86° W) are calculated. The largest connectivity extent between various WFS regions (specifically those that are close to the coast and estuaries) is provided by the deep-ocean forcing scenario, rather than the primarily local forcing scenario, although a combination of the two is most effective. While the overall displacement of particles is larger at the surface during the local forcing driven scenarios, these particles tend to be transported either to the outer shelf or downwelled rather than being useful for advecting inorganic nutrients to the near shore.

3.2 Tools

3.2.1 Model

Model simulation/hindcast information from the West Florida Coastal Ocean Model (WFCOM) consisting of the Finite Volume Coastal Ocean Model (FVCOM) nested in the Gulf of Mexico Hybrid Coastal Ocean Model (GOM HYCOM) were used in this study for the purpose of comparing particle trajectory calculations in multiple locations during unique events. FVCOM was originally developed at the University of Georgia in 1999 by Chen, Liu and

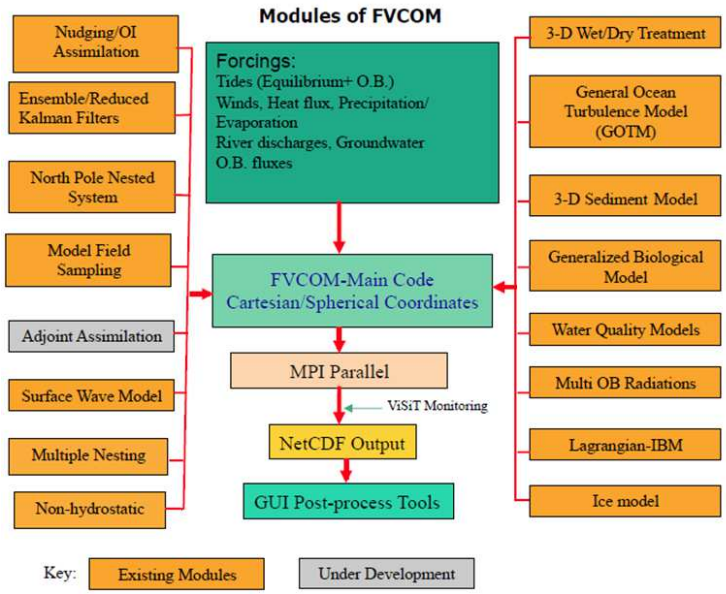

Figure 3.1: Modules of FVCOM and their plug-in features. [*Chen*, 2013]

Beardsley. The original version was able to simulate the 3-D currents and transport within an estuary/tidal creek/inter-tidal salt marsh complex [*Boucher et al.*, 2013]. The model was officially submitted to the Journal of Atmospheric and Ocean Technology and published in 2003. Through various updates, FVCOM now has a variety of functions to include (but not limited to) forecast modeling, research modeling, 2D and 3D, ecology modeling, and works through a plug-in module system (Figure 3.1).

What makes FVCOM different from other models available? The most difficult problems with modeling coastal areas are resolving irregular coastal geometry and conserving heat, momentum and mass. FVCOM combines the benefits of two popular previously developed model types, the finite difference (FD) and finite element (FE) styles [*Chen et al.*, 2013a]. It is computationally efficient in the FD style, while having good geographical flexibility via the use of an unstructured mesh as the FE style of models do (Figure 3.2). FVCOM is a globally used model, with more than 1000 users/institutions in 38 countries applying the model to their research questions [*Chen*, 2013].

FVCOM is widely applicable both in specific fields of research as well as geographic regions. It has been used to investigate the circulation of the Tampa Bay estuary system [*Weisberg and Zheng*, 2006a], hurricane storm surge in two and three-dimensions [*Chen et al.*, 2014b; *Weisberg et al.*, 2009a; *Weisberg and Zheng*, 2006b, c], inundation calculations

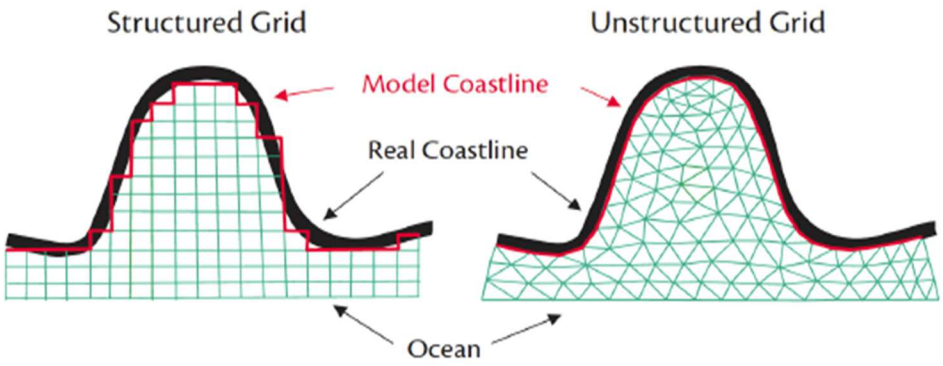

Figure 3.2: Graphic comparing the basic difference between structured (left) and unstructured (right) grid approaches. [*Chen*, 2013]

[*Chen et al.*, 2014a], an estuary system with complicated coastline and geometry requiring resolution to include creeks and multiple narrow channels [*Zheng and Weisberg*, 2010], the effects of deepening and widening a shipping channel [*Zhu et al.*, 2015], larvae tracking due to dynamics in environment for recruitment information [*Boucher et al.*, 2013; *Huret et al.*, 2007; *Weisberg et al.*, 2014b], investigating plankton blooms [*Ji et al.*, 2006; *Ji et al.*, 2007], and

copepod transport and retention [*Johnson et al.*, 2006] to name a few. FVCOM can be coupled with other models as demonstrated in the example of *Johnson et al.* [2006] to a NPZD (nitrogen, phytoplankton, microzooplankton, detritus) model. Other applications include nutrient flux via tidal pumping [*Hu et al.*, 2008] and nitrogen cycles examination [*Ji et al.*, 2007]. Estuarine and shelf hydrodynamics [*Chen et al.*, 2013b; *Chen et al.*, 2003], cross-frontal transport [*Isobe and Beardsley*, 2006] and the modeling of eddy formation [*Chen et al.*, 2014b] have also all found significant applicability of the FVCOM. Sediment transport [*Lee et al.*, 2007] is an additional application that has accomplished by incorporating the USGS sediment concentration field measurements and scales.

An additional benefit of FVCOM is its ability to have its boundary conditions driven by a larger scale model. HYCOM has been used as a boundary model [*Zheng and Weisberg*, 2012] for not only FVCOM, but also for ROMS (Regional Ocean Modeling System) on the WFS [*Barth et al.*, 2008]. HYCOM is a well-tested and validated model for the basin scale. By using the HYCOM output for the large-scale to drive a regional model on the WFS (such as the FVCOM or ROMS), it allows for the strengths of each model to be taken advantage of. HYCOM is a model run by the US Navy. It is a data-assimilative hybrid isopycnal-sigma-pressure coordinate ocean model, meaning that it uses the vertical coordinate system it deems best for each individual location or depth which allows it the flexibility of choosing either an isopycnal, z or σ coordinate system. Driving the boundary conditions of FVCOM with HYCOM takes advantage of these benefits.

Zheng and Weisberg [2012] describe FVCOM with boundary conditions driven by specific parameters of the Global HYCOM (referred to as the West Florida Coastal Ocean model or WFCOM) and its features, configuration, grid, tidal constituents (8 used) and other details

while testing the model against in situ data for the year 2007. The goal of the particular study was to use the model setup to effectively downscale for physical processes from the open water of the GOMEX across the WFS and into the estuaries. The variables used for forcing the open boundary of WFCOM were sea level, water velocity, and temperature. WFCOM is atmospherically forced by NOAA's North American Mesoscale Forecast System (NAM) for the entirety of the data sets used in this study.

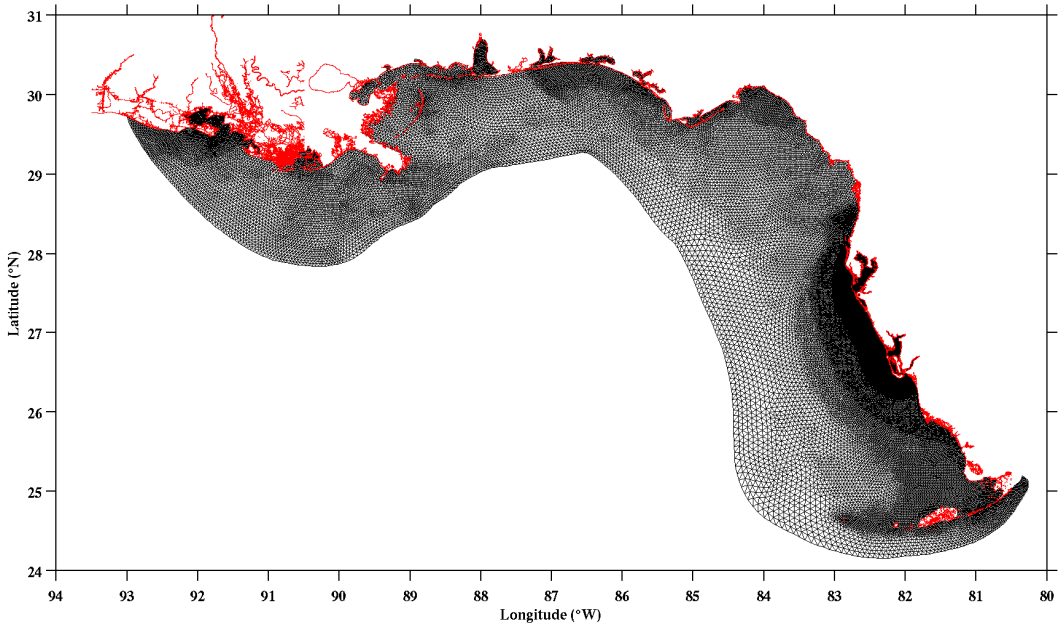

Figure 3.3: WFCOM domain and unstructured grid used for this study. The resolution is approximately 12 km at the model boundary, and increases to 150 m in the estuaries with the majority of the grid having a resolution of 250 m - 500 m.

The setup proved appropriate with a couple of noted issues. The issues identified were 1- neither the Global HYCOM nor FVCOM handled the seasonal sea level fluctuations for the area, and 2- errors in HYCOM may be propagated via the one-way nesting scheme through the FVCOM domain. The second error was able to be identified by comparing the influenced modeled velocity field with velocity observed from moored buoys. Improvements were subsequently made to the nested FVCOM setup of *Zheng and Weisberg* [2012], and these are discussed in *Weisberg et al.* [2014b]. The version of WFCOM used here has an increased

domain (Figure 3.3), stretching past the De Soto Canyon around the northern edge of the GOMEX to include the Mississippi River Delta, and is nested in the GOM HYCOM (resolution 1/25°) rather than the Global HYCOM (1/12°) providing an improved resolution in the outer domain of the nested setup. This version of FVCOM also has an increased number of sigma levels from 21 to 31 to provide increased vertical resolution.

3.2.2 Data Sets

Stored WFCOM information: WFCOM model simulations (from year 2004 through 2014) were run prior to the onset of this project. The resulting data fields were put into NetCDF files upon completion and were used for the specific data calls and trajectory calculations as detailed in section 3.3. The calculations for particle trajectories were calculated using the hourly mean data in the NetCDF files. Quasi-isopycnal particle trajectories are the preferred method for use in this study because a Lagrangian fluid parcel without changing its density cannot cross an isopycnal surface. Mixing as occurs within an Eulerian simulation allows the fluid parcel to change its density so the combination of the Eulerian simulation and the quasi-isopycnal, Lagrangian particle trajectory calculation provides a reasonable approach to determining fluid pathways for this study.

Buoy 42039 Meteorological Data: Historical meteorological data is used from NOAA's National Data Buoy Center's website for Buoy 42039 which is located approximately 115 nm ESE of Panama City, Florida. The data encompasses the timeframes for Front 1 (18-28APR2012) and Front 2 (13-18APR2007). The raw data is analyzed for narrowing down the timing of the cold fronts at the buoy's location for each front, helping to further classify the fronts as well as calculating a horizontal speed of passage for the fronts over the WFS.

Satellite Altimetry Data: As a supportive tool used for indicating the proximity of the LC and

potential impingements upon the WFS, satellite altimetry data is used (Figure 3.4). The Mean Dynamic Topography (MDT) auxiliary data from AVISO [*Rio et al.*, 2011] is added to the Ssalto/Duacs gridded Sea Level Anomaly (MSLA) data to get absolute sea surface height. Surface geostrophic velocities are then derived. The details of this procedure are described in *Liu et al.* [2011a] and *Liu et al.* [2014]. Of note, it is clear by looking at the series of graphics that the 45-day case study starting in January 2007 was at a time free of LC impingement (deep-ocean forcing), while the case starting in late March 2007 was an instance with considerably more LC impingement on the WFS.

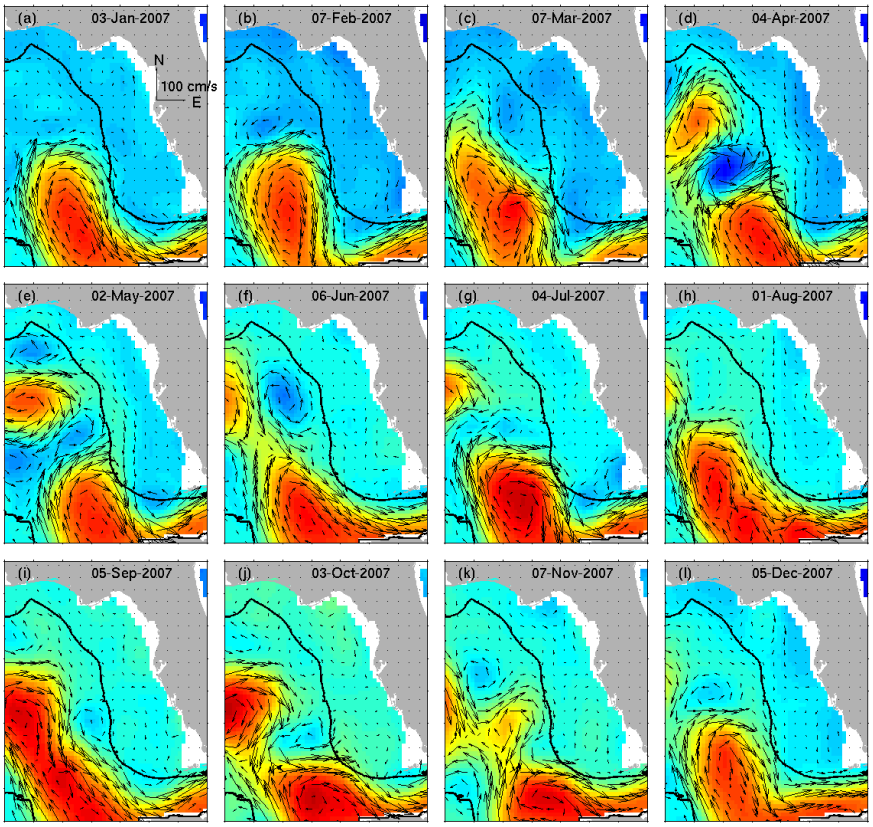

Figure 3.4: AVISO Monthly snapshot of altimetry data showing the Loop Current in 2007. Sea surface heights are shown in color contours (with higher values in red) and geostrophic velocity vectors are indicated in arrows. The 200 m isobath is also shown as a thick black line.

KSRQ Meteorological Observational Data: Historical observation data is used from The Weather Company owned website www.weatherunderground.com for the meteorological observations at KSRQ (Sarasota-Bradenton International Airport) for the timeframes encompassing the case

studies Front 1 (18-28APR2012) and Front 2 (13-18APR2007). The observations are used for narrowing down the passage of the cold front in Sarasota to find the horizontal speed of the front as it traversed the breadth of the WFS.

Salinity and Near-Surface Current Simulations: These graphics are an automatically generated product that is published each day by Dr. Zheng of the University of South Florida's Ocean Circulation Group on his research-publishing website http://ocgweb.marine.usf.edu/~zheng/ . The product (Figure 3.5) is an overlay of the WFCOM near surface current (displayed as vectors) and the salinity (displayed as a color scale).

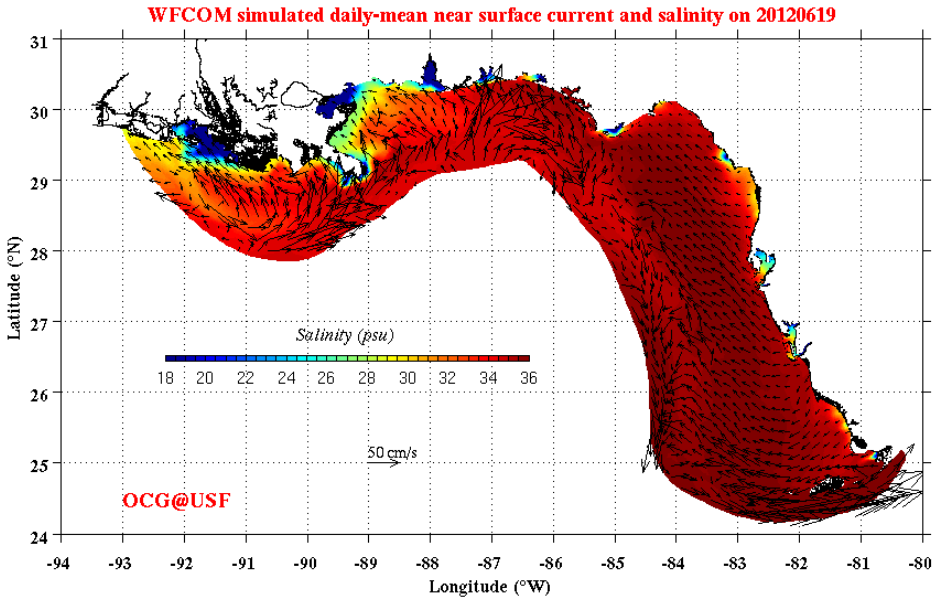

Figure 3.5: Example of WFCOM simulated daily-mean near surface current and salinity product from Dr. Zheng's research website (link detailed above). This particular image is simulated for 19JUN2012.

FVCOM 3.5-day Forecasted Trajectories: These graphics are another automatically generated product that is published each day by the University of South Florida's Ocean Circulation Group on their website http://ocgweb.marine.usf.edu/. The product is a 3.5-day trajectory calculation based on the previous FVCOM domain (not that of WFCOM). The product plots the trajectories both with starting points at the surface and at the bottom along 4 transects running east to west across the broadest part of the WFS (Figure 3.6).

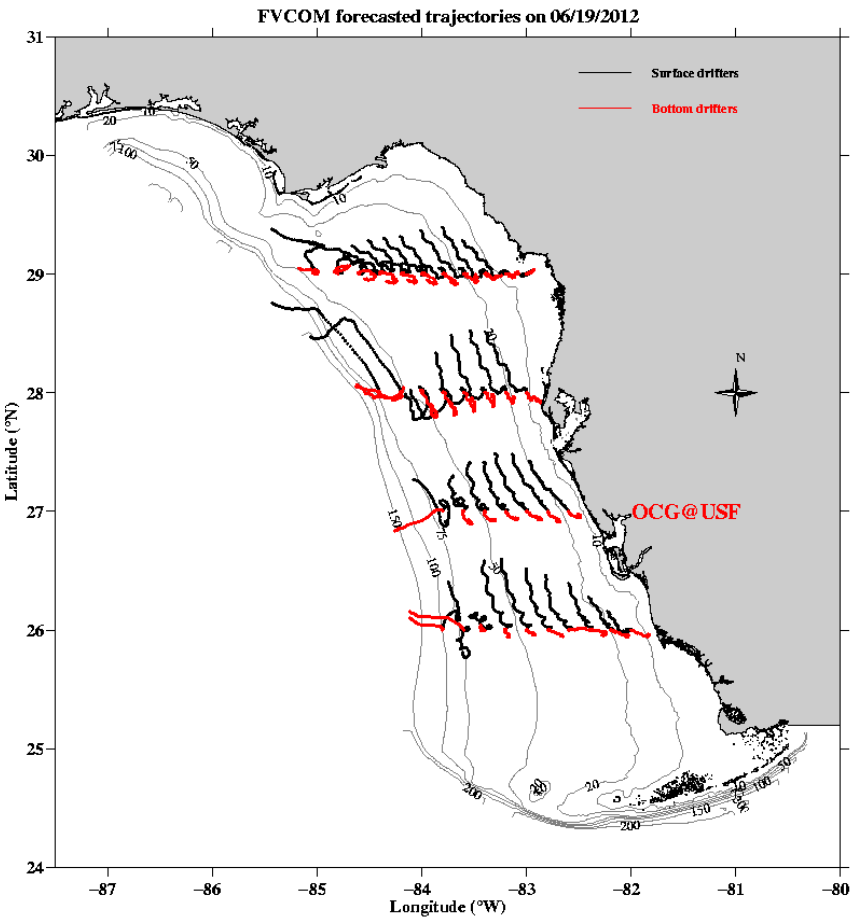

Figure 3.6: Example of FVCOM daily forecasted trajectories starting at the surface (black) and bottom (red) for a 3.5-day period. The product is from the USFCMS Ocean Circulation Group website (http://ocgweb.marine.usf.edu/Models/FVCOM/fvcom_index.html). This particular image is forecast for 19JUN2012.

3.3 Experiment Design

Question: Under primarily deep-ocean or local forcing influences, what are the ranges of upwelling and advection of water parcels both vertically and horizontally across the various regions of the WFS?

i. Given a period of time when we know the deep-ocean influence was strong on the WFS, what were the pathways of water parcel delivery from the region of the shelf slope to the near shore?

ii. Given a period of time when we know the local forcing influence was strong on the WFS, what were the pathways of water parcel advection across the WFS?

By answering the two sub-questions, a more holistic approach to the primary question is possible.

The first sub-question (steps 1 and 2 below) is specifically geared towards a period of time when the deep-ocean influence on the WFS was considerable. The case study that was used to investigate this question is the 45-day period of 29 March -13 May 2007, which was chosen for this study due to a) its prevalent upwelling across the shelf break, b) the impact of the Loop Current on the overall WFS circulation (Figure 3.4), c) the prior work done investigating the red tide event of that summer in *Walsh et al.* [2009] and d) the research regarding the movement of gag grouper larvae that spring in *Weisberg et al.* [2014b].

1- Trajectory calculations were initiated forward in time at the shelf break (75 m) along the entirety of the WFS, spanning the 45 days defined previously. The output provided details a new location (horizontal, vertical, and grid cell) as well as density, and temperature (°C) data every hour as the particles are advected. See sections 3.2.1 and 3.2.2 for specifics regarding the particle trajectories and the model data used.

2- Trajectory calculations were also initiated along 7 transects along the bottom of the water column simultaneously during the 45-day period spanning the WFS from south of Marcos Island to Pensacola (Figure 3.7 and Table 1). These locations were chosen based on their marking the extent of the WFS, locations of interesting changes bathymetrically, and for their fisheries, recruitment, and nutrient transport importance.

Table 1: Transect end points.

Pensacola	Panama City	Big Bend	Cedar Key	Tampa Bay	Sanibel Island	South of Marcos Island		
30.3	30.1	29.76	29.3	27.69	26.69	25.5	Latitude (degrees N)	Shoreward
87.3	85.75	84.5	83.25	82.8	82.3	81.26	Longitude (degrees W)	
29.15	29.15	28.39	27.92	27.23	26.15	25.5	Latitude (degrees N)	Shelfward
87.3	86.36	85.54	85.18	84.8	84.45	84.45	Longitude (degrees W)	

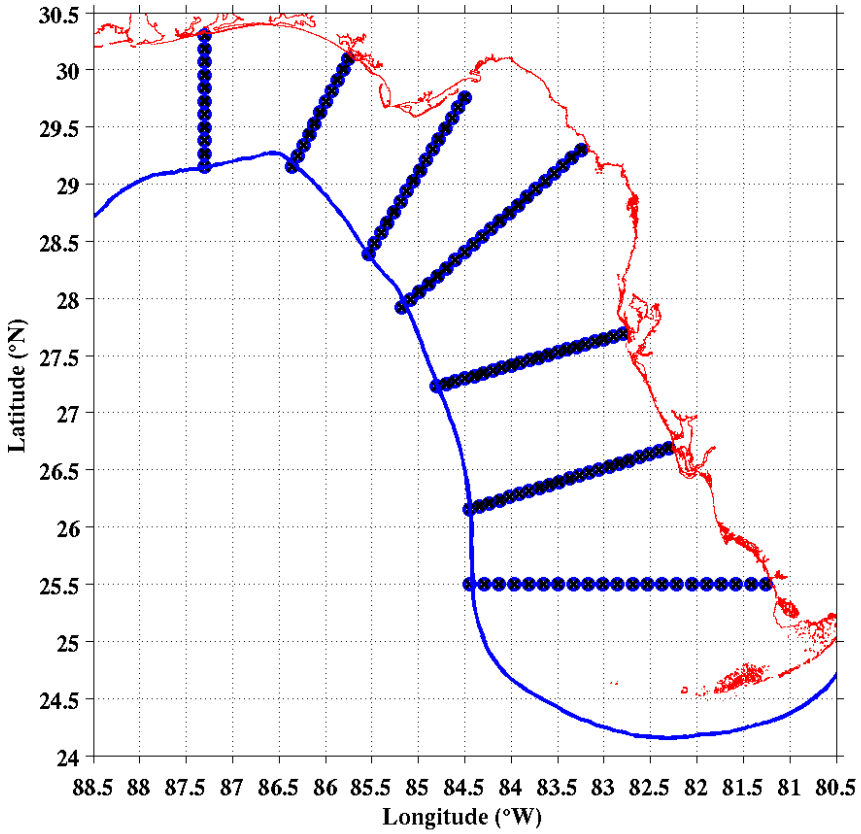

Figure 3.7: Transects and particle trajectory starting points in relation to the coastline of Florida (red) and the open boundary of the model domain (blue solid line).

The second sub-question (steps 3-4 below) is specifically regarding a time of weak deep-ocean forcing influence. Multiple time frames were considered appropriate for this particular question. For comparison purposes to sub-question 1, the 45 days spanning 01JAN-15FEB2007 are considered.

3- Step 1 was repeated for the new timeframe.

4- Step 2 was repeated for the new timeframe.

To facilitate finding the range of vertical and horizontal advection due to local forcing (continuing to address sub-question 2), two synoptic scale meteorological frontal passages are investigated across the WFS using the same transects specified previously, then compared to the extreme example of a tropical storm going through the area and making landfall in Florida from the GOMEX. The two fronts considered are in April 2007 and April 2012 and the tropical storm to be considered is Debby (AL042012). These case studies provide a thorough approach to the local forcing effects and particle advection maximum and minimums at depth and at the surface, allowing for a more complete comparison to be made against the deep-ocean forcing studied in March through May 2007 in sub-question 1.

The two cold fronts mentioned previously in April 2012 (Figure 3.8) and April 2007 (Figure 3.9) are displayed in Figure 3.10, and analyzed for speed and classification by comparing the meteorological data from the NDBC buoy 42039 (bottom panel), and the KSRQ (top panel) observations. Figure 3.10 is a dual panel of the surface analysis product made my NOAA's Hydrometeorological Prediction Center for Front 1 and 2, with both images being in local time. When comparing the data in all three figures, it is imperative to note the buoy data is in GMT, and the KSRQ and surface analysis graphic data are in EST time. For Figures 3.8-3.10, EST is four hours behind GMT. So 6 am in the buoy data (GMT) is 2 am in the KSRQ and surface analysis graphic (EST) time. Figure 3.8 and 3.10 (left panel) support a cold front passage at buoy 42039 for Front 1 at 2 am EST (6 am GMT), and passing KSRQ at 7 am EST (11 am GMT) the same day, indicating the front traveled 336 km horizontally in 5 hours (67.2 kph or 36.4 kts) making it a fast moving front. Figure 3.9 and 3.10 (right panel) support a cold front passage at

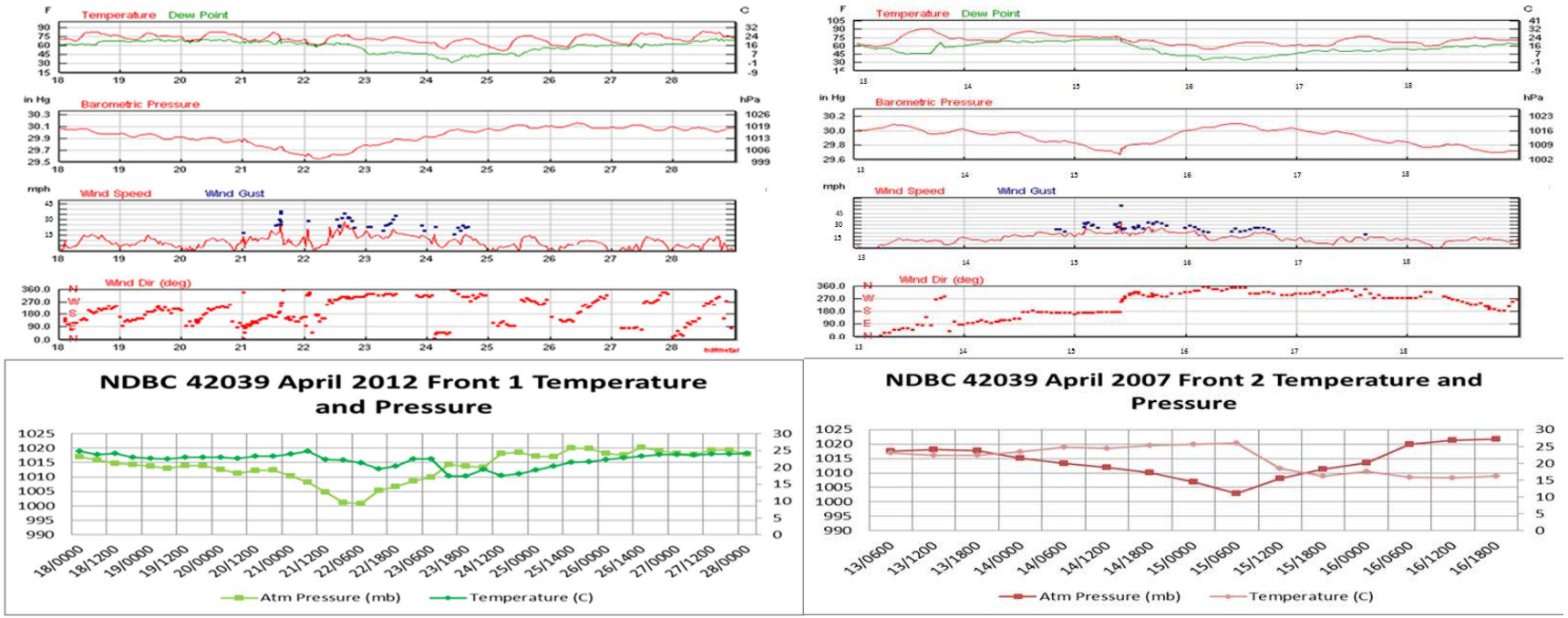

Figure 3.8: Top panel is KSRQ meteorological observations (Front 1) 18-28APR2012 [*Weatherunderground*, 2015]. Bottom panel is temperature and air pressure records at Buoy 42039 [*Center*, 2015].

Figure 3.9: Top panel is KSRQ meteorological observations (Front 2) 13-18APR2007 [*Weatherunderground*, 2015]. Bottom panel is temperature and air pressure records at Buoy 42039 [*Center*, 2015].

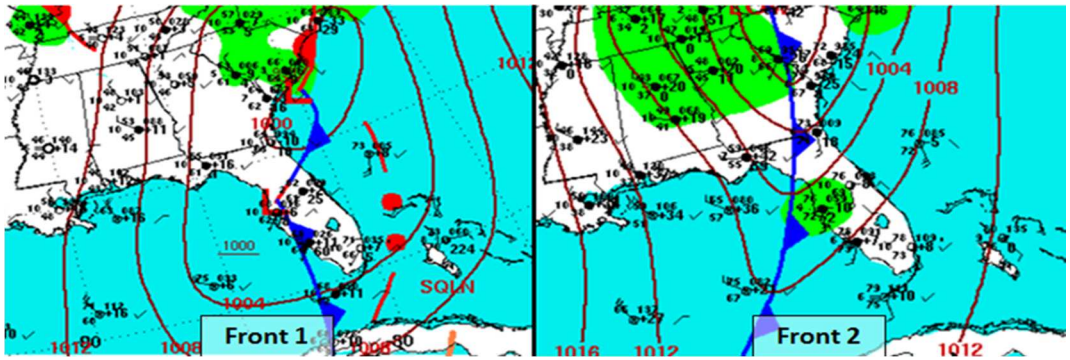

Figure 3.10: Surface analysis products from NOAA's Hydrometeorological Prediction Center for Front 1 (22APR2012, 0700 EST) in the left panel [*Otto*, 2007], and Front 2 (15APR2007, 0700 EST) in the right panel [*Monarski*, 2012].

buoy 42039 for Front 2 at 5 am EST (9 am GMT), and passing KSRQ at 11 am EST (3 pm GMT) the same day, indicating the front traveled the 336 km horizontally in 6 hours (56 kph or 30.3 kts). Based on their characteristics and speeds, these two fronts are comparable.

The main difference between the two fronts is that Front 1 provides a strictly local forcing effect on the waters of the WFS, while Front 2 occurred with a moderate amount of deep-ocean forcing at the same time on the WFS. This means the resulting effects of the water flow and trajectories may be different due to a difference in forcing. Specifically for Front 1 and 2, the seven transects were used again for starting points of the particle trajectory calculations both along the bottom and at the surface of the water column, allowing the results to be comparable to those from TS Debby and each other.

Tropical Storm Debby (23-27JUN2012) had a central pressure of 990mb, and maximum sustained winds of 55kts. She made landfall in the Big Bend region of Florida (Figure 3.11) near Steinhatchee, FL. The impact of Debby's passage across the WFS is investigated by comparing particle trajectory calculations both at the surface and at depth along the seven transects defined previously across the WFS for the timeframe of 19JUN-01JUL2012. The time period investigated allows for the consideration of the approach, passage, landfall, and subsequent weakening of the storm.

In addition to looking at the multi-day particle trajectory calculations at the surface and at depth using WFCOM along the seven transects across the WFS, a series of daily FVCOM forecasted trajectories (each displaying a 3.5-day forecast) for the surface and bottom of the water column encompassing the WFS area from Naples to the Big Bend region are also considered.

By comparing the two fronts as well as the information from TS Debby which had little to no deep-ocean forcing at the time, an initial estimation about the importance of local and

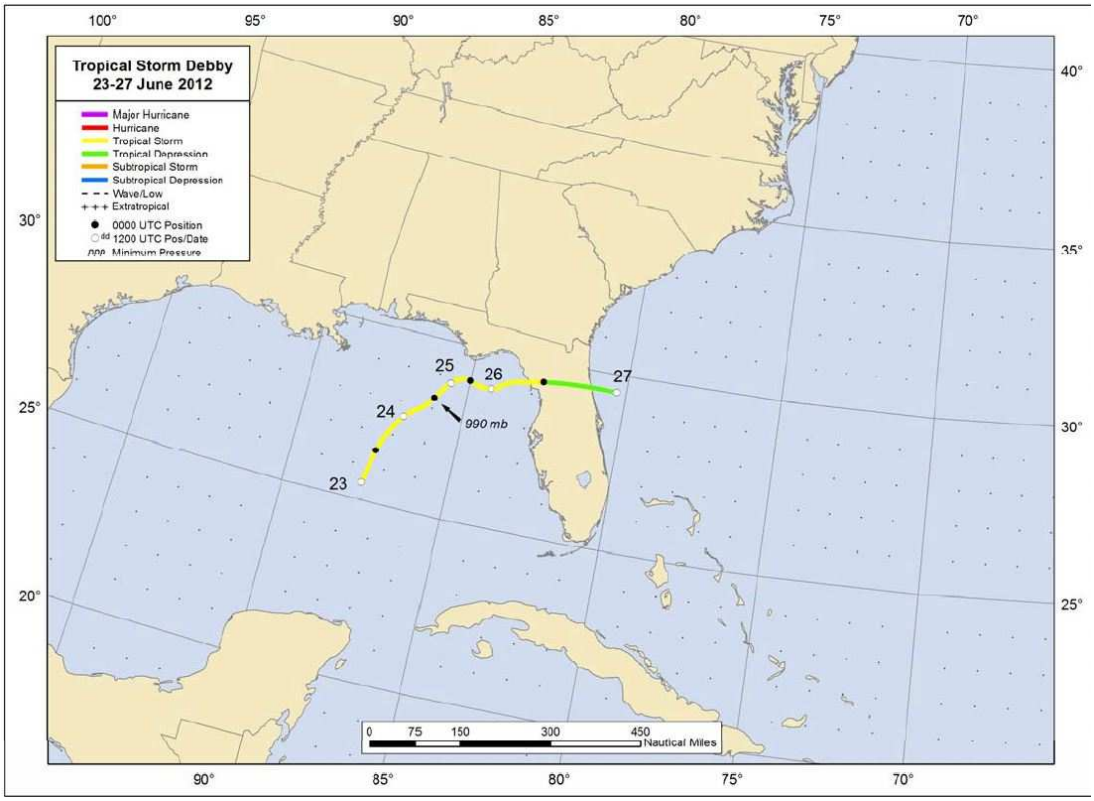

Figure 3.11: Tropical Storm Debby's track. [*Kimberlain*, 2013]

deep-ocean forcing in how they affect overall particle trajectories on the WFS will be able to be compared to the two 45-day particle trajectory calculations that were also run during the times of primarily local forcing and primarily deep-ocean forcing.

3.4 Design Limitations and Assumptions

The study is limited by the tools used and by the specific case studies investigated. The WFCOM domain in itself is also a limitation. While significantly improved from the FVCOM domain previously used to study the area of interest on the WFS, it is still limited in its scope as it does not include the entirety of the GOMEX, and instead must be nested into a larger regional scale model. The WFCOM data used are simulated data, and although these have been

quantitatively assessed relative to in situ observations in previous studies, they remain model-simulated data subject to errors in offshore boundary values, local forcing and model parameterizations and resolution.

The timeframes chosen for the case studies limit the investigation in that the upwelling in the March-May 2007 timeframe is not the peak of the upwelling event locally, but rather is the beginning of the event. This 45-day period as well as that of the January-February period in 2007, while good examples of local forcing and deep-ocean forcing, they deliberately do not overlap timeframes previously studied and published by others so the works can be looked at from a more holistic view of the WFS for the entirety of the 2007 year, rather than as overlapping piecemeal works.

3.5 Data Analysis Methods

For all the five case studies investigated for both sub-questions in this portion of the exploratory study conducted, trajectory calculations were done starting with particles released at the surface and at depth. Each of these resulting data sets was then analyzed for general statistics. The initial release location was compared to the final location for each particle trajectory calculation. The difference in position (displacement) was computed irrespective of the path the particle took to get there, so the resulting distance was viewed as a straight-line distance traveled horizontally across the WFS in meters. Each transect for each timeframe was then considered individually for the average distance travelled in the east-west and north-south directions in addition to considering all particles in total between all the transects. This average distance traveled by all the particles from all transects for each timeframe was used as the mean for each data set. The scatter plots specifically do not include particles originating west of 86°W, or the

Pensacola or Panama City transects as they are all in the Florida Panhandle. Due to the almost 90° turn from the overall direction of the majority of the rest of the WFS and the significant narrowing of the shelf itself due to the presence of the De Soto Canyon, the data is not

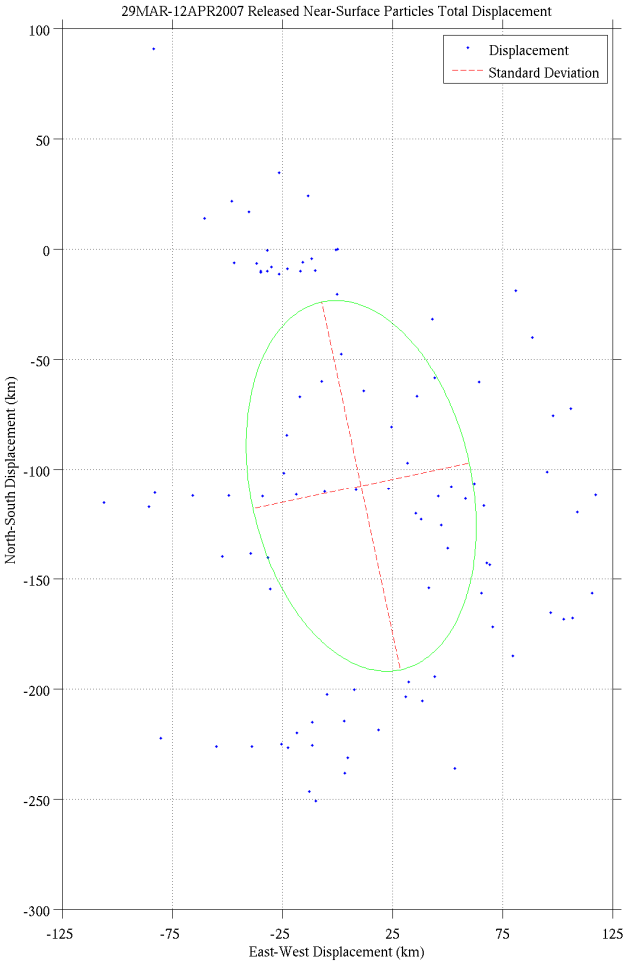

Figure 3.12: Example of particle trajectory displacement plot used for displaying the mean, standard deviation from the mean of the data set, and overall movement for a set timeframe and location. This particular example is a 15 day window from 29MAR-12APR 2007, encompassing the five transects on the WFS proper, not including those originating in the Florida Panhandle. This example specifically displays particles released at the surface at the beginning of the timeframe. The standard deviation plot is centered on the mean displacement, and the angle of offset from True North is indicated by the tilt in the major axis in the clockwise direction.

considered in the graphics or the numerical results displayed in Table 2. Though they are not considered in the statistics, they are still displayed in the particle trajectory calculation graphics. Figure 3.12 serves as an example of the statistics display used for each trajectory calculation time

frame. For reference when considering the amount of displacement shown in the graphics, each degree of latitude is ~111km, and each degree of longitude is ~97km.

3.6 Results

3.6.1 Sub-question 1: Deep-ocean forcing; Material advection from the shelf break

This sub-question focuses on the 45-day period of 29MAR-13MAY2007 using both the shelf break as the starting point for particle trajectory calculations as well as the seven transects across the WFS.

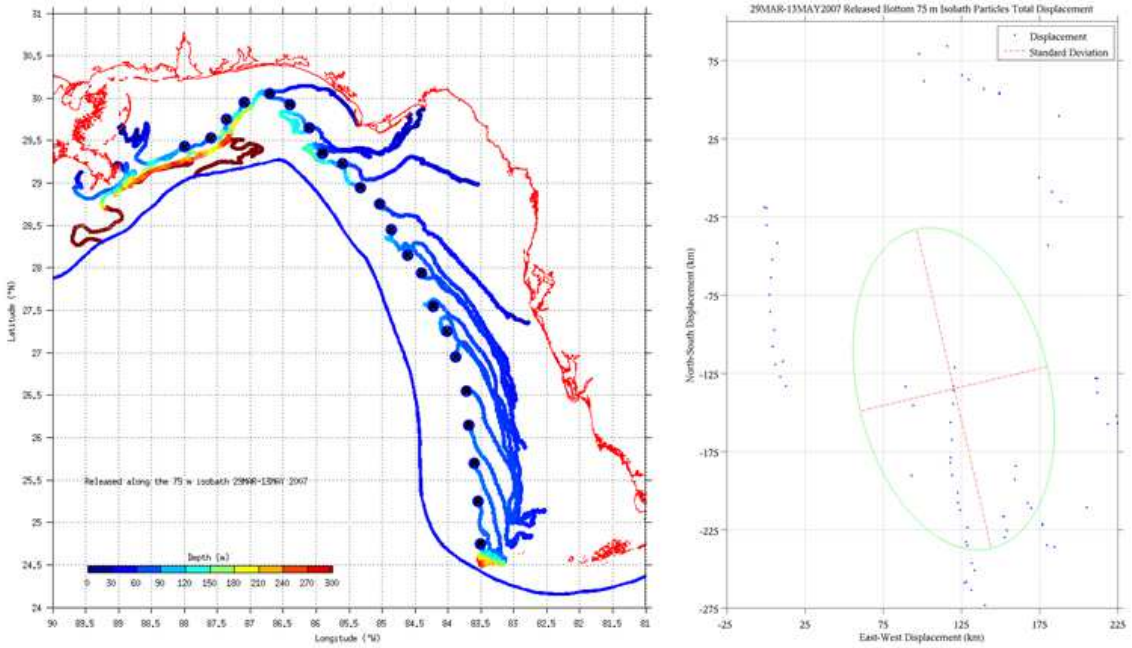

Figure 3.13: Near-bottom release of particles along the 75 m isobath (shelf-break) along the WFS, 29MAR-13MAY2007. The left panel color is saturated as the particles near the De Soto Canyon and the mouth of the Mississippi River are at a depth greater than the 300 m the colorbar extends to. This was done intentionally so there would be a measure of detail available in the color differences for the rest of the particles in the figure. The right panel statistical graphic shows the standard deviation along the major and minor axis for the data set, as well as the mean displacement of the set (shown by the center of the ellipse). The x-axis represents the displacement in kilometers in the east-west direction, with negative values corresponding to westward. The y-axis is north-south displacement, with negative values corresponding to southward displacement.

This particular timeframe was chosen as a comparison to the JAN 2007 timeframe used in sub-question 2. It is a period of anomalous upwelling, and shows the responses of the surface and bottom water particles to a primarily deep-ocean driven upwelling event on the shelf. This

specific case study is highly influenced by the LC as it impinged upon the shelf slope early in the timeframe. As the period progressed, the impingement and strength of the LC and subsequent deep-ocean forcing effects increased as the upwelling scenario developed, with the peak upwelling across the shelf occurring after the conclusion of the 45-day timeframe. The 45-day trajectory calculations of particles released along the 75 m isobath near the bottom of the water column are shown in Figure 3.13 (left panel). With few exceptions the particles clearly demonstrate the upwelling occurring across the shelf, driven by the bottom boundary layer dynamics and deep-ocean forcing.

Table 2: Statistic results for particle trajectory calculations.

(all units in km)*	**Mean East-West (+) (-)**	**Mean North-South (+) (-)**	**Standard Deviation (major axis)**	**Standard Deviation (minor axis)**	**Degrees of offset from True North (clockwise (+), counterclockwise (-))**
Study 1-Shelf-Break	120.2	-135.0	104.8	61.4	-13.2°
Study 1- Surface	-5.8	-219.7	171.1	54.8	-14.3°
Study 1- Surface 1st 15 days	10.8	-107.6	85.5	50.2	-12.0°
Study 1- Surface 2nd 15 days	-8.1	-83.6	114.4	23.8	-0.2°
Study 1- Surface 3rd 15 days	-8.8	-27.9	66.3	15.8	8.1°
Study 1- Bottom	67.4	-71.8	101.5	51.3	-38.9°
Study 2- Shelf-Break	-104.3	48.6	143.8	59.4	-65.9°
Study 2- Surface	-186.3	90.3	151.4	87.4	-30.8°
Study 2- Bottom	-0.7	-4.3	98.7	34.0	-58.3°
Study 3- Front 1 Surface	19.7	-13.2	30.7	23.0	-22.5°
Study 3- Front 1 Bottom	16.3	-11.9	27.0	13.4	-22.5°
Study 4- Front 2 Surface	20.7	-63.5	57.4	25.5	-8.1°
Study4- Front 2 Bottom	16.3	-23.4	35.7	17.6	-18.9°
Study 5- TS Debby Surface	-35.0	50.4	89.7	73.4	-41.9°
Study 5- TS Debby Bottom	8.2	-6.1	29.7	17.7	-27.6°

* Values calculated including any data points that exited the model domain in the timeframe. All data points outside of the Florida Panhandle were used.

Figure 3.13 (right panel) shows the statistics for the entirety of the data set that was calculated. The trajectories displayed in the left panel are limited to a sample of 22 of the 73 calculated for the sake of not having an overly cluttered graphic. The details of the statistics are provided in Table 2 for all five case studies examined in this chapter. The majority of the particles in the data set displaced primarily to the southeast, which is to be expected for the location and timeframe of these particles. If they had been released later in the upwelling scenario when it was fully developed (after the 45-day period, which is outside of the scope of this project), they would have had a larger eastward trajectory.

When looking at the right panel of Figure 3.13 there are two lines that run almost vertical which require further explanation. These odd arrangements are due to the particles leaving the model domain and similar groupings can be found in a few of the graphics that will be discussed in this chapter. These particular groupings demonstrate that two groups of the particles moved in

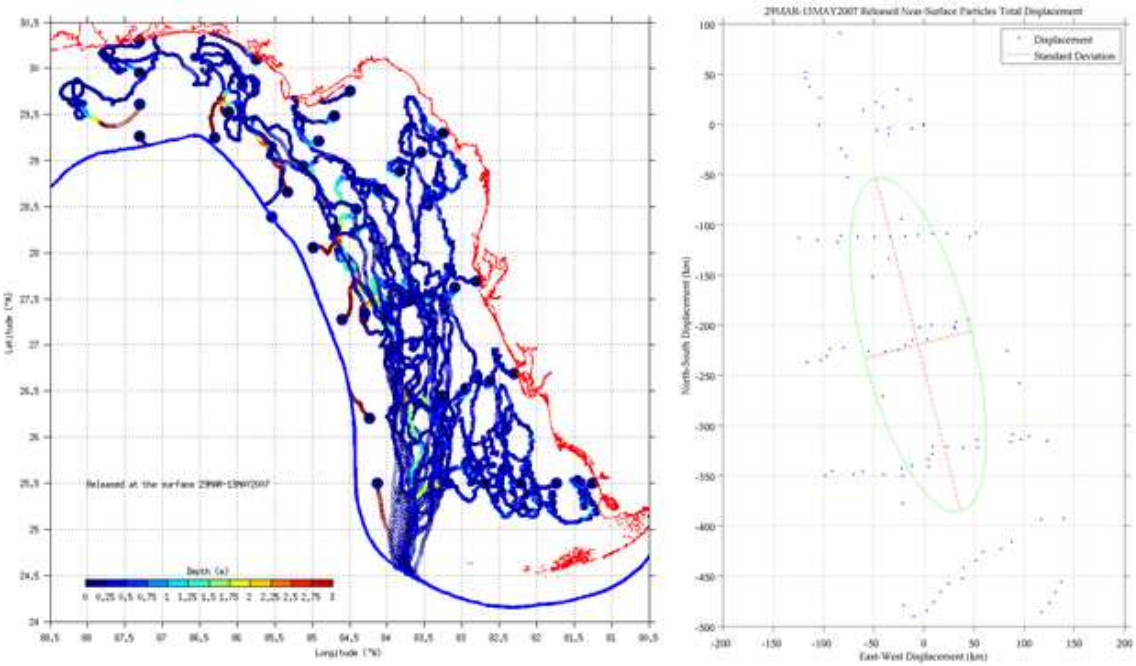

Figure 3.14: Near-surface release of particles along seven transects, 29MAR-13MAY2007.

the same general pattern, towards the same exit point of the model domain. In this specifice instance, the particles leaving the model domain are those along the southern portion of the WFS

(particles to the south of approximately 27°N), while the rest of the particles that are more random in appearance are from the northern portion of the shelf.

Considering now the surface released particles (Figure 3.14) along the seven transects rather than along the shelf break, there is some movement towards shore particularly in the northern parts of the shelf, though the majority of the particles are displaced away from the shore. There is quite a bit of advection along the ~100 m isobath area as a large amount of the particles converge and flow southward, many leaving the model domain. Again, the semi-straight lines (this time horizontally oriented) in the right panel of Figure 3.14 are due to particles leaving the model domain as in Figure 3.13. Many of the particles made it out of the model domain due to the long timeframe and the speeds at which they were being advected. In order to address the actual particle movements with as little domain boundary interference as possible, the dataset was split into three smaller pieces, each 15 days long (Figure 3.15).

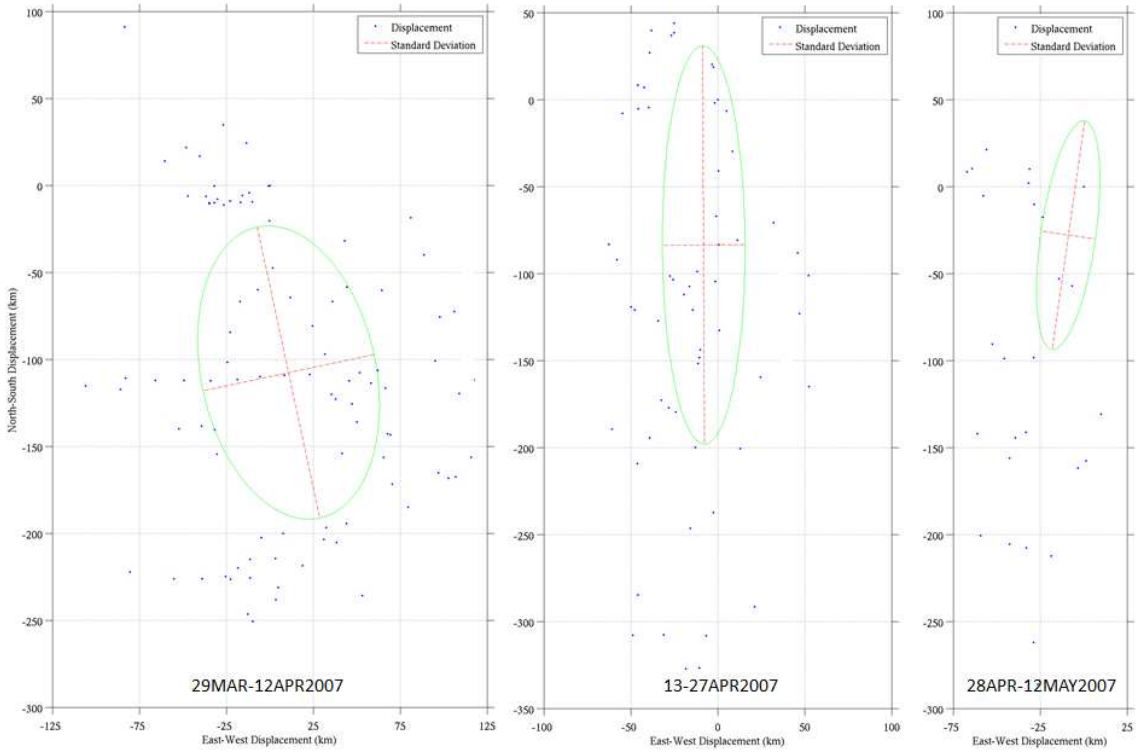

Figure 3.15: The surface particle trajectories from the 45-day period starting 29MAR2007 split into three 15-day periods (left to right).

When comparing the data displayed in the right panel of Figure 3.14 to those of Figure 3.15, the decision to split the timeframe into more manageable pieces for the purpose of mitigating the model domain boundary is supported as the right choice. By looking at Table 2 the smaller timeframes provide a clearer picture of the movement of the particles over time. In the first timeframe (Figure 3.15 left panel), the data has a mean displacement to the southeast. Compared to that of the next 15-day period (middle panel), the overall flow was almost entirely in the southward direction, albeit with less total displacement than the first 15-day period. The mean of the particle displacements were to the west, with a very small standard deviation in the east west direction, suggesting little across shelf transport, and primarily down-shelf transport instead.

The final 15 days of the 45-day period (Figure 3.15 right panel) showed a small standard deviation in the minor axis direction as well, but the overall advection speed was less. This is also the first time a positive angle of inclination is seen in the transport over the course of the 45-day period. The average advection of the data in the east-west direction was comparable to that of the previous 15-day period, but again the total displacement was considerably less (~83.6km/15day vs. ~27.9 km/15day) in the southward direction.

A point of caution for these three breakdowns is that the information is skewed. Of the 100 particles tracked during the 45-day period, only 26 of them were still in the model domain during the last 15-day period, compared to the previous 15 days which was able to track 62 particles in the domain, and the first 15-day period which saw all 100 particles initially in the domain. This oddity means the overall statistics are more strongly skewed to the origin in the later portions of the 45-day run as a larger percentage of the particles had exited the domain as time progressed.

To this point, the only bottom released particles that have been discussed are those released along the 75 m isobath. When considering the particles released at the bottom of the water column along the seven transects (Figure 3.16), the flow is a little more coherent and slower. These particles were released in the bottom boundary layer across the breadth of the WFS and a good portion of the shelf slope in many cases. The comparatively smooth trajectories calculated are due to the dynamic restrictions the particles must adhere to in the bottom boundary layer, and the relatively consistent forcing mechanisms the particles experience over the timeframe. The particles that made the largest advection were those from the midshelf area and

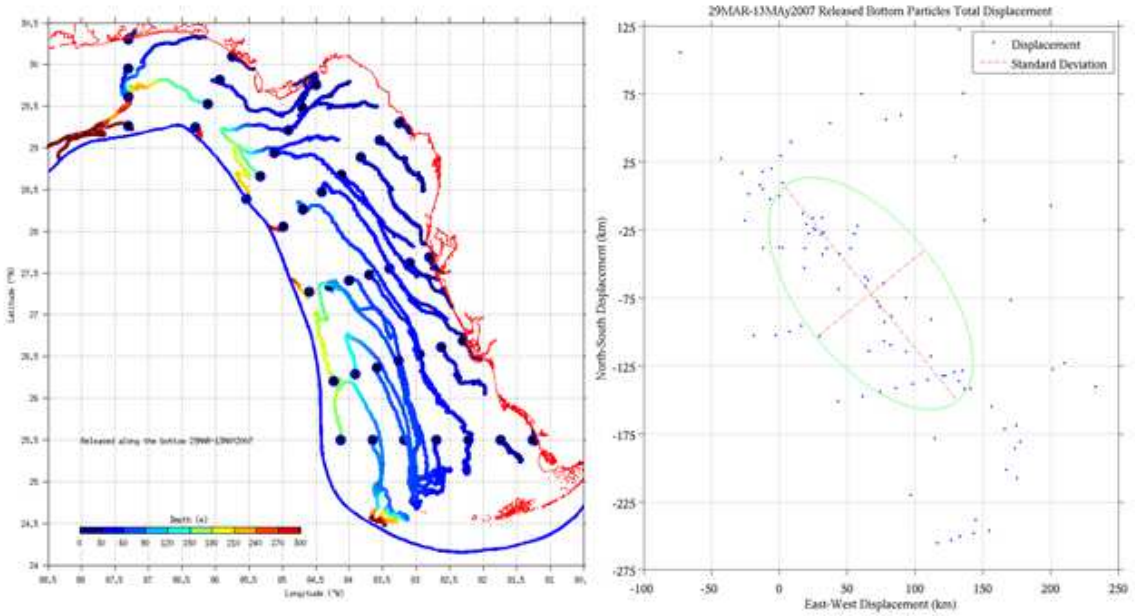

Figure 3.16: Near-bottom release of particles along seven transects, 29MAR-13MAY2007. Once again, the color in the left panel is saturated as the particles near the De Soto Canyon are at a depth greater than the 300 m the colorbar extends to. This was done intentionally so there would be a measure of detail available in the color differences for the rest of the particles in the image.

the outer shelf. They had comparatively longer trajectories than those in the inner shelf. Many of the particles that were released on the shelf slope and rise originally advected northward, then reversed direction part way through the period and advected southward with the rest of the particles. From the Tampa transect north, the outermost particles tended to downwell and leave the model domain rather quickly, compared to the particles on the shelf, which tended to upwell

slightly, and flow generally along-isobath with time. Many of the very near shore particles upwelled and were transported into local estuaries or other bodies of water, remaining trapped close to the coast. The right panel of Figure 3.16 shows the significant mean transport was to the southeast, with a larger standard deviation along the major axis direction by almost twice as much as that of the minor axis direction. The plot itself is organized primarily with the northernmost transect considered (Big Bend) plotting to the farthest left of the ellipse. Progressively working southward through the transects on the WFS, the displacements plot to the southeast roughly along the major axis, with the exception being the clear horizontal line of particles from approximately (50,-150) to (130,-130) which is from the Sanibel Island transect.

Largely, the deep-ocean forcing that played a primary role in the 45-day period of 29MAR-13MAY2007 on the WFS supported upwelling, across shelf transport, and significant advection speeds at various areas of the shelf. Most notable of these were the areas on the shelf slope and rise, as they were impacted the most directly by the LC and associated deep-ocean forcing mechanisms. The mid and outer shelf, however, also saw some large amounts of transport throughout the period, both at surface and at depth. While the surface particle trajectories were more irregular and variable in their actual paths due to the additional forcing of local winds, overall the entirety of the WFS was impacted in some way by the upwelling scenario, even though this time period wasn't at the height of the event.

Considering the connectivity of various parts of the WFS, the surface (Figure 3.14 left panel) does not provide a significant amount of connectivity between the estuaries and other near-shore areas. The locations of connectivity are more in the Panhandle as the particles that make it around the De Soto Canyon work their way shoreward and towards the waterways along the coast. The rest of the particles were primarily advected out towards midshelf rather than up

along the coastline. The strongest horizontal advection at the bottom of the water column (Figure 3.16 left panel) appears to be in the midshelf region where the velocities are the largest. The connectivity enabled by the bottom transport between locations is much more prevalent than that provided at the surface. There are a number of particles that end up in the Tampa Bay area from midshelf off the Cedar Key transect and the Big Bend transect. The same can be said of the Sanibel Island area.

3.6.2 Sub-question 2: Local forcing; Extreme and Moderate case studies

This sub-question starts by addressing the 45-day period of 01JAN-15FEB2007, then proceeds to investigate the two frontal passage case studies, and concludes with the case study of the extreme local forcing event of TS Debby (AL042012).

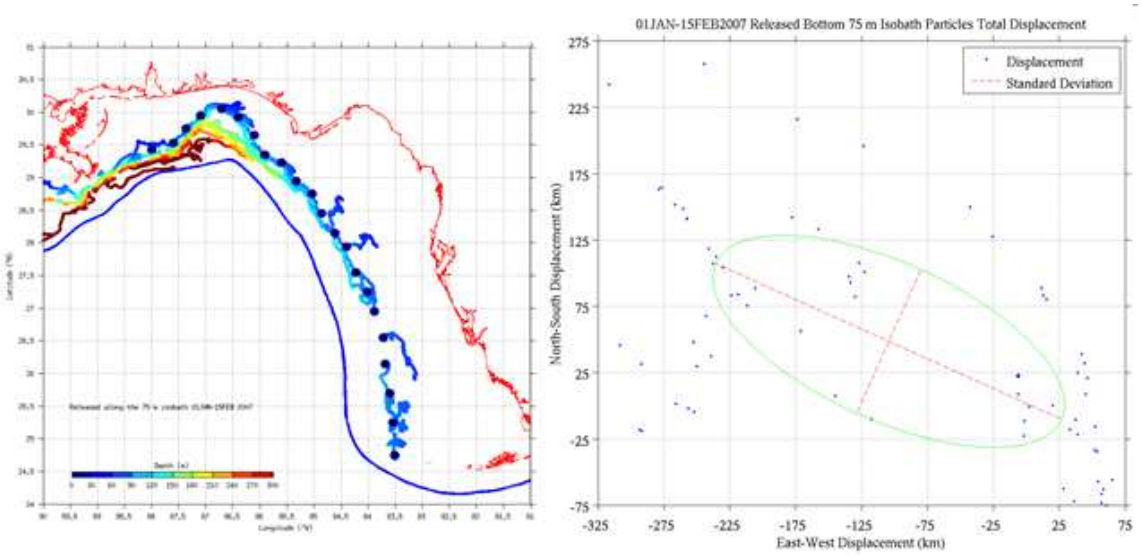

Figure 3.17: Near-bottom release of particles along the 75 m isobath (shelf-break) along the WFS, 01JAN-15FEB2007. The left panel color is saturated as the particles near the De Soto Canyon and the mouth of the Mississippi River are at a depth greater than the 300 m the colorbar extends to. This was done intentionally so there would be a measure of detail available in the color differences for the rest of the particles in the figure.

The 45-day period was chosen due to it being a timeframe with little/no deep-ocean forcing effects, allowing the advection of the particles to be driven almost exclusively by local forcing. The time period is one of primarily downwelling, with the particle trajectory calculations clearly showing this.

Figure 3.17 shows the particle trajectories along the 75 m isobath (same points used as in the previous section) 01JAN-15FEB 2007. The left panel shows the particles' primarily along isobath advection for the majority of the shelf, mostly to the north. The advection is very slight due to the lack of LC interaction or other deep-ocean forcing effects. As one looks at the Florida Panhandle and De Soto Canyon portions of the WFS, there is still a clear tendency for the particles to be transported north along their isobath and the northern-most edge of the Canyon, but there is also some significant downwelling occurring as demonstrated by those particles that are transported deeper in the water column (greens and reds on the graphic). These particles were downwelled to a deeper isobath offshore of the Big Bend area then slowly advected towards the De Soto Canyon at which point many of them downwelled farther as they continued their journey towards the Mississippi/Louisiana shelf. Figure 3.17 (right panel) shows the particle displacements during the timeframe. Worth mentioning is the lack of straight line groupings as was displayed in the upwelling timeframe previous discussed in section 3.6.1. The vast majority of these particles remained in the model domain through the entirety of the timeframe. The average advection was strongly to the west and moderately north. The majority of the deviation was in the major axis direction, though it was comparable to that of the March 75 m isobath (Figure 3.13) deviation. This particular standard deviation is greater than all the others in the entirety of this study (with the exception of the surface particles released for both 45-day periods), suggesting the particles did not advect uniformly in their direction or distance over the course of the timeframe as occurred in the other case studies.

The particles released along the seven transects at the surface (Figure 3.18 panels A and C) over the same 45-day timeframe had a strong tendency to move away from the coastline and be transported towards the shelf break. Upon reaching the shelf break the velocity of the particles

increased and they were advected mainly northward along the length of the WFS in the surface layer of the water column just above the ~100 m isobath. The majority of the particles advected north and west along the WFS, with only a few exceptions moving south towards the Florida Straits.

An area with a few interesting trajectories is that of the shoreward portion of the Marco Island transect. This area had a few particles that, while they moved in the same general pattern

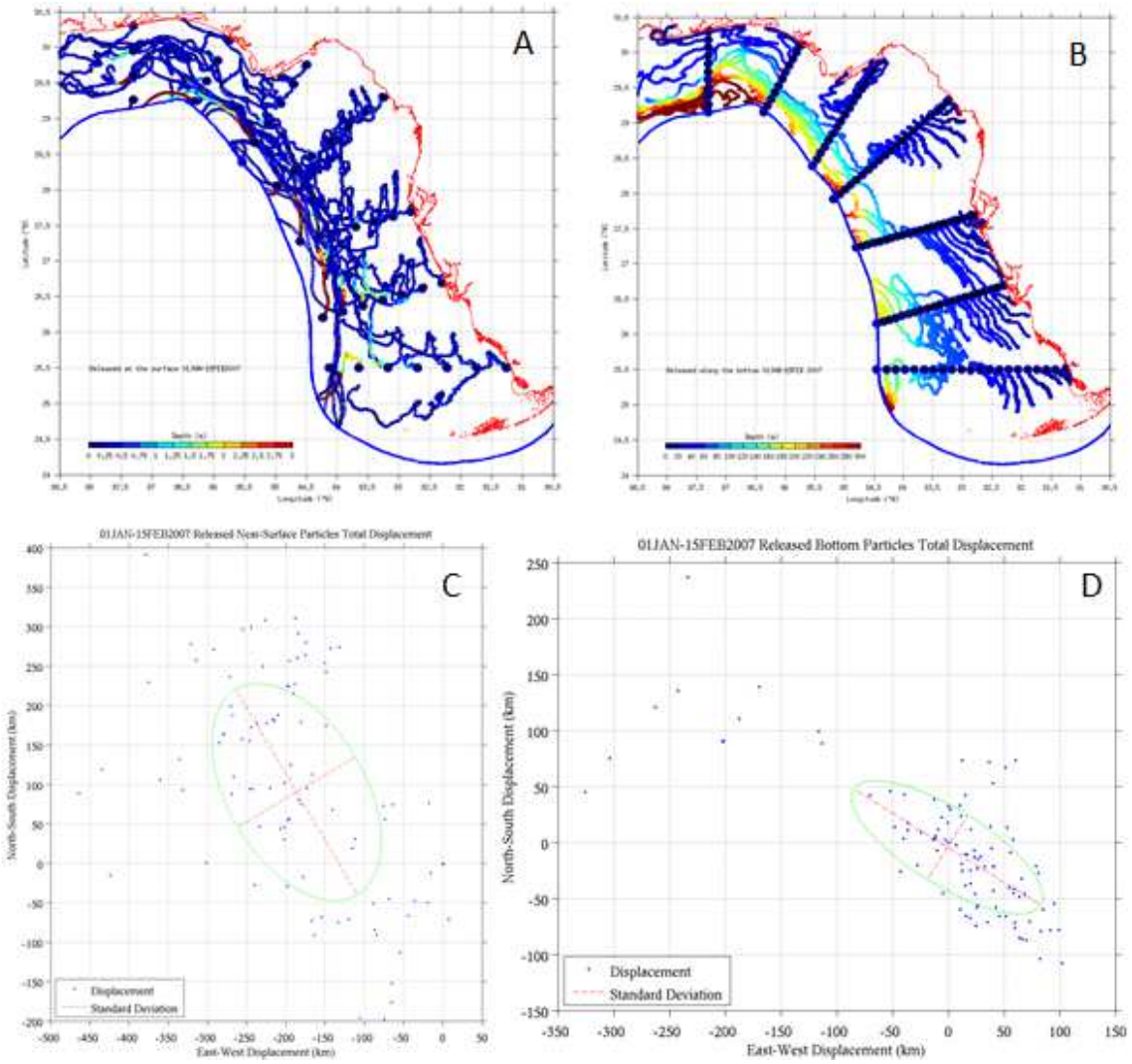

Figure 3.18: Near-surface (Panels A and C) release of particles along the seven transects, 01JAN-15FEB2007. Near-bottom release of particles for the same timeframe and locations (Panels B and D).

as the rest (northwestwards with a slight dip and strong westward movement before increasing speed to travel north again), the northwards movement was significantly less pronounced than

the rest, while their westward movement was significantly more. They travelled almost the entirety of the model domain (longitudinally) in the 45-day period, while remaining in the top one meter of the water column. Seeing such movement of the particles and having them not be caught in the off-shelf movement towards the Florida Straits is interesting, and another supporting reason why looking at the transport of water masses on the WFS needs to be considered as separate local and deep-ocean forcing examples as much as possible to try and identify the driving factors of the water transport.

The displacement of the surface particles (Figure 3.18 Panel C) was on average very strongly to the west and about half as strong to the north overall. The majority of deviation was along the major axis direction, with again about half the magnitude of deviation in the direction of the minor axis. Connectivity on the WFS is shown by the nearshore particles by Sanibel Island that tracked northward along the coast towards the Tampa Bay area before they reversed and headed south and west across the shelf. The particles that are closest to Apalachicola work their way along the coastline past Panama City and to the Fort Walton Beach area over the timeframe. Interestingly, most other particles remain away from the coastline, even after making the turn onto the narrow part of the shelf by De Soto Canyon. The particles with the largest horizontal advection over the 45-day period were those that started along the shelf break area. Generally, the closer the particles were to the coast, the shorter the distance they moved.

Contrasting to the surface particle trajectories, the bottom particle trajectories (Figure 3.18 panels B and D) from the midshelf and inner shelf are primarily advecting slightly shoreward and to the south. Another distinct difference is the smaller velocity of the bottom particles as evidenced by the much shorter trajectories, especially in the inner and mid shelf regions. This example is a good example of the non-homogeneous flow that can occur on the

shelf. On the WFS proper in this instance, the majority of the flow is to the southeast (panel D, most of the particles in the bottom right section of the graphic), while the area past the shelf break flows almost entirely to the north or west in a strongly downwelling fashion, oftentimes leaving the model domain (the particles in the top left portion of the panel). The area of reversal in direction is the easiest to see in Panel B. The change right around the shelf break is very clear, and significant. Panel D supports the reversal of transport between the different portions of the shelf by showing the mean is very near to zero displacement, and the major and minor axis standard deviations are relatively small as well (smaller than those from the previous 45-day period). There isn't much connectivity between the areas present in the bottom transport of the water column in this timeframe, and the little that there is, is limited to the nearshore areas in the Florida Panhandle.

The next case study is that of Front 1: 18-28APR2012. This cold front was chosen for its lack of deep-ocean forcing influence, which allows for (almost exclusively) only the local forcing effects to be considered. The majority of the surface particles (Figure 3.19 Panels A and a) reverse direction from northward to southward after the front passes. The front passed buoy 42039 at approximately 2 am EST on 22APR, and made its way to KSRQ in Sarasota, FL by approximately 7 am EST the same day. This front was a fast moving front, which is supported by the reversal mentioned previously. The mean displacement of the surface particles during the frontal passage was to the southeast (Panel a), with similar standard deviations in both the major and minor axis directions. This similarity in magnitudes suggests there was a relatively broad distribution of displacement directions and magnitudes in all directions about the mean of the data set.

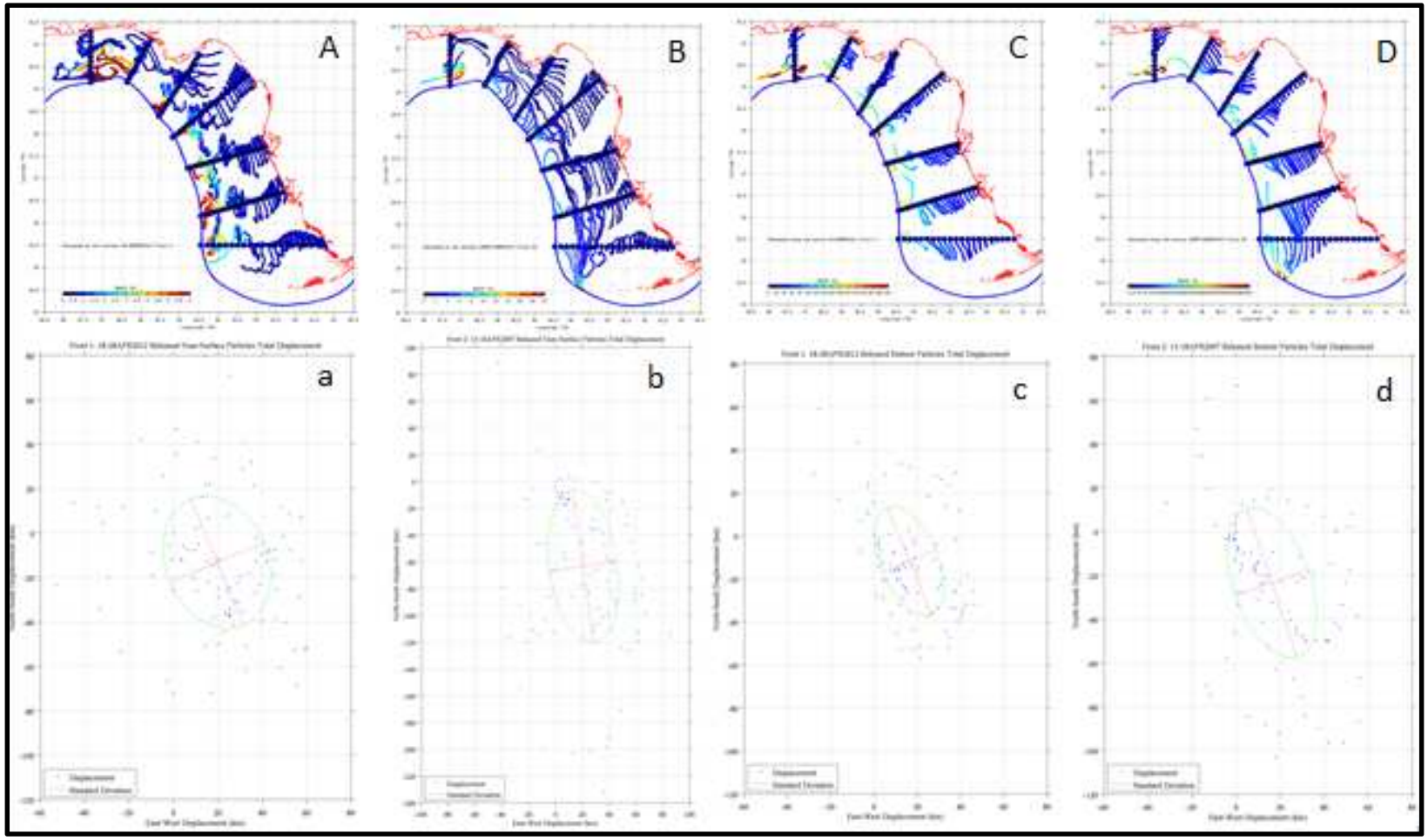

Figure 3.19: Front 1 and 2 surface and bottom trajectory calculations and statistics. Panels A and a are Front 1 surface calculations; B and b are Front 2 surface calculations; C and c are Front 1 bottom calculations; D and d are Front 2 bottom calculations.

The connectivity across the areas of the shelf isn't really influenced too much with this frontal passage via surface transport. The particles that moved the most were out past the shelf break area and in the area of the De Soto Canyon. The particles nearshore had small transport Distances that didn't allow for exchange between estuaries. The option with the most potential for success in that region, however, would probably be the Big Bend and Cedar Key area, as everything else was working its way towards midshelf and the shelf break.

The bottom released particle trajectories (Figure 3.19 Panels C and c) are for the most part all towards the south along the shelf. There is a little bit of reversal past the shelf break, but not with all the particles. The particles closest to the edge of the model domain are all heading south along the isobaths, albeit very slowly and with little movement. The mean displacement was similar to that of the surface displacement, though slightly less, with the standard deviation being almost twice as large along the major axis direction compared to that of the minor axis (Panel c). Interestingly, the angle of transport for the data set was almost exactly that of the surface particles for the duration of the frontal passage. These trajectories do not support any connectivity between the areas of the shelf. Due to the lack of deep-ocean forcing in this example, there is little overall advection and poor connectivity both at the surface and at depth.

The next case study is that of Front 2: 13-18APR2007. This front occurred at a time with some deep-ocean influence in addition to the local forcing provided by the passage of the cold front. The actual frontal passage at buoy 42039 was approximately 5 am EST on 15APR. The front made it to KSRQ at approximately 11 am EST the same day. It was a relatively fast moving front. The passage of the cold front is reflected by the shift in the surface particles' trajectories (Figure 3.19 Panel B). The particles closer to shore in the Big Bend area and further south along the coast also show the passage of the front via an abrupt change in direction. They initially were

going north, then reversed direction and tracked south and seaward slightly. The surface particles (Panel B and b) have a larger amount of horizontal advection than those of the bottom (Panels D and d) particles. Similarly to the previous examples, there are multiple particles that advect southward along the shelf break area. Up in the Florida Panhandle area and into the Big Bend area it is interesting to note the multiple particles that worked their way to the southwest and out of the model domain as the front passed. The area of the shelf with the greatest horizontal advection is that of the midshelf and the shelf break region. The particles that were in the inner shelf initially tended to not have as large of an advection (with the noted exception of the Florida Panhandle area).

Looking at the bottom trajectories (Panels D and d) there is comparatively little movement (as with Front 1). The inner shelf area sees the least amount of advection, especially the further south along the shelf one looks. Midshelf again sees the most advection, and it is primarily to the southeast along the length of the shelf. The deep-ocean forcing is apparent in the reversal of the transport seaward of the shelf break, though it is not very strong.

A key point to remember when comparing the two fronts used as case studies is that the particles were tracked for ten days for Front 1, and five days for Front 2. The mean displacement in the east-west direction both at the surface and at depth for Front 2 is almost the same as that of Front 1. The big difference is in the north-south mean displacement values. The Front 2 displacement is significantly larger than that of Front 1. At the surface, the mean displacement was almost five times larger in Front 2 and the bottom particles displaced almost twice as much as in Front 1. The standard deviation along the major axis direction was larger than in Front 1, while they are almost the same for both the surface and the bottom particle displacements between the studies.

Looking now past the typical synoptic scale events and to a more extreme example of local forcing that is available to the WFS, TS Debby was a tropical storm with very little deep-ocean forcing at the time of her passage.

Figure 3.20 shows the progression of WFCOM simulated daily-mean near surface current and salinity for the duration of the timeframe considered in this study (19JUN-01JUL2012). These figures are very helpful in viewing the surface velocities as the storm approached and how the connectivity between different areas was impacted via the salinity movement through the series, because if the less saline bodies of water can progress along the coastline and move to other areas, then additional nutrients and water properties can be transported as well in the water parcels. The movement of less saline water masses along the FL coastline was limited primarily to those areas up in the Big Bend region. This area saw the extension of a less saline area of water by Cedar Key become more restricted to the coastline as Debby's winds forced the deeper, more saline waters closer towards the coast, and the less saline waters stretched northward along the coast further into the Bend. Of note, the strong surface currents that were developed as a result of Debby's active passage also served to push water of a higher salinity into some of the estuaries, with Tampa Bay serving as an example. The flux of water into the Bay was not prolonged, but it was enough to drive the salinity levels of the Bay up at the mouth of the Bay, while further restricting the less saline waters to the inner Bay, despite the rain associated with Debby's passage and bands.

While some of the increase in less saline water in the Big Bend region may be attributed to the increase in fresh water (rain) from Debby, it is not so much the increase or decrease of less saline water which is important in this particular instance, but rather the movement from one area of the coastline to another and the actual advection of the properties (salinity in this case)

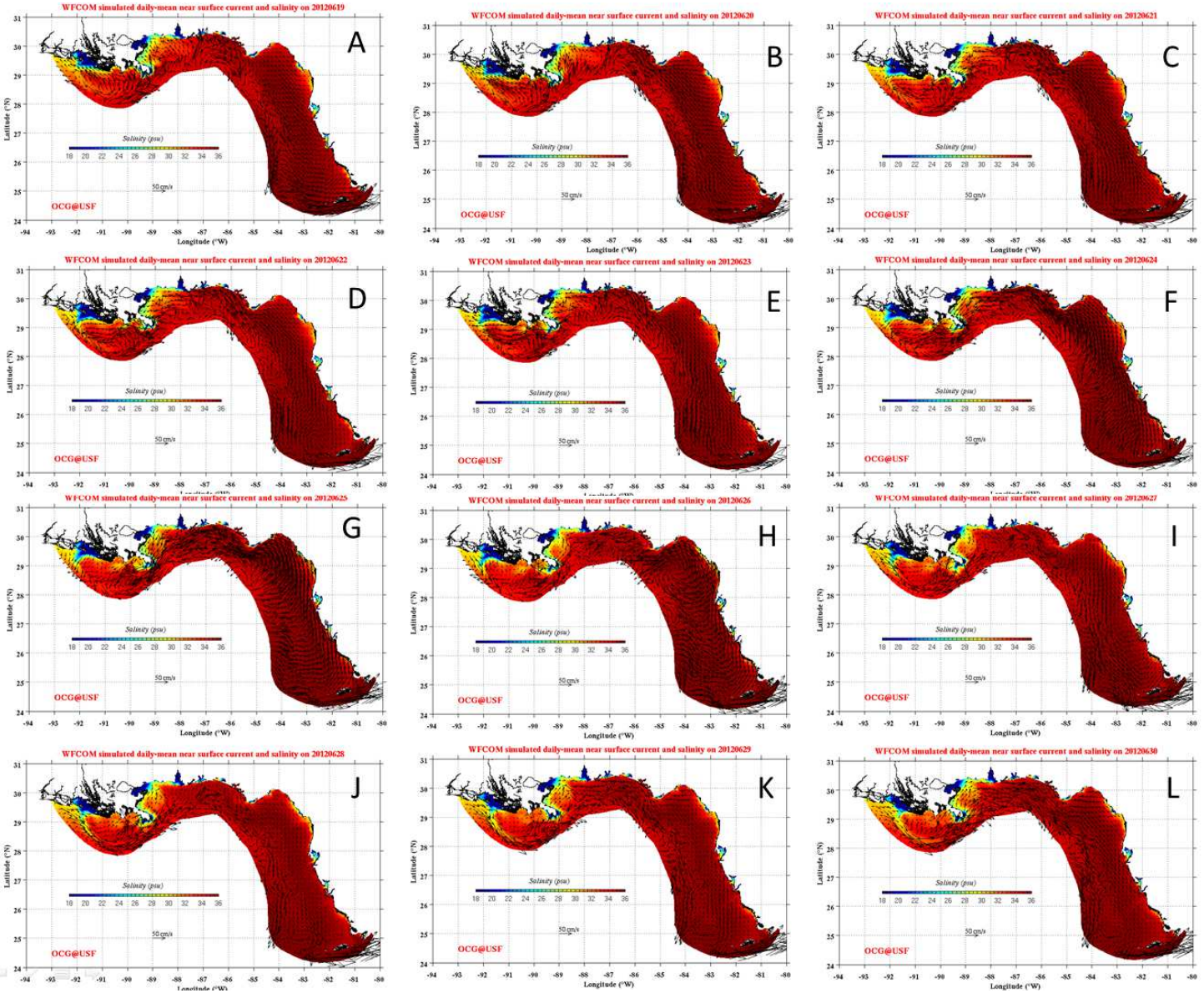

Figure 3.20: Salinity and near-surface current simulations in WFCOM 19-30JUN2012. Each panel is the average for one specific day, consecutively from Panel A (19JUN) through L (30JUN).

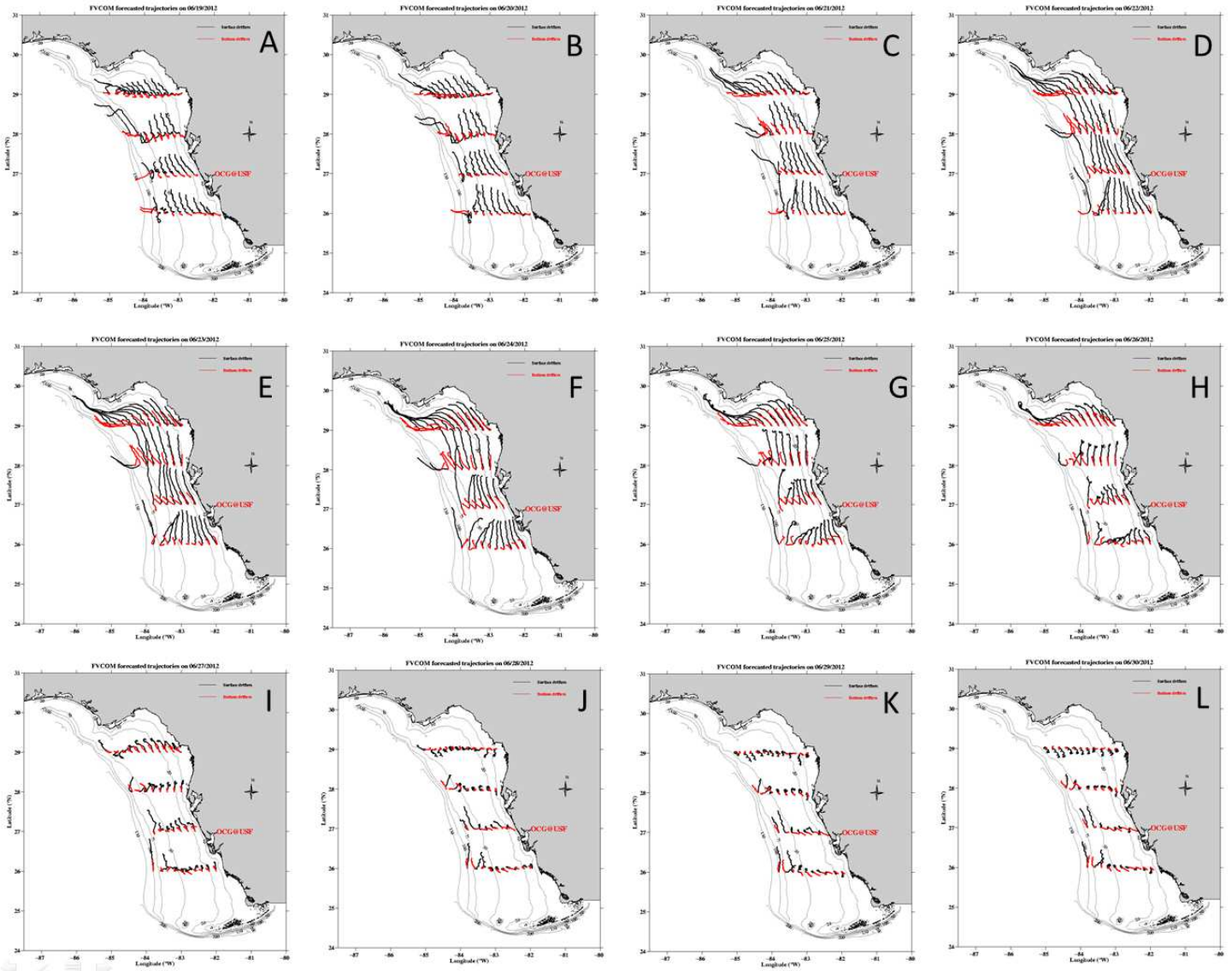

Figure 3.21: FVCOM 3.5-day forecasted trajectories. 19-30JUN2012. Black lines are surface trajectories, red lines are bottom trajectories. The panels progress consecutively with one each day starting on 19JUN (Panel A) through 30JUN (Panel L).

accompanying such movement of water. If the storm had slowed its forward progress and remained over the WFS waters longer, the substantial winds would have had a longer period of time to cause the waters to transport along the coastline, demonstrating a more extensive level of connectedness between areas. However, Debby proceeded to make landfall, and as such, her forcings and the drive to move the waters of the WFS went with her.

Figure 3.21 shows the lack of strong deep-ocean influences along the deeper parts of the model domain specifically when looking at the westernmost points on each of the four transects plotted. Through the first portion of the timeframe, the bottom particles at those locations downwell and are transported off of the WFS, while after Debby leaves the area, the overall transport at the bottom reduces to very small amounts for the 3.5-day forecasted periods. Overall, the bottom particle forecasted trajectories are very short as the storm approached, they increased in distance (and hence speed) as the storm passed and the extreme strength of the local forcing (winds) relative to normal synoptic frontal passages influenced through the depth of the water column across the entirety of the WFS which forced the particles at the bottom to advect in-line with those at the surface. Once the storm tracked towards the Big Bend area and made landfall, the trajectories began to progressively show less and less impact from the storm's forcing, beginning with the southernmost transect. These forecast trajectories show the strong material transport throughout the water column to the north and around the bend into the Florida Panhandle area of the WFS. As Debby progressed through the local area, the waters at all depths were advected with great speed due to her strength and the depth at which she was able to influence the water column. Such storms as Debby (hurricanes, tropical storms, etc.) are known for their pull of energy from the uppermost 150-200 m of the water column, and their resulting

mixing and physical movement of the water mass they are acting upon as they track over the water.

Figure 3.22 supports the information in Figures 3.20 and 3.21. Looking at the surface particles (Panels A and C) the majority of the particles moved quickly north around the shelf as Debby approached and made landfall. This provided for a solid opportunity for connectivity between the areas of the shelf at the surface. Waters from the Marco Island area made it up to

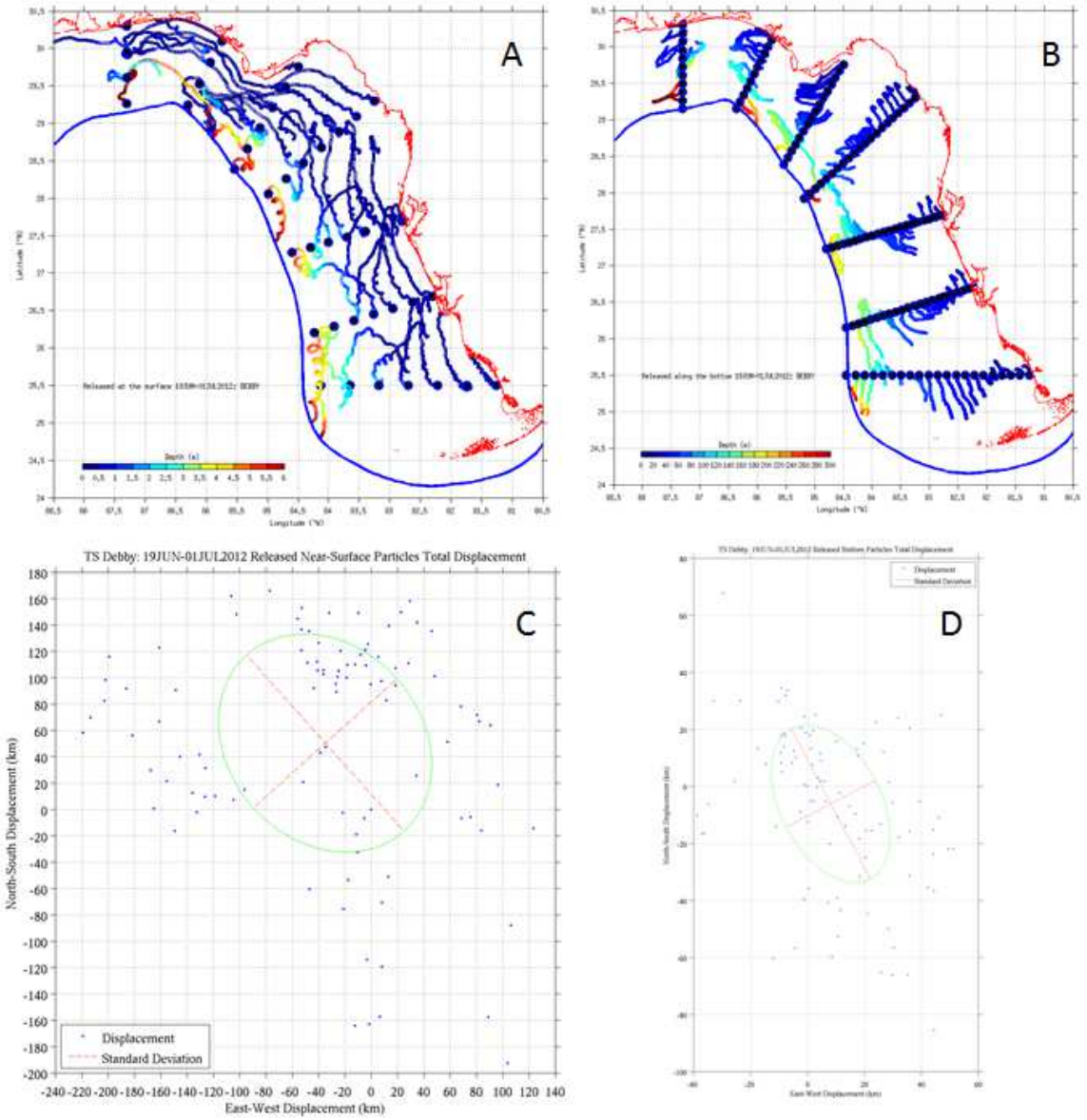

Figure 3.22: Tropical Storm Debby (19JUN-01JUL2012) particle trajectory calculations and resulting statistics for the surface (Panels A and C) and near-bottom (Panels B and D).

the Sanibel Island area, Sanibel Island waters made it up to Tampa Bay, while waters from Tampa Bay almost made it as far as Cedar Key to the North. The waters from Cedar Key, the Big Bend, and Panama City all made it to the Florida Panhandle and around towards Pensacola. The bottom trajectories (Panel B and D), while smaller in magnitude compared to those at the surface, they are still quite large compared to those of the two fronts previously investigated (Figure 3.19). Interestingly the inner shelf and midshelf trajectories bend with time showing a shift in their path as the storm passes.

The average displacement at the surface (Panel A and C) was moderately to the northwest, as was apparent via the other products considered (Figures 3.20 and 3.21), and was expected due to the counterclockwise rotation of the storm. The standard deviation along the major and minor axis directions were quite large over the data set, suggesting the movement was not homogeneous across all particles, as there was a larger spread in the displacement values. The bottom particles (Panels B and D) had a significantly smaller overall movement. The mean displacement was slightly to the southeast, and the standard deviations were also considerably smaller suggesting there was greater coherency in the trajectories of the particles at the bottom of the water column.

3.7 Discussion

When considering the first sub-question which was

"given a period of time when we know the deep-ocean influence was strong on the WFS, what were the pathways of water parcel delivery from the region of the shelf slope to the near shore?" the pathways that were determined in section 3.6.1 were those of bottom layer Ekman transport towards the shore, and an across-isobath movement due to the LC influence (deep-ocean forcing)

which helped to trigger an upwelling event which was in its early stages for the first case study. By having a deep-ocean driven upwelling event on the WFS, the entirety of the shelf is able to be impacted, and "new" water masses are able to be transported from the shelf break and slope area into the mid and inner shelf regions.

Looking at the second sub-question of

"given a period of time when we know the local forcing influence was strong on the WFS, what were the pathways of water parcel advection across the WFS?"

the downwelling prominent timeframe of 2007 and the three case studies in 2007 and 2012 were considered. The primary pathways of advection across the WFS (longitudinally) were not as prevalent or straight forward as in an upwelling scenario driven by the LC interactions with the shelf slope. The majority of the advection longitudinally was in the westward direction, away from the Florida coastline and her estuaries. The downwelling driven scenarios helped to drive the little bit of movement in the bottom layer that was in the longitudinal direction. The synoptic events, both those that occurred in the 45-day period January through February and those that were considered individually as case studies saw small amounts of horizontal advection, while most of the movement was in the north-south direction both at the surface and at depth. Due to the forcing being primarily local, the bottom particle trajectories were substantially less than those of the surface, and they tended to follow the isobaths along the shelf until they reached a point at which they were forced to either mix or downwell. Even Tropical Storm Debby, the extreme local forcing case study, only served to move the trajectories a little more at depth than the synoptic cold frontal passages did. This was due to her quick movement and the deficient amount of time for the bottom layer of the water column to be sufficiently influenced to advect as substantially as the waters at the surface did. The large potential transport for the bottom

particles was clearly demonstrated in Figure 3.21, showing what could have happened each day if Debby had remained stationary for the next 3.5 days. There is not much connectivity to be seen at depth, but the larger flow in general helps out some, especially when compared to the other examples of local forcing (Fronts 1 and 2). Compared to the fronts, the surface advection and opportunity for connectivity was much greater, which is to be expected from an extreme case of local forcing such as a tropical storm.

Considering the two frontal case studies specifically, their resulting comparison suggests that a combination scenario of local and deep-ocean forcing is preferred for getting the most advection and the best chances of connectivity between the shelf's waters and estuaries. This finding is also supported by the connectivity and relatively larger transport distances found in the first sub-question (section 3.6.1), which was driven primarily by a strong deep-ocean forcing event, but still had local forcing influences due to the normal synoptic weather patterns that passed through the area on a regular basis in the Spring.

Now for the final over-arching question of

> "under primarily deep-ocean or local forcing influences, what are the ranges of upwelling and advection of water parcels both vertically and horizontally across the various regions of the WFS?"

the ranges of upwelling driven advection in the horizontal (latitudinally and longitudinally) are moderate over the early stages of such a scenario. The longitudinal transport was found to reach up to 225 km in a 45 day period (Figure 3.13 right panel) when considered from the shelf break specifically, and 250 km over the same period (Figure 3.16 right panel) when considered from the transects along the bottom of the water column. In the latitudinal direction however, the surface particle displacement was larger. When considered as a whole 45-day time period, some

of the surface particles from sub-question one traveled 500 km south before exiting the model domain prior to the conclusion of the period. When considered individually in 15-day increments, the same timeframe yielded 250 km, 420 km, and 280 km southward displacements in each increment, respectively. In the vertical, the results suggest that the particles did not upwell from depth directly into the surface layer of the water column, but rather slowly traveled in the vertical direction as they horizontally advected across isobaths, making their way closer towards the inner shelf, thus bringing them slowly into the surface layer (that which is directly influenced by the local forcing and mixing that occurs near the air-sea interface). While some were able to make the journey quicker than others, the early stages of the upwelling scenario considered in this study do not suggest a quick transference between the bottom layer and surface layer of the water columns when originating from the shelf break during a deep-ocean upwelling event.

Primarily local forcing scenarios (sub-question two) can have very large displacements over time periods, both latitudinally and longitudinally (particularly at the surface), but they are not upwelling driven. They have a slightly smaller standard deviation compared to the results from the upwelling scenario, suggesting slightly more coherency in the displacements of the particles over the timeframes considered for each case study. The local forcing driven scenarios tend towards downwelling, both at the surface and at depth. The particles tend to be pulled towards the outer shelf or off the shelf entirely, and those at the surface, if they do not remain at the surface, are downwelled slightly (maximum of ~2 m) through the course of their timeframe.

Local forcing alone does not provide the connectivity between areas of the WFS that would be primarily useful for moving larvae, eggs, or required nutrients about the shelf between estuaries or from the outer shelf into estuaries for further development. While the overall physical displacement distances can be quite large, the majority of that displacement is away

from the inner shelf area, and up around the De Soto Canyon in the Florida Panhandle. That area is one in which the particles increase their speed as they follow the isobaths westward (at depth) and the surface currents around the De Soto Canyon towards the Mississippi River Delta. There are some instances where particles will get downwelled into the De Soto Canyon and remain at significant depths through the rest of the timeframe, but most of the particles do not get transported in such a manner. The overall best connectivity is provided by the deep-ocean upwelling scenario, or a combination of local and deep-ocean forcing influences.

CHAPTER 4

QUESTION #2

4.1 Abstract

Forward and backward particle trajectory calculations are made using a 4th order Runge-Kutta numerical scheme, comparing both start and end points as well as the overall shape and location of the calculated trajectories. Comparisons are made along the 75 m and 15 m isobaths of the WFS at 12 locations, at the near-bottom and middle depths of the water column, resulting in a total of 24 particle trajectories being calculated forward and backward. While this approximation method is more precise than Euler's method, there are still situations in which the discrepancies between the forward and backward calculations are considered too large for some applications. Instances where the particles encounter large or quickly changing fluctuations in velocity or direction are not adequately replicated. Particles in the surface or bottom boundary layers have greater fidelity in their backward replication trajectory calculations than those not restricted by the boundary layer dynamics. The backward calculations may provide a means for crudely estimating particle source regions, it must be recognized that they are not the same as forward calculations except for steady and relatively unstructured flow fields. Pathlines are not streamlines for unsteady flows, and spatial structure further impacts discretized calculations both in time and space.

4.2 Tools

4.2.1 Numerical scheme

When solving Ordinary Differential Equations (ODE), there are many tools available for use depending on the problem and desired type of solution. Methods for solving them in the forward direction include examples such as the Euler method, Leapfrog method, variable order methods such as Richardson extrapolation and the Bulirsch-Stoer algorithm, and the alternative options of the Hermite-Obreschkoff method and Fehlberg methods. Over time, many basic methods have been expanded in their application and refined for specific fields of interest and application (i.e. compressible fluid dynamics, strongly turbulent flows, mechanical engineering, particle dispersion, etc.). As a result of such expansion, many tools have been developed that are very specific in their realm of applicability. One such example is the extensive investigative work that has been done in considering the simulation of steady and unsteady incompressible flows in fluid dynamics. By taking a comparably simple lattice Boltzmann method (LBM) and expanding it into a high-order compact finite-difference lattice Boltzmann method that utilizes a 4^{th} order RK method to discretize the temporal term, increased accuracy for flows with low and high Reynolds numbers are able to be attained in the forward direction [*Hejranfar and Ezzatneshan*, 2014]. Along with examples of such numerical tool development, the various methods used to calculate truncating error and compare error estimates for multi-step algorithms have also been further advanced (e.g. [*Shampine and Watts*, 1971], [*Butcher and Johnston*, 1993]).

The Runge-Kutta (RK) method is a more precise way to calculate an Ordinary Differential Equation (ODE) than the traditional Euler method,. The history of the RK method and its development over the years is covered thoroughly in *Butcher* [1996]. RK takes a

weighted average of the slope for each step starting with the initial slope at some start point, resulting in a more accurate and precise solution to the ODE. The general RK 4th order equation shows clearly that each step in the calculation is based on the previous step (Figure 4.1). This dependency upon the previous step in the calculation is important because any uncertainty or discrepancy added into the calculation at step 1 is going to be carried over and built upon in steps 2, 3, and so on. When trying to work backward from the last approximation step in the calculation, the ability to replicate the forward calculation is made more difficult by trying to incorporate what the forward intermediate steps calculated without the initial point (since one is now working from the opposite direction).

$$p_{i+1}=p_i + (1/6)\Delta t[\bar{v}_i + 2\bar{v}^1_{i+1} + 2\bar{v}^2_{i+1} + \bar{v}^3_{i+1}]$$

p_i: initial point
p_{i+1}: successive point after initial point, Δt away
Δt: step size between points p_i and p_{i+1}
$\bar{v}_i$: velocity vector associated with point p_i

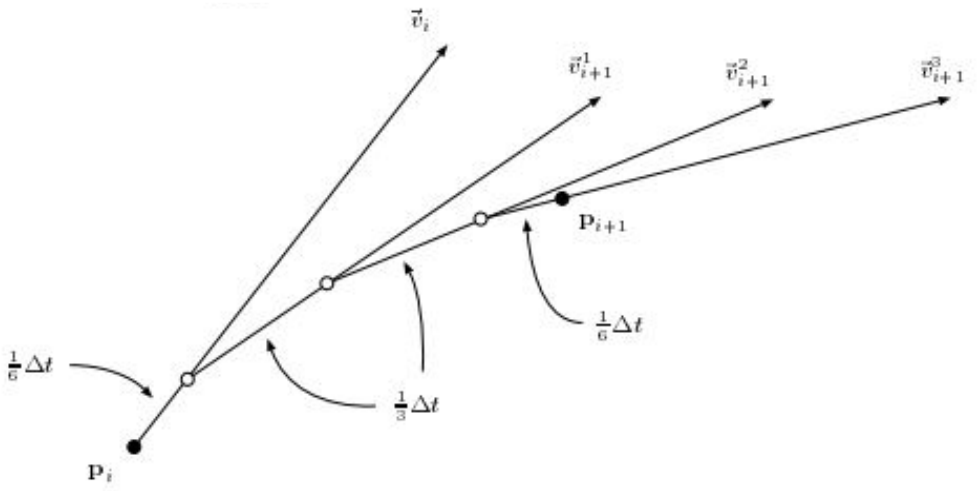

Figure 4.1: 4th order Runge-Kutta diagram [*Joy*, 1999].

RK method is a numerical scheme used to approximate a time dependent solution to an ODE through iterative steps. As summarized in *Varsakelis and Anagnostidis* [2016], previous

studies have shown that using the same initial data sets, various numerical schemes can lead to solutions that are substantially different. The main cause for such discrepancies is noted as the analytic dependence of the resultant particle trajectory on the time-step of the method chosen. The time-step used in this study is calculated every hour as an hourly mean.

The 4th order RK scheme is widely used in Lagrangian trajectory simulations in coastal oceans (e.g., [*Hofmann et al.*, 1991; *Zheng and Weisberg*, 2012]) and oil spill tracking applications (e.g., [*Liu et al.*, 2011b, c; *Weisberg et al.*, 2011]). Most of these trajectory simulations are calculated forward in time to predict future particle/drifter locations. However, there are needs for accurate backward trajectory simulations as well, for example, in the case of determining the source location of pollution or floating objects in the ocean.

Investigations into multiple areas of study have been conducted to find similar comparative studies into forward and backward in time particle trajectory calculations and the use of the RK numerical scheme for such calculations. These areas include, but are not limited to, the field of air pollutant dispersement [*Stein et al.*, 2015], magnetic diffusion [*Pries and Hofmann*, 2015], satellite orbits [*Anastassi and Simos*, 2005; *Aristoff and Poore*, 2012], solids and structures (specifically spring-mass systems) [*Kaunda*, 2015], meteorology and the dynamics of the atmospheric boundary layer [*Nazari et al.*, 2014], and linear shallow water flows [*Beljadid et al.*, 2013] to name a few. Through all of the studies, while they are looking forward in time and using one form of a numerical approximation scheme or another, they do not address the direct comparison between forward and backward in time numerical scheme calculations for a non-stochastic dynamically driven, diffusion affected, non-linear incompressible flow. There are many discussions on the forward trajectory and overall approach to limiting chaos and finding a balance with superstability, but no true backward in time calculations or comparisons to the

forward in time calculations. There are a multitude of studies using backward-facing calculation schemes such as the backward-difference method applied to the numerical scheme of their choice, but this is not truly doing the calculation backward but rather taking the forward calculation and finding the difference between two time steps t and Δt-1. This process still utilizes the forward calculation process.

One study that has some similarities to the study conducted in this Thesis is that of *Batchelder* [2006]. This particular study investigates plankton advection and dispersion through the water column and along a near-shore region using a 3D physical circulation model (Spectral Element Ocean Model) for a timeframe of 30 days with constant salinity, varying temperature, a rectangular coordinate system, idealized boundary conditions and bathymetry, and with an upwelling-favorable fluctuating wind regime. The intent of the study was to demonstrate the need for taking into account diffusion in particle tracking simulations and to show the potential usefulness of backward-in-time-trajectory simulations by investigating source and receptor discrepancies for plankton in various life-stages. The study first conducts backward simulations, then compares the results to forward simulations started from the last point of the backward simulations for the duration of the timeframe available in the physical circulation model. Advection only simulations were compared to advection and added vertical diffusion simulation results. Vertical diffusion was incorporated via a random walk, while horizontal diffusion was not considered. The actual calculation method used for the backward in time trajectories that were calculated is not thoroughly explained, nor is the method for calculating the forward trajectories. This lack significantly limits the comparability between the two studies. Nothing may be noted about the schemes chosen, the errors induced and integrated, if the backward

calculations are truly backward in time or if they are instead backward-facing steps like those mentioned previously, or the approach to the diffusivity problem.

Despite the differences in goals, foci, and approaches, some similar conclusions were reached in *Batchelder* [2006] and this Thesis. Areas of strong nonlinear flows and interactions have the largest impact in trajectory fidelity between forward and backward calculations. The scale of the model grid plays a role, as well as the important inclusion of diffusivity (though it is accounted for in *Batchelder* [2006] via a random walk) in particle tracking of ocean ecosystem processes. Also that irreversible processes are exactly that- irreversible. While estimations can be made of the results moving backward, they are not exact solutions. Advection-only particle trajectory calculations are reversible, but without accounting for diffusion, the resultant trajectories are useless. However, diffusion is irreversible backward in time. As a tool however, backward in time calculations under certain circumstances can prove to be useful in the form of likelihood or probability maps of potential solutions for sources of particles, though not necessarily exact solutions.

4.2.2 Data

Stored WFCOM data: The same WFCOM model simulations that were used for question #1, sub-question 1 are once again used for calculating particle trajectories at different locations on the WFS, with date ranges of 29MAR-13MAY 2007. The model calculated trajectory data are hourly means, and the model mesh grid horizontal resolution varies from 150 m to 12 km, with the largest amount of grid cells falling into the 250-500 m resolution dimension [*Zheng and Weisberg*, 2012]. The WFCOM based trajectory simulation was evaluated against the satellite-tracked surface drifter data observed in summer 2010 [*Liu et al.*, 2014]. The mean Lagrangian separation distance after 3 days' simulation was 38 km on the WFS, and the mean skill score was

0.39, in termos of the normalized cumulative Lagrangian separation proposed by *Liu and Weisberg* [2011]. The WFCOM performed better than the other three models and the altimetry data products on the shelf during that three months period of 2010 [*Liu et al.*, 2014]. An even better model-data comparison was reported for the inner shelf area [*Zheng and Weisberg*, 2012].

4.3 Experiment Design

Question: Is it reasonable to expect forward and backward particle tracking to be the same? If so, under what conditions?

In order to address this question, forward and backward particle trajectory calculations over the same period and locations were compared. The focus of this study was the differences between the simulated paths and start/end point agreement (or discrepancy) for both sets of trajectory calculations. It was anticipated that particles encountering strong eddies or large changes in velocity would have the most error in their backward trajectories, resulting in the largest discrepancies between the two data sets. In order to investigate this, the following steps were taken:

1- The forward trajectory calculations from the shelf break near-bottom release along the 75 m isobath for chapter 3 sub-question 1 (29March-13May 2007) were expanded to include a release in the middle of the water column. This timeframe was chosen in order to not only be supplemental to the previous question, but also to consider a time of primarily deep-ocean forcing. With the goal of keeping this study on a smaller scale than the previous chapter, a sub-sample of six points along each isobath were focused on in order to consider a range of dynamically and bathymetrically different locations. By focusing on a sample of points rather

than an overview of the mass group trajectories, a greater level of detail can be considered for each trajectory.

2- Forward particle trajectory calculations were completed starting at six comparable points along the 15 m isobath for the same timeframe and relative release depths in the water column as in step 1. This additional isobath provides an opportunity to consider the dynamics of the inner-shelf and if there is a difference in the applicability of the RK method in an area of the shelf which is not driven as strongly by deep-ocean forcing as that of the shelf break.

3- The end points of the selected sample of forward trajectory calculations that originated at the 75 m and 15 m isobaths were used as the starting points for backward particle trajectory calculations. The goal was to try and replicate the forward calculations, seeing how close the backward calculations match the forward calculations in both pathway and termination point. For those points that left the model domain within the 45-day timeframe, their last hourly position in the model domain from their forward trajectory calculation was used as their starting location and time for the backward trajectory calculation. This means the backward trajectory calculations were considered for individual particles, with some being considered for the entirety of the 45-day period, and others as few as 20, 31, 43 days to name a few. This difference between the individual points is accounted for in the analysis by calculating their daily discrepancy rate based on the individual number of hours each particle remained in the model domain.

4- The best and worst results from each set of particle trajectory calculations were

compared to find commonality amongst them in an effort to describe the conditions that are the most and least favorable for backward tracking using the RK method for quasi-isopycnal particles.

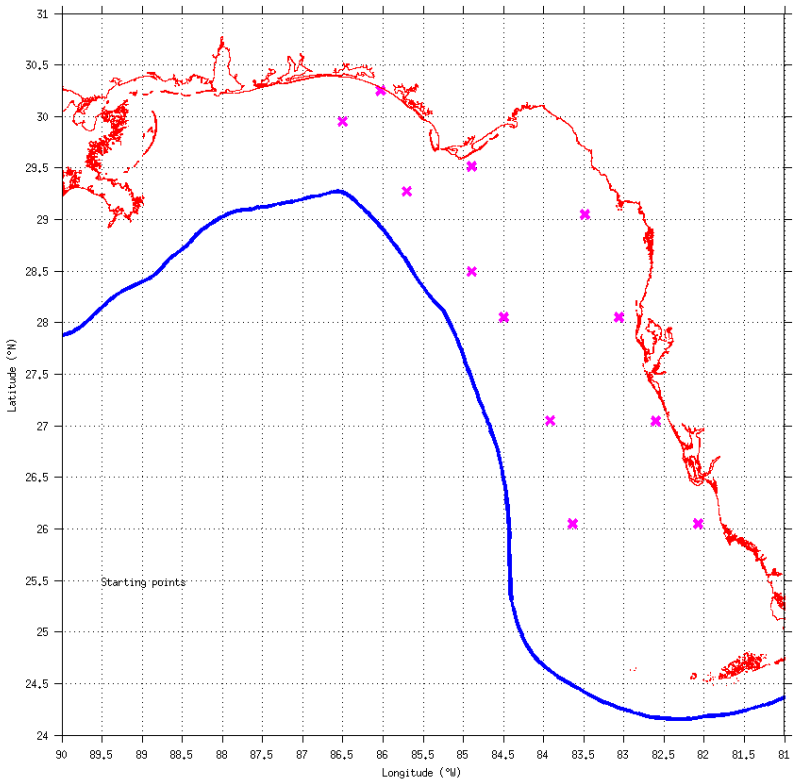

Figure 4.2: Magenta x's designate the 12 starting locations for the particles along the 75 m and 15 m isobaths on the WFS. The blue line represents the WFCOM model boundary.

The RK method mentioned previously is the method used for calculating the forward (and backward) particle trajectory locations in a step-wise fashion in this study. For the entirety of this study (both chapters 3 and 4), the calculation used is a 4^{th} order RK. Initially, one might think that in order to have a calculation for a particle trajectory proceed backward in time, one must only adjust the velocity vectors or other portion of the forward calculations by (-1) in order for them to progress in the reverse direction. Unfortunately, this seemingly straight forward solution does not work realistically in all situations when the forward calculation was

accomplished with the RK method. If a strictly linear interpolation was being used for the forward trajectories, then a strictly linear backward interpolation would be significantly more feasible and realistic in its ability to reproduce the trajectories that resulted from the forward calculations. Due to the numerical scheme building each successive step on the previous step, the RK method results in some instances where the backward trajectory is significantly different both in shape, length, and the final point than the forward calculation.

4.4 Design Limitations and Assumptions

Any particles that went outside the model domain by the end of the 45-day period were looked at individually to find their last hourly position in the model domain as a valid point. These points (and corresponding shorter time frames) were then considered for their individually appropriate time frames and trajectories, so not all particles were considered for the entire 45-day period. The only particles considered in this study were the 24 specified (12 along the 75 m isobath, and 12 along the 15 m isobath in Figure 4.2). For each trajectory, the discrepancy was calculated as a straight line distance between the original forward particle trajectory release point and the final point of the backward trajectory. If at any point in time other than the end of the calculation for each timeframe had a larger discrepancy than the final point discrepancy, it was not calculated quantitatively, though it was considered qualitatively (shape).

As discussed in section 4.3, this study specifically considered only a limited sub-sample of points along two specific isobaths as release locations in order to conduct a closer analysis of each particle than was previously feasible in Chapter 3. While having a more robust set of particles would be beneficial for a stronger statistical analysis of the data, it was deemed acceptable for the purposes of this particular study to limit the number of particles.

4.5 Data Analysis Methods

Once the forward trajectory calculations were completed, every result was considered individually. The last hourly location that was in the model domain during the 45-day calculation period was taken to be the "final point" of each particle's trajectory. This location and time was then used as the starting point for the backward trajectory calculations, with the intent being to replicate the forward calculations in the backward direction. To quantify how well the replication occurred, the discrepancy was calculated by finding the straight line distance between the final point of the backward trajectory and the original point of the forward trajectory.

From the discrepancy calculations, the arithmetic mean, variance, and standard deviation were calculated for all of the particles, those released at the near-bottom, those released in the middle of the water column, all particles from the 75 m isobath, and all from the 15 m isobath separately (Table 3).

Of the 24 particles considered, the distance discrepancy (m) was considered as a rate (day^{-1}) for each individual particle's total time in the model domain. This rate of m day^{-1} was compared at each level and location (i.e. the 15 m isobath middle of the water column particles, separate from the 15 m isobath near-bottom released particles). From each group, the best (green) and worst (red) daily discrepancy rates were highlighted (Table 4), and then the resulting four best rates were plotted together (Figure 4.7) and the four worst rates were plotted together (Figure 4.8) for comparison.

When considering the overall shape of the trajectories and how similar or dis-similar they were between the forward and backward calculations, the analysis is more qualitative rather than quantitative. If the general direction and shape of the trajectories were similar, they were considered of similar shape. Major differences in trajectory shape and location were investigated

for cause. Many times the presence of local eddies, significant velocity changes, or significant changes in forcing influences were found to have been the cause of the differences. Each of the figures showing the trajectories is slightly saturated in the depth color scheme so as to provide a little better precision for the depth changes in the shallower waters.

4.6 Results

Table 3 provides quantitative results for distance discrepancies and additional calculations. The origination location that had the best (smallest) overall distance discrepancy and resulting statistics across the board was the near-bottom released particles of both isobaths. Not only was the total discrepancy an order of magnitude less than those of the other locations, but the mean was less than half that of the middle particles and all the particles released at the 75 m isobath. The variance and standard deviation of the discrepancies was significantly less than all other sets that were considered, which is to be expected with a total discrepancy distance as relatively small as the bottom particles had.

Table 3: Distance discrepancy for each calculated set of particle trajectories relating forward to backward RK calculations.

	Total	**Bottom Particles**	**Middle Particles**	**75 m Isobath**	**15 m Isobath**
Number of Particles	24	12	12	12	12
Total Discrepancy (m)	1.629×10^{6}	4.92×10^{5}	1.137×10^{6}	1.007×10^{6}	6.221×10^{5}
Mean (m)	6.790×10^{4}	4.100×10^{4}	9.480×10^{4}	8.396×10^{4}	5.184×10^{4}
Variance (m^2)	5.181×10^{9}	1.558×10^{9}	7.356×10^{9}	5.507×10^{9}	4.338×10^{9}
Standard Deviation (m)	7.198×10^{4}	3.947×10^{4}	8.577×10^{4}	7.421×10^{4}	6.587×10^{4}

Comparing the 75 m and 15 m isobath results, they had comparable variance and standard deviation values despite the 15 m isobath out preforming the 75 m isobath results in

overall total discrepancy and mean discrepancy. This suggests the 15 m isobath saw less significant forcing changes during the timeframe and the backward calculations were better able to replicate the forward trajectories that those that originated at the shelf break.

Comparing the near-bottom and middle released particles, the near-bottom particles out preformed those released in the middle of the water column in every aspect. This suggests the particles released near the bottom had more consistent forcing influences with fewer abrupt changes over their timeframes. With few exceptions, the results from the bottom released particles from Chapter 3 across the entirety of the WFS had smaller velocities than those from

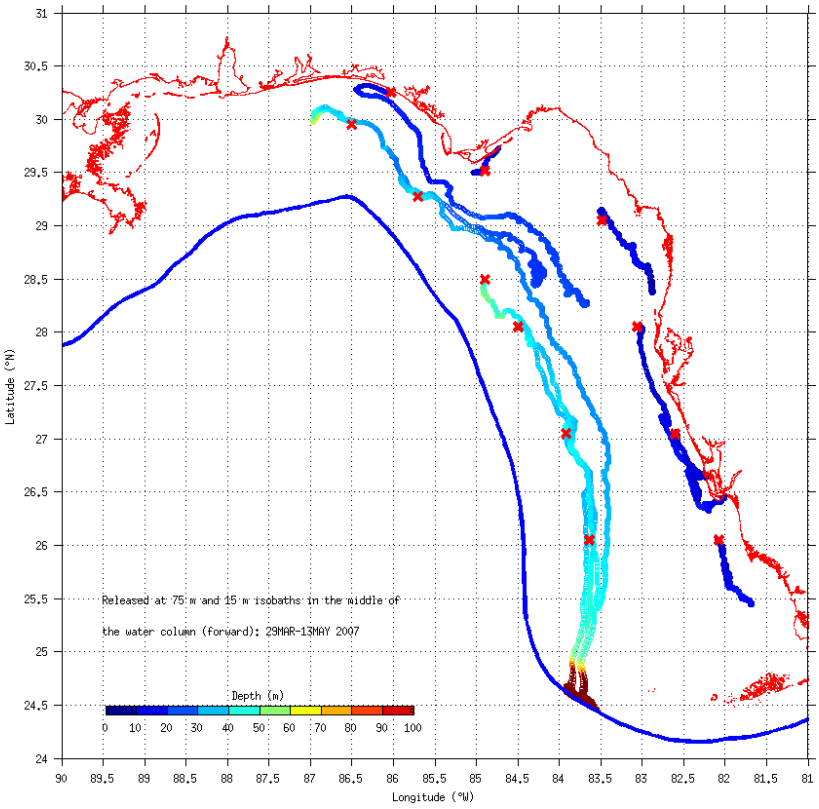

Figure 4.3: Forward particle trajectory calculations of particles at 75 m and 15 m isobaths released in the middle of the water column at the -0.5 sigma layer. Each red 'x' marks the initial release location.

the surface. Their trajectories also tended to be smoother and subject to less variation with the progression of time during the trajectory calculations. The results from the backward calculations

in this study strongly suggest those tendencies may be a large factor in the comparatively outstanding performance of those particles compared to those of the other areas.

Looking strictly at the trajectories themselves now, the forward trajectory calculations of the particles released in the middle of the water column (Figure 4.3) advected generally southeastward along the shelf. The particles released along the 75 m isobath travelled farther than those along the 15 m isobath over the time period, and many of them exited the model domain by the end of the period. The four particles released along the 15 m isobath east of 83.5°W stayed close to the shoreline, generally following the isobath until the end of the period in which they turned shoreward. The two particles west of 84.5°W along the 15 m isobath

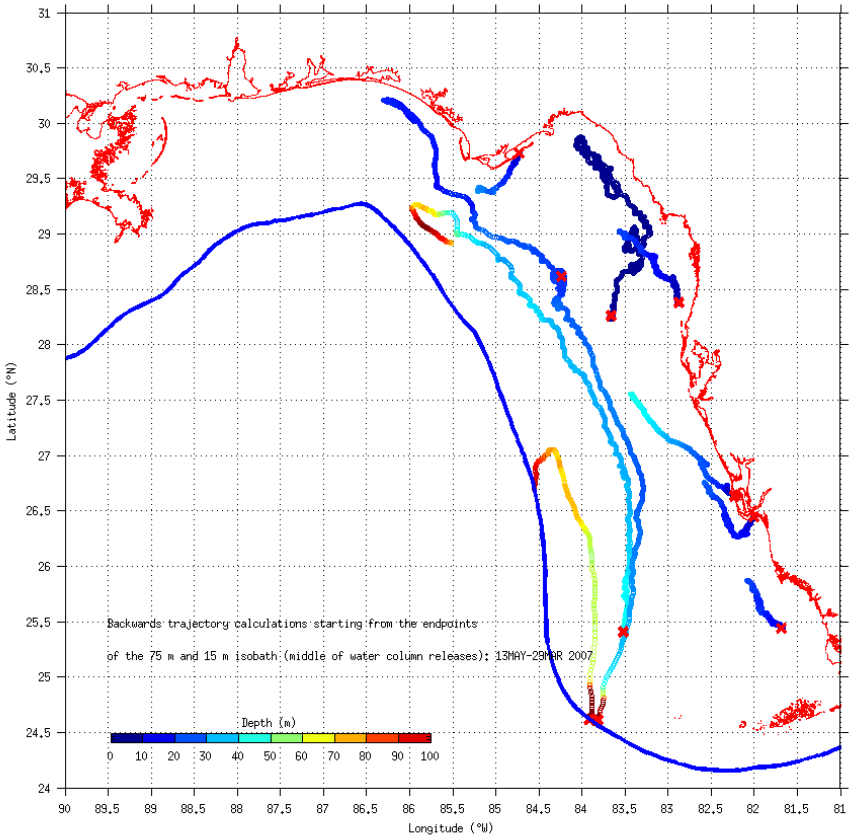

Figure 4.4: Backward particle trajectory calculations. The particles are those that were originally released at the 75 m and 15 m isobaths in the middle of the water column at the -0.5 sigma layer when they were calculated forward in time. Each red 'x' marks the final location of the forward trajectories, which are the initial locations for the backward trajectory calculations.

behaved differently. The particle at 86°W had a similar behavior as those released along the 75 m isobath. This is due to the considerably steeper gradient at that portion of the shelf. The presence of the De Soto Canyon makes the shelf relatively narrow in the Florida Panhandle which allows the deep-ocean forcing and the dominant local forcing in the area to impact the particles in the shallow waters. The remaining particle along the 15 m isobath had the shortest transport over the timeframe, and almost immediately was advected shoreward to St. George Island outside of Apalachicola, FL. Figure 4.4 provides the backward trajectory calculations

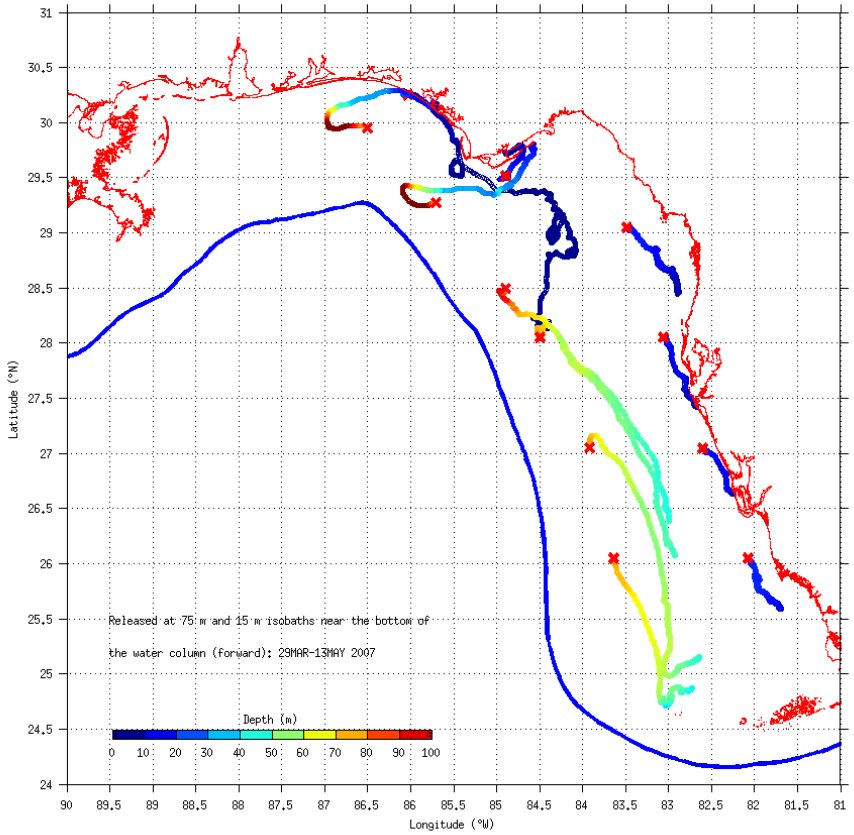

Figure 4.5: Forward particle trajectory calculations of particles at 75 m and 15 m isobaths released near the bottom of the water column at the -0.95 sigma layer. Each red 'x' marks the initial release location.

associated with the forward calculations in Figure 4.3. Overall the paths of the particle trajectories correspond well between the forward and backward calculations. The 15 m particles

are the easiest to qualitatively verify their performance as they stayed mostly close to the coastline and their shape and transport distance were similar. The particle that behaved the most uniquely started backward near Charlotte Harbor (and corresponds to the forward released particle starting just north of Tampa Bay). Though initially it behaved similar to the others in that it advected northward and generally along the isobath, it then slowly was transported across the isobaths into deeper water.

The 75 m isobath particles in the same two Figures managed to demonstrate the mostly along isobath transport and larger velocities compared to the shallower particles of the inner shelf. Of the four particles that reached the model domain boundary in the forward calculations,

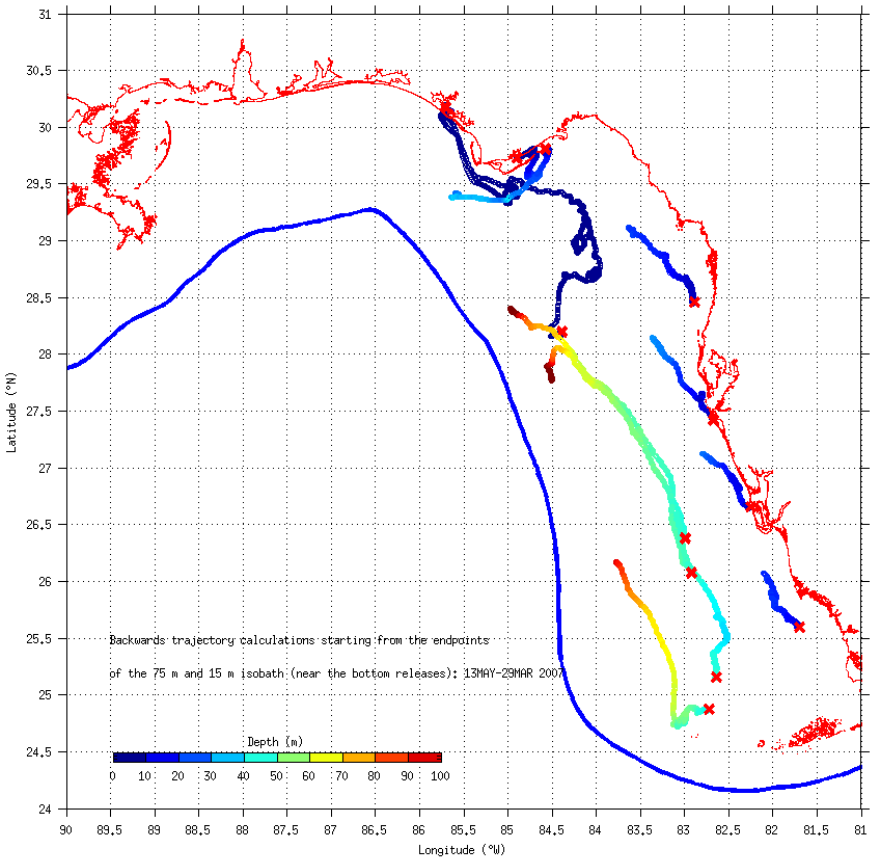

Figure 4.6: Backward particle trajectory calculations. The particles are those that were originally released at the 75 m and 15 m isobaths near the bottom of the water column at the -0.95 sigma layer when they were calculated forward in time. Each red 'x' marks the final location of the forward trajectories, which are the initial locations for the backward trajectory calculations.

only two of them were transported away from the model boundary and northward along the shelf when calculated backward. One of those two never made it back over the shelf break, and was transported instead out of the model domain around 26.7°N. The other particle advected north above 28.5°N in relatively good agreement with most of the corresponding forward trajectory, though it stopped short of the initial forward release point of 29.9°N 85.7°W. The two remaining particles that started at the model domain boundary were not transported away from the boundary when calculated backward. After further investigation into the cause of the major discrepancies, that portion of the model domain boundary was found to be experiencing large velocities with frequent direction changes through the entire time period due to both local and deep-ocean forcing.

Moving to the near-bottom released particles (Figures 4.5 and 4.6), the shape and actual trajectory locations were replicated significantly better than in the middle released particles. The four 15 m particles that were calculated forward starting at 83.5°W and eastward all had good replication of their forward calculations. The particle farthest to the south reproduced the trajectory shape, depth, and reached the appropriate points almost exactly. The two particles that originated near Charlotte Harbor and Tampa Bay also did well with the overall shape and direction of trajectory though they both continued too far to the northwest having longer trajectories moving into deeper water. The particle that was released forward at 83.5°W had very good trajectory shape and depth replication, with only a minor over-extension to the northwest of the forward starting point. The remaining two 15 m particles had very good path replication and depth replication. Surprisingly, the RK was able to calculate the particle that entered the waters just outside of Apalachicola's path back out into the GOMEX. The distance discrepancy was

small, demonstrating that relatively complex calculations around landmasses are possible as long as the forcing influences are consistent.

Looking at the 75 m released particles, the four southernmost particles had good replication backward in depth, shape, and actual location. The particle that was released forward at 27.1°N fell short and east in the backward, but the shape was still mostly correct. The two

Table 4: Distance discrepancy in meters for each of the 24 particles, their daily discrepancy rate (m day^{-1}), and the release location.

Discrepancies (m)	Rate (m day^{-1})	Release Location
239098	**5313**	15 mid
30323	1418	15 mid
7493	**166**	15 mid
65916	1686	15 mid
32322	718	15 mid
19567	434	15 mid
135142	**3003**	15 btm
17647	438	15 btm
15725	349	15 btm
33015	1481	15 btm
21735	896	15 btm
4114	**91**	15 btm
53095	1179	75 mid
43392	**964**	75 mid
58943	2199	75 mid
150791	**7492**	75 mid
272864	6063	75 mid
163875	6343	75 mid
86022	1968	75 btm
20344	641	75 btm
14942	**332**	75 btm
27550	612	75 btm
96426	**2142**	75 btm
19332	429	75 btm

* "15" and "75" represent the 15 and 75 m isobaths respectively, and "mid" represents middle of the water column (-0.5 sigma layer), and "btm" represents the bottom (-0.95 sigma layer) release location in the water column. The green values are the best rates for each of the four release locations, while the red values are the worst for each. These specific particles are plotted in Figure 4.7 (best) and Figure 4.8 (worst) respectively.

particles in the Florida Panhandle from the forward trajectory had strong replication backward until the upwelling pattern needed to be replicated. The northern-most particle replicated very well backward until it came time to break away from the shallow depths and move into deeper water. The same can be said of the other particle which had good replication until the shelf break

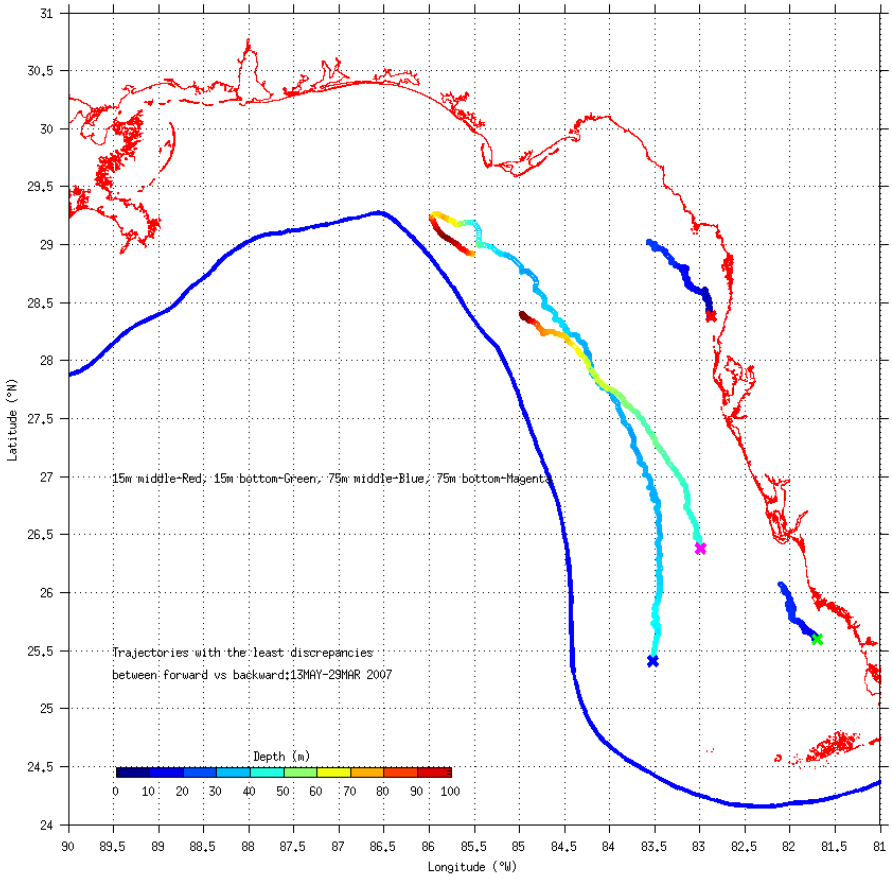

Figure 4.7: The four particles with the best distance discrepancies (smallest) in each of the four release sets (see Table 4.2). The trajectories displayed are the backward calculations. The colored 'x' at each trajectory marks the final location of the forward trajectory calculation (initial point of the backward trajectory calculation). Red marks the 15 m middle of the column, green marks the near-bottom of the 15 m isobath particle, blue is the 75 m middle released particle, and magenta is the 75 m bottom released particle.

was encountered where the rapid shift between downwelling and upwelling needed to be replicated. Each of the four sets of particles (15 m isobath middle, bottom and 75 m middle and bottom) had a particle that was replicated with the smallest (best) distance discrepancy rate and one that had the largest (worst). These particle trajectories are displayed in Figures 4.7 and 4.8,

and listed in Table 4. The particles that had the best backward RK replication were those that didn't have any large velocity or direction changes over the time period, weren't trapped near the model domain boundary, and didn't have to try and replicate an abrupt change from downwelling to upwelling. These trajectories are relatively smooth and consistent in their

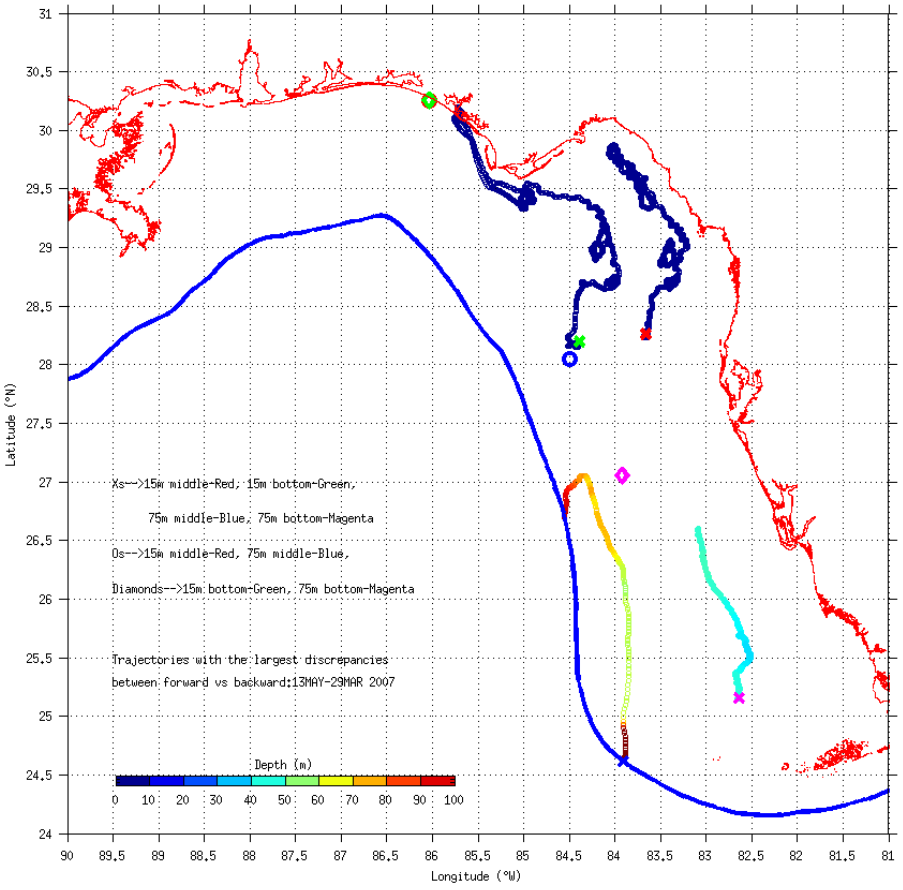

Figure 4.8: The four particles with the worst distance discrepancies (largest) in each of the four release sets (see Table 4.2). The trajectories displayed are the backward calculations. The colored 'x' at each trajectory marks the final location of the forward trajectory calculation (initial point of the backward trajectory calculation). The diamonds are the initial forward trajectory locations of the bottom released particles, and the circles are the initial forward release locations of the middle of the water column particles. Red marks the 15 m middle of the column, green marks the near-bottom of the 15 m isobath particle, blue is the 75 m middle released particle, and magenta is the 75 m bottom released particle. Ideally, the 'x' of a particular color would have a trajectory ending at the diamond or circle of the same color. Of note, the red diamond and green circle are overlapping, demonstrating the worst particle for the 15 m isobath at both release depths was at the same location.

velocity and overall path. Figure 4.8 shows three particles that replicate the general shape of their forward trajectories (green, blue, and magenta markers). Each of these trajectories falls well

short of their target end point when calculated backward with RK, but their path is comparable. Their discrepancies came from either not being able to replicate the total distance to the end point, or they were in the wrong location on the shelf, though with the right overall shape. The particle that truly is a poor replication in every way is the red particle. This particle followed a forward trajectory that travelled slightly to the west paralleling the coastline for a brief period of time before reversing direction and flowing south along the shelf. From this point the particle had the largest velocity of all of the 15 m isobath particles that were released in the middle of the water column (Figure 4.3) for the forward calculations. The backward calculation got caught in the Big Bend and paralleled the coastline rather than going into relatively deeper waters and advecting to the northwest into the Florida Panhandle towards the original release point of the forward calculation.

4.7 Discussion

Based on the variety of replication results using the 4^{th} order RK method for forward and backward particle trajectory calculations, there are multiple situations with relatively large discrepancies between the original initiation in the forward and the final point in the backward calculations. These situations may need to be approached using a different mathematical tool to account for the discrepancies between the forward approximation and the attempt to replicate the approximation calculation in the backward direction. The particles that encounter large changes of velocity, direction, or both simultaneously are prime candidates for considering an alternative calculation method approach. These particles end up trapped against the boundary (shoreline or model domain boundary) and are not appropriately transported across isobaths and out of their initial bathymetric area (i.e. remain trapped in shallow (deep) water). The particles do not cross

locations on the shelf like the shelf break or the inner shelf boundary. Examples of such dynamic situations that could cause such discrepancies are eddies, current reversals, and strong frontal passages that cause significant reversals in the overall water advection in an area.

Another situation in which the discrepancies would most likely be too large to be worth using the RK for backward calculations is where particles need to replicate downwelling and upwelling in quick succession. The quick change in required direction and depth over such a short time period isn't calculated reliably by the RK. The result tends to completely ignore the quick and large changes in the trajectory and remain relatively stationary instead of transporting the particle to greater depth. This makes it appear as if the velocity abruptly decreases with no reversal, and the particle's total transport distance is shorter than it actually is. This was primarily a problem with the particles that originated at the 75 m isobath. The trend could most likely be applied to other locations in the outer shelf where movement across the shelf break and deep-ocean forcing both play key roles in the particle transport.

Instances where the RK works most reliably in the backward direction are those of consistent forcings (deep-ocean or local), with little to no abrupt direction reversals or velocity changes. The smoother the forward trajectory calculated by RK, the smoother and more likely the RK calculations backward will reliably replicate the forward calculations. In such cases, there are less fluctuations in the calculation's step-wise process forward, which makes it easier to recreate the same approximations backward since there are no "hidden" variations or fluctuations that the step sizes mask. In addition to this, the particles that were in the boundary layers performed the best at all locations. This is due to the dynamic restrictions and comparatively less chaotic resultant flows that are found in such areas of the water column. The middle of the water column locations that were selected, especially those at the 75 m isobath, were able to be in

between the surface and bottom boundary layers, allowing for relatively more freedom of movement of the particles compared to those in the boundary layers. This increased movement in the middle of the water column led to increased errors that were compounded as the iterative steps in the RK were calculated.

As mentioned previously, the distance between grid points in any calculation are going to play a role in the solution's accuracy. The nature of the unstructured mesh that allows for downscaling from the open boundary into the estuaries and rivers of the WFS in the WFCOM has areas of varying resolution. The open boundary is as coarse as 12 km, while the estuaries and rivers see resolution as fine as 150 m. The paths the particles took between one successive time step and another in many cases crossed into grid cells of multiple sizes and areas of varying resolution. This process will impact the calculations forward and backward in time as the physical resolution of each calculation step can only be as fine as the resolution of the grid cells the particle is in.

This study has shown that while there is some validity in using a 4^{th} order RK method forward in time for isopycnal particle trajectory calculations in a non-stochastic environment forced by both local and deep-ocean forcing influences, the backward calculations serve best as estimations and as a way to get a first approximation of where a particle originated from in time. This model does not include a random walk like so many others do to account for diffusivity. The fact that the trajectories and dynamics are non-linear forward in time yield an immediate assumption that the backward in time cannot mathematically yield an exact replication of the forward calculations. Those particles that are restricted in their flows due to surface and boundary layer conditions are most likely to have a high fidelity in their replication calculations. It is a useful tool for areas of little oscillation, velocity, and forcing changes, with the

understanding that it is still an approximation (as is the forward RK method) to the actual solution of the ODE.

CHAPTER 5

SUMMARY

The distribution of water properties within the coastal ocean is determined by a combination of the coastal ocean circulation that is driven by both local and deep-ocean forcing and the biological and chemical interactions that consume and transform nutrients. Sound ecologically based management of the West Florida Shelf (WFS) and elsewhere thus requires an understanding of these processes beginning with the advection of nutrients into the euphotic zone of the continental shelf and hence the primary productivity from which most of the coastal ocean ecology, and resulting economic stimulus to the state economy, derives.

The purpose of this thesis project was to study the connections in response to local and deep-ocean forcing on waters of the WFS. The inclusion of upwelling of waters from the deeper ocean across the shelf break onto the WFS and the further investigation into the transport of waters throughout the WFS from the shelf break to the shoreline was a natural extension. These movements and responses to forcing influences are what set the stage for the ecology of the WFS. The approach entailed the use of an improved Eulerian numerical scheme (4^{th} order Runge-Kutta) applied to numerical coastal ocean circulation model simulations to estimate Lagrangian particle trajectories. An ancillary investigation was made regarding the differences that occurred when tracking particles either forward or backward in time. In other words if two different questions were to be asked: 1) if a particle originated at a given location and time where would it end up at

a later time, or 2) if a particle originated at a given location and time where did it originate, would similar answers be obtained?

The forcing influences on the WFS were explored, specifically comparing the local and deep-ocean forcing effects on water particle transport. A period of upwelling of deeper Gulf of Mexico (GOMEX) water across the shelf break and onto the WFS was considered as a deep-ocean forced event. This period was compared to a period of downwelling of equal duration. The local forcing influence on the WFS waters was approached by considering the downwelling period as well as utilizing case studies. The case studies included an extreme example (Tropical Storm Debby in 2012 (AL042012)) and the passage of two cold fronts. One of the frontal passages occurred during a time of deep-ocean forcing influence as well as local forcing, providing an example of both influences to be considered with those of the extreme local forcing and the synoptic scale local forcing (the other front). The different case studies demonstrate the complexity of the connections that are present on the WFS. The particle trajectory calculations for all examples were considered for connectivity purposes across the WFS, and what general forcing influence would be potentially the most efficient at moving water masses to various areas on the shelf, especially between estuaries and other areas of juvenile fish recruitment importance.

It was found that under primarily deep-ocean forcing and in an upwelling event, the bottom Ekman layer is the primary conduit for transporting parcels from the shelf break towards the shore and estuaries. Under primarily local forcing, the majority of the longitudinal movement was found to be mostly towards the west, though there was more movement in the north-south direction than longitudinally both at the surface and at depth. The connectivity of the various

parts of the WFS has the best chance of occurring to the greatest extent when both local and deep-ocean forcing occurs simultaneously.

Chapter 4 took a closer look at the actual particle trajectory calculation method that was used for the study in Chapter 3. A 4th order Runge-Kutta method was used for the calculations forward in time. Investigating the applicability of the same method to calculate the trajectories backward in time and to compare the results in both directions and the potential causes for the discrepancies that resulted was the purpose of the study. Both particles originating at the near-bottom and in the middle of the water column at locations along the 75 m and 15 m isobaths were considered during the 29MAR2007-13MAY2007 45-day period of upwelling that was investigated in Chapter 3.

The largest discrepancies in the backward calculations were found with events of large changes in velocity, direction, or both simultaneously. Examples of such instances would be eddies, current reversals, or strong frontal passages. There was also a consistent problem with the backward calculations for instances of upwelling and downwelling changing in quick succession. The Runge-Kutta method had comparatively strong success in those events when the forcings (local or deep-ocean) were consistent, and where there were little or no abrupt changes in direction or velocity of the water parcel transport.

As an exploratory study, there is room for further research and expansion. Limited by only a few case studies, this work does not provide a large enough ensemble of events from which meaningful statistics may be arrived at. Connectivity, deriving from a combination of local and dep ocean forcing, warrants a much more exhaustive set of calculations for determining a probabilistic distribution of particle translations and a set of outlying situations for which water properties may deviate from the norm. This in fact is the crux of the connectivity question. For a

broad continental shelf that is generally depleted of nutrients, i.e., oligotrophic, how is it possible to support an abundant and diverse set of ecosystems services? Connectivity under certain conditions provides an answer, and this study is an initial, exploratory step in defining such an answer. Future work may include exploring many more case studies in Chapter 3 and further refining the initial results of Chapter 4.

REFERENCES

Allen, T., and R. Southwick (2007), Sportfishing in America: An Economic Engine and Conservation Powerhouse, edited by M. J. Williamson, Southwick Associates.

Anastassi, Z. A., and T. E. Simos (2005), An optimized Runge-Kutta method for the solution of orbital problems, *Journal of Computational and Applied Mathematics*, *175*(1), 1-9, doi:10.1016/j.cam.2004.06.004.

Anderson, D. M., P. Hoagland, Y. Kaoru, and A. W. White (2000), Estimated annual economic impacts from Harmful Algal Blooms (HABs) in the United States, 1-101 pp, Woods Hole Oceanographic Institution.

Aristoff, J. M., and A. B. Poore (2012), Implicit Runge-Kutta Methods for Orbit Propagation, in *AIAA/AAS Astrodynamics Specialist Conference*, edited, American Institute of Aeronautics and Astronautics, Inc., Minneapolis, MN, doi:10.2514/6.2012-4880.

Arnold, W. S., et al. (2002), An Ecosystem Model of the West Florida Shelf for use in Fisheries Management and Ecological Reserach: Volume II. Model Construction, 163 pp, St Petersburg, FL.

Barth, A., A. Alvera-Azcarate, and R. H. Weisberg (2008), A nested model study of the Loop Current generated variability and its impact on the WFS, *Journal of Geophysical Research*, *113*, 18, doi:10.1029/2007JC004492.

Barton, E. D., A. Huyer, and R. L. Smith (1977), Temporal variation observed in the hydrographic regime near Cabo Corveiro in the northwest African upwelling region, February to April 1974, *Deep-Sea Research*, *24*, 17, doi:10.1016/0146-6291(77)90537-9.

Batchelder, H. P. (2006), Forward-in-Time-/Backward-in-Time-Trajeectory (FITT/BITT) Modeling of Particles and Organisms in the Coastal Ocean, *Journal of Atmospheric and Oceanic Technology*, *23*, 727-741, doi:10.1175/JTECH1874.1.

Beljadid, A., A. Mohammadian, and H. M. Qiblawey (2013), An unstructured finite volume method for large-scale shallow slows using the fourth-order Adams scheme, *Journal of Computers and Fluids*, *88*, 579-589, doi:10.1016/j.compfluid.2013.10.018.

Boicourt, W. C., W. J. Wiseman, Jr, A. Valle-Levinson, and L. P. Atkinson (1998), Continetal shelf of the southeastern United States and the Gulf of Mexico: in the shadow of the western boundary current, in *The Sea: The Global Ocean: Regional Studies and Synthesis*, edited by A. R. Robinson and K. H. Brink, pp. 135-182, John Wiley & Sons, New York, NY.

Boucher, J., C. Chen, Y. Sun, and R. C. Beardsley (2013), Effects of interannual environmental variability of the transport-retention dynamics in haddock melanogrammus aeglefinus larve on Georges Bank, *Marine Ecology Progress Series*, *487*, 201-215.

Brink, K. H., F. F. G. Abrantes, P. A. Bernal, R. C. Dugdale, M. Estrada, L. Hutchings, R. A. Jahnke, P. J. Muller, and R. L. Smith (1995), Group report: How do coastal upwelling systems operate as integrated physical, chemical and biological systems and influence the geological record? The role of physical processes in defining the spatial structures of biological and chemical variables, paper presented at Upwelling in the ocean: Modern Processes and Ancient Records, John Wiley & Sons, Berlin, Germany.

Bumpus, D. F. (1973), A description of the circulation on the continental shelf of the east coast of the United States, *Progress in Oceanography*, *6*, 111-157, doi:10.1016/0079-6611(73)90006-2.

Butcher, J. C. (1996), A history fo Runge-Kutta methods, *Applied Numerical Mathematics*, *20*(3), 247-260, doi:10.1016/0168-9274(95)00108-5.

Butcher, J. C., and P. B. Johnston (1993), Estimating local truncation errors for Runge-Kutta methods, *Journal of Computational and Applied Mathematics*, *45*(1-2), 203-212, doi:10.1016/0377-0427(93)90275-G.

Center, N. D. B. (2015), Station 42039 (LLNR 141) Pensacola, edited, NOAA NWS NSBC, Stennis Space Center, MS.

Chen, C. (2013), FVCOM- An unstructured grid Finite-Volume Community Ocean Model, edited, p. 56.

Chen, C., et al. (2013a), An unstructured grid, finite-volume community ocean model: FVCOM User Manual, edited, p. 416, SMAST/UMASSD.

Chen, C., R. C. Beardsley, Q. Xu, G. Cowles, and R. Limeburner (2013b), Tidal dynamics in the Gulf of Maine and New England Shelf: An application of FVCOM, *Journal of Geophysical Research*.

Chen, C., Z. Lai, R. C. Beardsley, J. Sasaki, J. Lin, H. Lin, R. Ji, and Y. Sun (2014a), The March 11, 2011 Tohoku M9.0 earthquake-induced tsunami and coastal inundation along the Japanese coast: A model assessment, *Progress in Oceanography*, *123*, 84-104, doi:10.1016/j.pocean.2014.01.002.

Chen, C., et al. (2014b), Process modeling studies of physical mechanisms of the formation of an anticyclonic eddy in the central Red Sea, *Journal of Geophysical Research: Oceans*, *119*(2), 20, doi:DOI: 10.1002/2013JC009351.

Chen, C., H. Liu, and R. C. Beardsley (2003), An unstructured, finite-volume, three-dimensional, primitive equation ocean model: application to coastal ocean and estuaries, *Journal of Geophysical Research*, *20*, 159-186.

Florida Department of Agriculture and Consumer Services (2013), Florida Agriculture Overview and Statistics, edited, Tallahassee, FL.

Florida Fish and Wildlife Conservation Commission (2015), The Economic Impact of Saltwater Fishing in Florida, edited, Tallahassee, Florida.

Hamilton, P., and T. N. Lee (2005), Eddies and jets over the slope of the northeast Gulf of Mexico, *Circulation in the Gulf of Mexico: Observations and Models*, *161*, 123-142.

He, R., and R. H. Weisberg (2002), Tides on the West Florida Shelf, *Journal of Physical Oceanography*, *32*, 3455-3473.

He, R., and R. H. Weisberg (2003), A Loop Current Intrusion Case Study on the West Florida Shelf, *Journal of Physical Oceanography*, *33*, 13.

He, R., R. H. Weisberg, H. Zhang, F. E. Muller-Karger, and R. W. Helber (2003), A cloud-free, satellite-derived, sea surface temperature analysis for the West Florida Shelf, *Geophysical Research Letters*, *30*(15), doi:10.1029/2003GL017673.

Heil, C. A., et al. (2014), Blooms of Karenia brevis (Davis) G. Hansen & O. Moestrup on the West Florida Shelf: Nutrient sources and potential management strategies based on a multi-year regional study, *Harmful Algae*, *38*, doi:10.1016/j.hal.2014.07.016.

Hejranfar, K., and E. Ezzatneshan (2014), A high-order compact finite-difference lattice Boltzmann method for simulation of steady and unsteady incompressible flows, *International Journal for Numerical Methods in Fluids*, *75*, 713-746, doi:10.1002/fld.3916.

Hetland, R. D., Y. Hsueh, R. R. Leben, and P. P. Niiler (1999), A loop current-induced jet along the edge of the West Florida Shelf, *Geophysical Research Letters*, *26*(15), 2239-2242, doi:10.1029/1999GL900463.

Hofmann, E. E., K. S. Hedstrom, J. R. Moisan, D. B. Haidvogel, and D. L. Mackas (1991), Use of Simulated Drifter Tracks to Investigate General Transport Patterns and Residence Times in the Coastal Transition Zone, *Journal of Geophysical Research*, *96*(C8), 12, doi:10.1029/91JC00832

Holligan, P. J., M. Viollier, D. S. Harbour, P. Camus, and M. Champagne-Philippe (1983), Satellite and ship studies of coccolithophore production along a continental shelf edge, *Nature*, *304*, 339-342, doi:10.1038/304339a0.

Hu, J. R. Nelson, E. Johns, Z. Chen, R. H. Weisberg, and F. E. Muller-Karger (2005), Mississippi River water in the Florida Straits and in the Gulf Stream off Georgia in Summer 2004, *Geophysical Research Letters*, *32*(L14606), doi:10.102/2005GL022942.

Hu, D. W. Townsend, C. Chen, G. W. Cowles, R. C. Beardsley, R. Ji, and R. W. Houghton (2008), Tidal Pumping and nutrient fluxes on Georges Bank: A process-oriented modeling study, *Journal of Marine Systems*, *74*, 528-544, doi:10.1016/j.jmarsys.2008.04.007.

Huret, M., J. Runge, C. Chen, G. Cowles, Q. Xu, and J. Pringle (2007), Dispersal modeling of fish early live stages: Sensitivity analysis with application to Atlantic Cod in the western Gulf of Maine, *Marine Ecology Progress Series*, *347*, 261-274.

Hurlburt, H. E., and J. D. Thompson (1980), A Numerical Study of Loop Current Intrusions and Eddy Shedding, *Journal of Physical Oceanography*, *10*(10), 1611-1651, doi:10.1175/1520-0485(1980)010<1611:ANSOLC>2.0.CO;2.

Isobe, A., and R. C. Beardsley (2006), An estimate of the cross-frontal transport at the shelf break of the East China Sea with the Finite Volume Coastal Ocean Model., *Journal of Geophysical Research*, *111*(C03012), doi:10.1029/2005JC002390.

Ji, R., C. Chen, P. J. S. Franks, D. W. Townsend, E. G. Durbin, R. C. Beardsley, R. G. Lough, and R. W. Houghton (2006), The Impact of Scotian Shelf Water "cross-over"on the plankton dynamics on Georges Bank: A 3-D experiment for the 1999 spring bloom, *Deep-Sea Research Part Ii-Topical Studies in Oceanography*, *53*(23-24), 2684-2707, doi:10.1016/j.dsr2.2006.08.007.

Ji, R., C. Davis, C. Chen, D. W. Townsend, D. G. Mountain, and R. C. Beardsley (2007), Influence of ocean freshening on shelf phytoplankton dynamics, *Geophysical Research Letters*, *34*(L24607), doi:10.1029/2007GL032010.

Johnson, and P. D. Killworth (1975), A Bottom current along the shelf break, *Journal of Physical Oceanography*, *5*(1), 185-188, doi:10.1175/1520-0485(1975)005<0185:ABCATS>2.0.CO;2.

Johnson, C., J. Pringle, and C. Chen (2006), Transport and retention of dormant copepods in the Gulf of Maine, *Deep-Sea Research Part Ii-Topical Studies in Oceanography*, *53*(23-24), 2520-2536, doi:10.1016/j.dsr2.2006.08.016.

Joy, K. I. (1999), Numerical Methods for Particle Tracing in Vector Fields, edited, Department of Computer Science University of California, Davis.

Kaunda, A. E. (2015), Forward-backward-difference time-integrating schemes with higher order derivatives for non-lnear finite element analysis of solids and structures, *Computers and Structures*, *153*, 1-18, doi:10.1016/j.compstruc.2015.02.026.

Kelly, K. A., and D. C. Chapman (1988), The Response of Stratified Shelf and Slope Waters to Steady Offshore Forcing, *Journal of Physical Oceanography*, *18*, 906-925, doi:10.1175/1520-0485(1988)018<0906.

Kildow, J. (2008), Phase II Florida's Ocean and Coastal Economies Report,*Rep.*, National Ocean Economics Program.

Kimberlain, T. B. (2013), Tropical Cyclone Report Tropical Storm Debby (AL042012) 23-27 June 2012, edited by N. H. Center, p. 51.

Lee, C., T. Khangaonkar, and Z. Yang (2007), Application of Hydrodynamic and Sediment Transport Model for the Restoration Feasibility Assessment- Cottonwood Island, Washington, paper presented at 10th International Conference, American Society of Civil Engineers, Newport, RI.

Lenes, J. M., B. A. Darrow, J. J. Walsh, J. M. Prospero, R. He, R. H. Weisberg, G. A. Vargo, and C. A. Heil (2008), Saharan dust and phopphatic fidelity: A three-dimensiona biogeochemical model of Trichodesmium as a nutrient source for red tides on the WFS, *Continental Shelf Research*, *28, 1091-1115*.

Lentz, S. J. (1995), Sensitivity of the Inner-Shelf Circulation to the Form of the Eddy Viscosity Profile, *Journal of Physical Oceanography*, *25*, 10.

Li, Z., and R. H. Weisberg (1999), West Florida continental shelf response to upwelling favorable wind forcing 2. Dynamics, *Journal of Geophysical Research*, *104*(C10), 16.

Liu, Y., and R. H. Weisberg (2005a), Momentum balance diagnoses for the West Florida Shelf, *Continental Shelf Research*, *25*, 2054-2074, doi:10.1016/j.csr.2005.03.004.

Liu, Y., and R. H. Weisberg (2005b), Patterns of ocean current variability on the WFS using the self-organizing map, *Journal of Geophysical Research*, *110*(C06003), 12, doi:10.1029/2004JC002786.

Liu, Y., and R. H. Weisberg (2007), Ocean Currents and Sea Surface Heights Estimated across the West Florida Shelf, *Journal of Physical Oceanography*, *37*, 1697-1713, doi:10.1175/JPO3083.1.

Liu, Y., and R. H. Weisberg (2011), Evaluation of trajectory modeling in different dynamic regions using normalized cumulative Lagrangian separation, *Journal of Geophysical Research*, *116*(C09013), doi:10.1029/2010JC006837.

Liu, Y., and R. H. Weisberg (2012), Seasonal variability on the West Florida Shelf, *Progress in Oceanography*, *104*, doi:10.1016/j.pocean.2012.06.001.

Liu, Y., R. H. Weisberg, and R. He (2006), Sea Surface Temperature Patterns on the WFS using growing hierarchial self-organizing maps, *Journal of Atmospheric and Oceanic Technology*, *25*, 325-338.

Liu, Y., R. H. Weisberg, C. Hu, C. Kovach, and R. Riethmuller (2011a), Evolution of the Loop Current system during the Deepwater Horizon oil spill event as observed with drifters and satellites, in *Monitoring and Modeling the Deepwater Horizon Oil Spill: A Record-Breaking Enterprise*, edited by Y. Liu, A. MacFadyen, Z.-G. Ji and R. H. Weisberg, pp. 91-101, AGU, Washington, D.C., doi:10.1029/2011GM001127.

Liu, Y., R. H. Weisberg, C. Hu, and L. Zheng (2011b), Tracking the Deepwater Horizon oil spill: A modeling perspective, *Eos 92*(6), 45-52, doi:10.1029/2011EO060001.

Liu, Y., R. H. Weisberg, C. Hu, and L. Zheng (2011c), Trajectory Forecast as a Rapid Response to the Deepwater Horizon Oil Spill, in *Monitoring and Modeling the Deepwater Horizon Oil Spill: A Record-Breaking Enterprise*, edited by Y. Liu, A. Macfadyen, Z.-G. Ji and R. H. Weisberg, pp. 153-165, American Geophysical Union, Washington, D.C., doi:10.1029/2011GM001121.

Liu, Y., R. H. Weisberg, S. Vignudelli, and G. T. Mitchum (2014), Evaluation of altimetry derived surface current products using Lagrangian drifter trajectores in the eastern Gulf of Mexico, *Journal of Geophysical Research Oceans*, *119*, 2827-2842, doi:10.1002/2013JC009710.

Lucas, A. J., R. A. Guerrero, H. W. Mianzan, and E.Marcelo (2005), Coastal oceanographic regimes of the Northern Argentine Continental Shelf (34-43*S), *Estuarine, Coastal and Shelf Science*, *65*(3), 405-420, doi:10.1016/j.ecss.2005.06.015.

Mapsofworld.com (2013), Florida River Map, edited, www.mapsofworld.com.

Meyers, S. D., E. M. Siegel, and R. H. Weisberg (2001), Observations of currents on the West Florida Shelf break, *Geophysical Research Letters*, *28*, 2037-2040.

Milliman, J. D., S. Huang-ting, Y. Zuo-sheng, and R. H. Mead (1985), Transport and deposition of river sediment in the Changjiang estuary and adjacent continental shelf, *Continental Shelf Research*, *4*(1-2), 37-45, doi:10.1016/0278-4343(85)90020-2.

Mitchum, G. T., and A. J. Clarke (1986), The frictional nearshore response to forcing by synoptic scale winds, *Journal of Physical Oceanography*, *16*, 13.

Monarski (2012), Surface Weather Map and Station Weather, edited, NOAA/National Weather Service National Centers for Environmental Prediction Weather Prediction Center, College Park, Maryland.

Nazari, F., A. Mohammadian, M. Charron, and A. Zadra (2014), Optimal high-order diagonally-implicit Runge Kutta schemes for nonlinear diffusive systems on atmospheric boundary layer, *Journal of Computational Physics*, *271*, 118-130, doi:10/1016/j.jcp.2014.01.039.

Oey, L.-Y. (1996), Simulation of Mesoscale Variability in the Gulf of Mexico: Sensitivity Studies, Comparison with Observations, and Trapped Wave Propagation., *Journal of Physical Oceanography*, *26*(2), 145-175, doi:10.1175/1520-0485(1996)026<0145:SOMVIT>2.0.CO;2.

Oey, L.-Y., T. Ezer, and H.-C. Lee (2005), Loop Current, rings, and related circulation in the Gulf of Mexico: A review of numerical models and future challenges, in *Circulation in the Gulf of Mexico: Observations and Models*, edited by W. Sturges and A. Lugo-Fernandez, pp. 31-56, American Geophysical Union, Washington D.C.

Otto (2007), Surface Weather Map and Station Weather, edited, NOAA/National Weather Service National Centers for Environmental Prediction Weather Prediction Center, College Park, Maryland.

Pitcher, G. C., F. G. Figueiras, B. M. hickey, and M. T. Moita (2010), The physical oceanography of upwelling systems and the development of harmful algal blooms, *Progress in Oceanography*, *85*(1-2), 5-32, doi:10.1016/j.pocean.2010.02.002.

Pries, J., and H. Hofmann (2015), Steady-state algorithms for nonlinear time-periodic magnectic diffusion problems using diagonally implicit Runge-Kutta methods, *Transactions on Magnetics*, *51*(4), 12, doi:10.1109/TMAG.2014.2344005.

Program, N. O. E. (2014), Coastal and Ocean Economic Summaries of the Coastal States, in *State of the U.S. Ocean and Coastal Economies*, edited, p. 62.

Rio, M. H., S. Guinehut, and G. Larnicol (2011), New CNES-CLS09 global mean dynamic topography computed from the combination of GRACE data, altimetry, and in situ measurements, *Journal of Geophysical Research*, *116*(C07018), 25, doi:10.1029/2010JC006505.

Schmitz, W. J., Jr., D. C. Biggs, A. Lugo-Fernandez, L.-Y. Oey, and W. Sturges (2005), A synopsis of the circulation in the Gulf of Mexico and on its continental margins, *Circulation in the Gulf of Mexico: Observations and Models*, *161*, 11-29.

Shampine, L. F., and H. A. Watts (1971), Comparing Error Estimators for Runge-Kutta Methods, *Mathematics of Computation*, *25*(115), 445-455, doi:10.1090/S0025-5718-1971-0297138-9.

Smith, R. L. (1995), The physical processes of coastal ocean upwelling systems, paper presented at Upwelling in the ocean: Modern Processes and Ancient Records, John Wiley & Sons, Berlin, Germany.

Stein, A. F., R. R. Draxler, G. D. Rolph, B. J. B. Stunder, M. D. Cohen, and F. Ngan (2015), NOAA's HYSPLIT Atmospheric Transport and Dispersion Modeling System, in *Bulletin of the American Meteorological Society*, edited, pp. 2059-2077, American Meteorological Society, doi:10.1175/BAMS-D-14-00110.1.

Strub, P. T., J. S. Allen, A. Huyer, R. L. Smith, and R. C. Beardsley (1987), Seasonal Cycles of Currents, Temperatures, Winds, and Sea Level Over the Northeast Pacific Continental Shelf: 35*N to 48*N, *Journal of Geophysical Research*, *92*(C2), 1507-1526.

Sturges, W. (2005), Deep-water exchange between the Atlantic, Caribbean, and Gulf of Mexico, *Circulation in the Gulf of Mexico: Observations and Models*, *161*, 263-278.

Summerhayes, C. P., K. C. Emeis, M. V. Angel, R. L. Smith, and B. Zeitzschel (1995), Upwelling in the ocean: modern processes and ancient records, paper presented at Upwelling in the ocean: Modern Processes and Ancient Records, John Wiley & Sons, Berlin, Germany.

Sverdrup, H. U. (1938), On the Process of Upwelling, *Journal of Marine Research*, *1*(2), 10.

Taylor, G. I. (1921), Experiments with Rotating Fluids, *Proceedings of the Royal Society of London. Ser. A*, *100*(703), 114-121.

Varsakelis, C., and P. Anagnostidis (2016), On the susceptibility of numerical methods to computational chaos and superstability, *Communications in Nonlinear Science and Numerical Simulation*, *33*, 118-132, doi:10.1016/j.cnsns.2015.09.007.

Virmani, J., and R. H. Weisberg (2006), The 2005 hurricane season: An echo of the past of a harbinger of the future?, *Geophysical Research Letters*, *33*(L05707), doi:10.1029/2005GL025517.

Walsh, J. J., et al. (2006), Red tides in the Gulf of Mexico: Where, when, and why?, *Journal of Geophysical Research*, *111*(C11003), 46, doi:10.1029/2004JC002813.

Walsh, J. J., et al. (2003), Phytoplankton response to intrusions of slope water on the West Florida Shelf: Models and observations, *Journal of Geophysical Research*, *108(C6)*(3190), doi:10.1029/2002JC001406.

Walsh, J. J., et al. (2009), Isotopic evidence for dead fish maintenance of Florida red tides, with implications for coastal fisheries over both source regions of the WFS and within downstream waters of the South Atlantic Bight, *Progress in Oceanography*, *80*, 51-73.

Weatherunderground (2015), Weather History for KSRQ, edited. Observation data from KSRQ for 18APR2012-2028APR2012 and 2013APR2007-2018APR2007.

Weisberg, R. H. (2011), Coastal Ocean Pollution, Water Quality, and Ecology, *Marine Technology Society Journal*, *45*(2), 35-42.

Weisberg, R. H., A. Barth, A. Alvera-Azcarate, and L. Zheng (2009a), A coordinated coastal ocean observing and modeling system for the West Florida Continental Shelf, *Harmful Algae*, *8*, 585-597.

Weisberg, R. H., B. D. Black, and Z. Li (2000), An upwelling case study on Florida's west coast, *Journal of Geophysical Research*, *105*(C5), 11.

Weisberg, R. H., B. D. Black, and H. Yang (1996), Seasonal modulation of the west Florida continental shelf circulation, *Geophysical Research Letters*, *23*(17), 2247-2250.

Weisberg, R. H., and R. He (2003), Local and deep-ocean forcing contributions to anomalous water properties on the West Florida Shelf, *Journal of Geophysical Research: Oceans*, *108*(C6), doi:10.1029/2002JC001407.

Weisberg, R. H., R. He, G. Kirkpatrick, F. Muller-Karger, and J. J. Walsh (2003), Coastal ocean circulation influences on remotely sensed optical properties: A West Florida Shelf case study *Oceanography*, *17*(2), 68-75, doi:10.5670/oceanog.2004.49.

Weisberg, R. H., R. He, Y. Liu, and J. I. Virmani (2005), West Florida Shelf circulation on synoptic, seasonal, and interannual time scales, in *Circulation in the Gulf of Mexico: Observations and Models*, edited by W. Sturges and A. Lugo-Fernandez, pp. 325-347, American Geophysical Union, Washington D.C.

Weisberg, R. H., Z. Li, and F. Muller-Karger (2001), West Florida shelf response to local wind forcing: April 1998, *Journal of Geophysical Research*, *106*(C12), 34.

Weisberg, R. H., Y. Liu, and D. A. Mayer (2009b), West Florida Shelf mean circulation observed with long-term moorings, *Geophysical Research Letters*, *36*(19), 6, doi:10.1029/2009GL040028.

Weisberg, R. H., and L. Zheng (2006a), Circulation of Tampa Bay driven by buoyancy, tides, and winds, as simulated using a finite volume coastal ocean model, *Journal of Geophysical Research*, *111*(C01005), doi:10.1029/2005JC003067.

Weisberg, R. H., and L. Zheng (2006b), Hurricane storm surge simulations for Tampa Bay, *Estuaries and Coasts*, *29*, 899-913.

Weisberg, R. H., and L. Zheng (2006c), A simulation of the Hurricane CHARLEY storm surge and its breach of north Captiva Island, *Florida Scientist*, *69*, 152-165.

Weisberg, R. H., L. Zheng, and Y. Liu (2011), Tracking Subsurface Oil in the Aftermath of the Deepwater Horizon Well Blowout, in *Monitoring and Modeling the Deepwater Horizon Oil Spill: A Record-Breaking Enterprise*, edited by Y. Liu, A. Macfadyen, Z.-G. Ji and R. H. Weisberg, pp. 205-215, American Geophysical Union, Washington, D.C., doi:10.1029/2011GM001131.

Weisberg, R. H., L. Zheng, Y. Liu, C. Lembke, J. M. Lenes, and J. J. Walsh (2014a), Why no red tide was observed on West Florida Continental Shelf in 2010, *Harmful Algae*, *38*, 119-126, doi:10.1016/j.hal.2014.04.010.

Weisberg, R. H., L. Zheng, and E. Peebles (2014b), Gag grouper larvae pathways on the West Florida Shelf, *Continental Shelf Research*, *88*, 11-23, doi:10.1016/j.csr.2014.06.003.

Werner, F. E. (1987), A numerical study of secondary flows over continental shelf edges, *Continental Shelf Research*, *7*(4), 379-409, doi:10.1016/0278-4343(87)90107-5.

Zhang, J.-Z. (2000), Shipboard automated determination of trace concentrations of nitrite and nitrate in oligotrophic water by gas-segmented continuous flow analysis with a liquid waveguide capillary flow cell, *Deep Sea Research Part I: Oceanographic Research Papers*, *47*(6), 1157-1171, doi:10.1016/S0967-0637(99)00085-0.

Zheng, L., and R. H. Weisberg (2010), Rookery Bay and Naples Bay circulation simulations: Applications to tides and fresh water inflow regulation, *Ecological modelling*, *221*, 986-996.

Zheng, L., and R. H. Weisberg (2012), Modeling the West Florida coastal ocean by downscaling from the deep ocean, across the continental shelf and into the estuaries, *Ocean Modeling*, *48*, 10-29.

Zhu, J., R. H. Weisberg, L. Zheng, and S. Han (2015), Influences of Channel Deepending and Widening on the Tidal and nontidal Circulations of Tampa Bay, *Estuaries and Coasts*, *38*, 132-150, doi:10.1007/s12237-014-985-4.

ABOUT THE AUTHOR

Amanda Sue Reinert was born in Long Prairie, Minnesota and has a younger brother. She graduated from the United States Naval Academy with Merit in May 2008 after earning a Bachelor's of Science in Oceanography. Her first duty station was USS FORREST SHERMAN (DDG 98) out of Norfolk, Virginia. She served as the Ordnance/Gunnery Officer June 2008-June 2009, earned her Surface Warfare designation, and served as the Force Protection and Assistant Weapons Officer until her detachment in June 2010. Upon detaching, Amanda transferred into the Meteorology and Oceanography community, getting stationed at the Naval Maritime Forecasting Center in Norfolk, VA (later known as the Fleet Weather Center-Norfolk) until August 2013. During her tour there she served as the lead officer (CDO) for a duty section on the high-tech 24/7 watch floor, was trained as a weather forecaster, earned her Information Dominance Warfare Officer designation, and qualified as the highest forecasting position of Duty Ship Routing Officer. She was also the Maritime Operations Officer and Sexual Assault Prevention and Response Program Manager for her command. Amanda voluntarily resigned her commission from the Navy in August 2013, and is now a graduate student at the University of South Florida, pursuing her Masters and Ph.D. in physical oceanography while raising her two young children. Upon completion of her Ph.D. she will be employed at the Naval Oceanographic Office at Stennis Space Center, Mississippi where she will once again contribute to the warfighter's mission success by providing operational oceanographic analysis and prediction products to the Fleet and its Allies.